Electrochemical approach to microfluidics

Yunus, Kamran

Award date:
2003

Awarding institution:
University of Bath

Electrochemical Approach to Microfluidics

Submitted by Kamran Yunus

for the degree of PhD

of the University of Bath

2003

Author's Signature.....

ProQuest LLC
789 East Eisenhower Parkway
P.O. Box 1346
Ann Arbor, MI 48106-1346

Acknowledgements

I would like to take this opportunity to thank Dr Adrian Fisher. Without his support and supervision I would have not been able to come this far with my education.

I would also like to thank all the members of the Electrochemistry Group based at the Chemistry Department in Bath University for welcoming me to their research team and for all the help and guidance given to me through the course of my PhD.

Special thanks to all the members of the optics group based at the Electronic and Electrical Engineering Department for their help and access to the microfabrication facilities. Thanks to Mr Trevor Ryan for all his training and priceless advice, and Dr J Sarma, Dr F Causa and Dr D Allsopp for welcoming me to their research group.

Finally, I will always be indebted to my family and friends who have always been a huge source of encouragement.

Abstract

This Thesis outlines the design, development and application of a new class of electrochemical device. Novel microelectrochemical reactors (MECR) are constructed using microfabrication techniques to provide structurally well-defined microchannels through which electrolyte solutions are pumped under microfluidic control and analysed using voltammetric techniques.

In depth studies and illustrations of microfabrication techniques are described for MECR development, with the potential benefits of microanalysis emphasised. Initial investigations focus on the development of a new voltammetric flow visualisation technique for the analysis of fluid flow properties within microreactors. Experimental studies are presented for monitoring the flow lines within channels with predefined obstructions and experimental results compared to computational predictions of the fluid dynamic properties using finite element method simulations.

MECR devices were developed to analyse the variation of the mass transport limited current variation as a function of solution flow rate within the cells, using microband electrodes sited on one wall of the microducts. The mass transport limited current was observed to vary linearly as a function of the cube root of volume flow rate, in an analogous manner to macroscopic flow cell devices. Three dimensional mass transport and fluid dynamics calculations were performed using a finite element technique in order to rationalise the observed behaviour. Examples of potential applications of MECR devices are also highlighted and preliminary studies detailed.

MECR techniques were also developed to evaluate the potential of creating parallel flows of immiscible liquids within the microreactor environments. Flow stability and voltammetric measurements are presented for a wide range of two and three phase immiscible flow regimes and the potential of the techniques to investigate phase transfer reactions are discussed.

Publications

1. Fisher, A. C.; A., G. K.; Henley, I. E.; Yunus, K. *Analytical Sciences* **2001**, *17*, i371.

2. Yunus, K.; Rickson, S. A.; Fisher, A. C.; Henley, I. E.; Allsopp, D. W. E.; Ryan, T. J. *Electrochemistry Communications* **2001**, *3*, 455.

3. Yunus, K.; Marks, C. B.; Fisher, A. C.; Allsopp, D. W. E.; Ryan, T. J.; Dryfe, R. A. W.; Hill, S. S.; Roberts, E. P. L.; Brennan, C. M. *Electrochemistry Communications* **2002**, *4*, 579.

4. Brookes, B. A.; Davies, T. J.; Fisher, A. C.; Evans, R. G.; Wilkins, S. J.; Yunus, K.; Wadhawan, J. D.; Compton, R. G. *Journal of Physical Chemistry B* **2003**, *107*, 1616.

5. Davies, T. J.; Brookes, B. A.; Fisher, A. C.; Yunus, K.; Wilkins, S. J.; Greene, P. R.; Wadhawan, J. D.; Compton, R. G. *Journal of Physical Chemistry B* **2003**, *107*, 6431.

6. Henley, I. E.; Yunus, K.; Fisher, A. C. *Journal of Physical Chemistry B* **2003**, *107*, 3878.

7. Hill, S. S.; Dryfe, R. A. W.; Roberts, E. P. L.; Fisher, A. C.; Yunus, K. *Analytical Chemistry* **2003**, *75*, 486.

8. Wadhawan, J. D.; Welford, P. J.; Yunus, K.; Fisher, A. C.; Compton, R. G. *Journal of the Brazilian Chemical Society* **2003**, *14*, 510.

9. Yunus, K.; Fisher, A. C. *Electroanalysis* **2003**, *15*, 1782.

Abbreviations

ACN	Acetonitrile
CT	Computer Tomography
DCE	1,2-Dichloroethane
DRIE	Deep Reactive Ion Beam Etching
ESR	Electron Spin Resonance
HF	Hydrofluoric Acid
IR	Infra Red
ITIES	Interface between Two Immiscible Electrolyte Solutions
μCP	Microcontact Printing
MECR	Microelectrochemical Reactor
MELL	Microelectrochemical Liquid-Liquid Techniques
MIMIC	Micromolding in Capillaries
μTM	Microtransfer Moulding
PIV	Particle Imaging Velocimetry
PSV	Particle Streak Velocimetry
PDMS	Poly(dimethylsiloxane)
KCl	Potassium chloride
REM	Replica Moulding
Re	Reynolds Number
SAMIM	Solvent-Assisted Micromolding
TBAP	Tetrabutyl ammonium perchlorate
TBPA	Tris(4-bromophenyl)amine
TMPD	N,N,N',N'-Tetramethyl-1,4-phenylene diamine
UV	Ultra Violet

Symbol	Definition	Units
A	Area of Electrode	cm^2
a	Radius of Electrode	cm
b	Length of Band Electrode	cm
C_e	Collection Efficiency	-
d	Width of Channel Flow Cell	cm
D_o	Diffusion Coefficient	$cm^2\ s^{-1}$
e	Electron	-
E	Potential	V
E_1	Initial Potential	V
E_2	Final Potential	V
E_p	Peak Current Potential	V
F	Faraday Constant	$C\ mol^{-1}$
h	Channel Flow Cell Half Height	cm
i	Current	A
i_L	Transport Limited Current	A
i_p	Peak Current	A
j	Surface Flux	$mol\ cm^{-2}\ s^{-1}$
j_p	Average Peak Current Density	$A\ cm^{-2}$
k_a	Rate of Anodic Reaction	$cm\ s^{-1}$
k_c	Rate of Cathodic Reaction	$cm\ s^{-1}$
l_e	Channel Flow Cell Inlet Length	cm
η	Over Potential	V
n	Number of Moles	-
r_a	Diffusion Layer Radial Distance at Short Time Scales	cm
r_p	Diffusion Layer Radial Distance at Long Time Scales	cm
Re	Reynolds Number	-
R	Gas Constant	$J\ K^{-1}\ mol^{-1}$
θ	Laplacian Variable	-

T	Temperature	K
t	Time	s
u	Ionic Mobility	$cm\ s^{-1}$
ν	Kinematic Viscosity	-
v	Voltage Scan Rate	$V\ s^{-1}$
v_x	Velocity	$cm\ s^{-1}$
v_o	Central Velocity	$cm\ s^{-1}$
V_{fr}	Volume Flow Rate	$cm^3\ s^{-1}$
ω	Rotation Speed	Hz
w	Electrode Width	cm
x_e	Electrode Length	cm

Contents

Chapter 1

Introduction

1.0. Introduction

The content covered in the course of this Thesis describes the development of novel microelectrochemical reactor (MECR) devices. The potential benefits of miniaturisation hold fundamental technological advances in many industrial processes as well as for academic research. In this Thesis a demonstration of how electrochemical techniques have been developed to probe and act as a tool to sense processes occurring within microreactors is given, and new experimental techniques have been set out to provide a quantitative description of the electrochemical response seen in MECR devices. Before describing in detail the work undertaken, this chapter reviews some of the important fundamental principles underlying the research area and highlights some of the electrochemical techniques already available to investigate electrode processes.

1.1. Reactions at the Solid-Liquid Interface

The pathway of many interfacial reactions at an electrode-liquid interface can be influenced where the electrode voltage, mass transport, electrode topography and the electrical double layer are some of the fundamental factors that can significantly affect the rate of an electrode reaction[1]. In this section, the fundamentals of these processes are described and their effect on electrolysis measurements highlighted.

1.1.1. The Mechanism of Electron Transfer at an Electrode

Equation 1.1 considers a typical electrolysis reaction, where the two main processes occurring are diffusion of material to and from the electrode surface where the reaction occurs and the electron transfer. Figure 1.1 illustrates the two steps occurring.

$$O(aq) + e^{-}(m) \Leftrightarrow R(aq)$$

Equ. 1.1

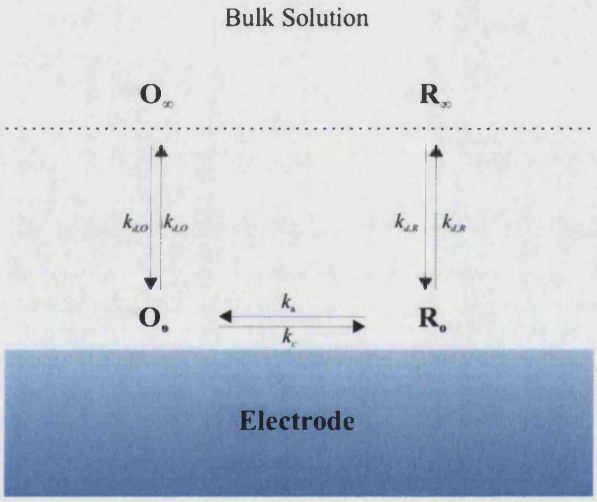

Fig. 1.1. Illustration of an electron transfer reaction.

The current induced by the electron transfer can be predicted using

$$i = nFAj$$

Equ. 1.2

where n is the number of electrons transferred, F the Faraday constant (C mol^{-1}), A the electrode area (cm^2) and j the surface flux (mol cm^{-2} s^{-1}) of the species (O or R) to or

from the electrode. Equation 1.3 can give the surface flux, where $[O]_o$ and $[R]_o$ are the surface concentrations of the species O and R respectively.

$$j = k_c[O]_o \text{ or } k_a[R]_o$$

Equ. 1.3

From Equation 1.2 it can be seen that the current can be limited either by the electrode kinetics (k_a, k_c) or how the concentration close to the electrode surface varies as a function of time. In the coming sections these two factors are discussed.

1.1.2. The Rate of Electron Transfer

For an electrolysis reaction as detailed in Equation 1.1, the Butler-Volmer Equation[2] can be used to describe how the observed current can vary as a function of the overpotential and transfer coefficient.

$$i = i_o\left(\frac{[R]_o}{[R]_{Bulk}}exp\left\{\frac{(1-\alpha)F\eta}{RT}\right\} - \frac{[O]_o}{[O]_{Bulk}}exp\left\{\frac{-\alpha F\eta}{RT}\right\}\right)$$

Equ. 1.4

where the overpotential is η and the exchange current i_o, which is defined as

$$i_o = nFAk_o[R]^{\alpha}_{Bulk}[R]^{(1-\alpha)}_{Bulk}$$

Equ. 1.5

When examining Equation 1.4 it is apparent that two limiting situations are possible, which depend on the value of i_o being large or small. When i_o has a large value

the system is referred to as reversible, as little or no overpotential is required to drive the reaction and both the anodic and cathodic current flow occurs readily. The opposite is observed for a small value of i_o, this is referred to as an irreversible system as a high overpotential is required to induce the current.

1.1.3. Mass Transport

As illustrated in Equation 1.2, the induced current due to electron transfer occurring at an electrode surface can be influenced by $[R]_o$ or $[O]_o$. The factors governing the values of $[R]_o$ or $[O]_o$ are dependent on the mass transport occurring within the bulk solution. These transport processes can occur via diffusion, convection and migration.

1.1.3.1. Diffusion

Diffusion arises from uneven distribution of concentration and acts to equilibrate the concentration gradient to give a uniform concentration within the solution. The rate at which diffusion occurs depends on the concentration gradient at any particular location in solution and is explained by Fick's 2nd law, which predicts diffusion as a function of time.

$$\frac{\partial [O]}{\partial t} = D_o \left(\frac{\partial^2 [O]}{\partial x^2} \right)$$

Equ. 1.6

where the diffusion coefficient of a species O is D_o and x is a one-dimensional Cartesian co-ordinate.

1.1.3.2. Convection

Convection can occur in two forms, natural convection and forced convection. Natural convection, is present in any solution and is caused from thermal gradients and/or density differences within a medium. Natural convection effects are typically seen in stagnant solution measurements, where the electrode has the dimensions in the magnitude of mm, and tends to become significant on time scales of 10 – 20 seconds or longer. Since this form of convection is difficult to predict mathematically it is generally undesirable.

Forced convection, is introduced by the application of an external force such as a gas bubbling through a solution, pumping, or stirring. In some electrochemical measurements forced convection is used and causes any effects due to natural convection to diminish, resulting in well-defined and reproducible experimental measurements. Forced convection measurements generally have well-defined hydrodynamic properties, enabling the establishment of a quantitative description of the solution. Concentration changes due to movement of solution with a velocity v_x can be given by

$$\frac{\partial[O]}{\partial t} = -v_x\left(\frac{\partial[O]}{\partial x}\right)$$

Equ. 1.7

1.1.3.3. Migration

During electrochemical measurements, the potential drop across the electrode-solution results in an external electric field ($d\phi/dx$), which is capable of exerting an electrostatic force on the charged species present in the interfacial region. These migration effects contribute to transport within electrochemical systems, and the

migratory flux (j_m) is proportional to the concentration of the ion, *[O]*, the electric field and the ionic mobility (u).

$$j_m \propto -u[O]\left(\frac{\partial \phi}{\partial x}\right)$$

Equ. 1.8

The ionic charge and its magnitude as well as the solution viscosity have an influence over the ionic mobility. The effects of migration can be eliminated by the addition of a high concentration of supporting electrolyte to the electrochemical cell, which causes a small electrical double layer close to the solution-electrode interface[3].

Having now established the processes that can influence electron transfer at a solution-electrode interface, detailed voltammetric techniques will be introduced.

1.2. Voltammetry

Voltammetry is a well-known electrochemical technique that has been used extensively for the experimental work carried out in this Thesis. This section, provides an introduction to the four most common forms of voltammetry.

1.2.1. Potential Step Voltammetry

In potential step voltammetry the applied voltage is instantaneously stepped between two values, E_1 and E_2 as demonstrated in figure 1.2.

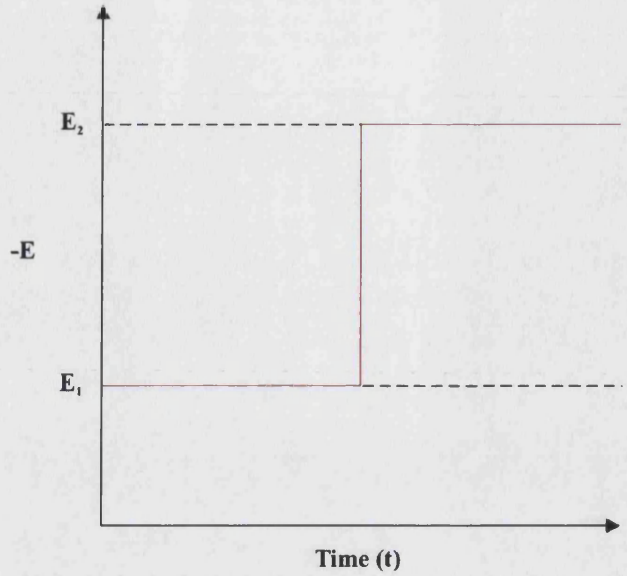

Fig. 1.2. The potential waveform employed in potential step voltammetry.

The resulting current is then measured as a function of time. In the case of a one-electron transfer reaction (Equation 1.1) the potentials would be set so that at E_1 no electrolysis of (O) occurs and at E_2 complete conversion of (O) at the electrode surface takes place. Under these conditions the current response is shown below.

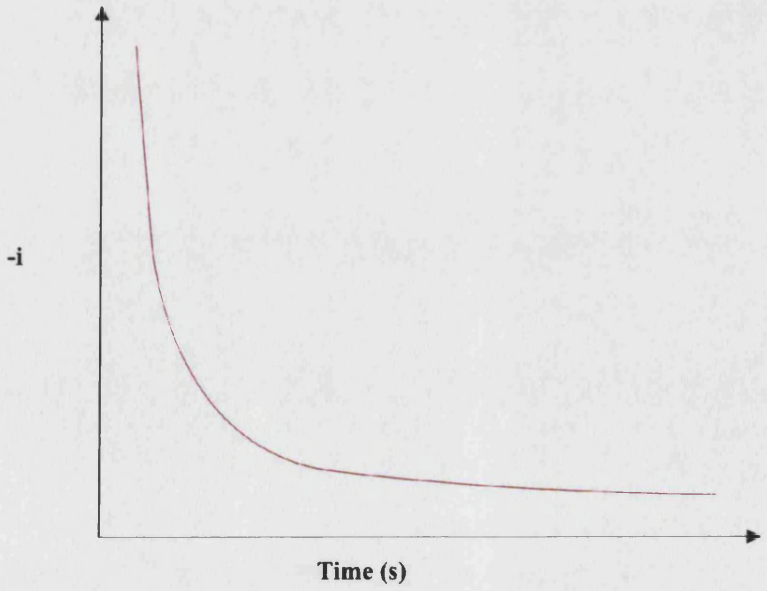

Fig. 1.3. Current response for a potential step experiment.

This response can be explained by the growth in the diffusion layer as a function of time. Mathematically, the Cottrell equation quantifies this behaviour[4].

$$|i| = \frac{nFAD_o^{1/2}[O]_{Bulk}}{\pi^{\frac{1}{2}} t^{\frac{1}{2}}}$$

Equ. 1.9

1.2.2. Linear Sweep Voltammetry

Another type of voltammetry used is linear sweep voltammetry and the potential waveform applied is shown in Figure 1.4.

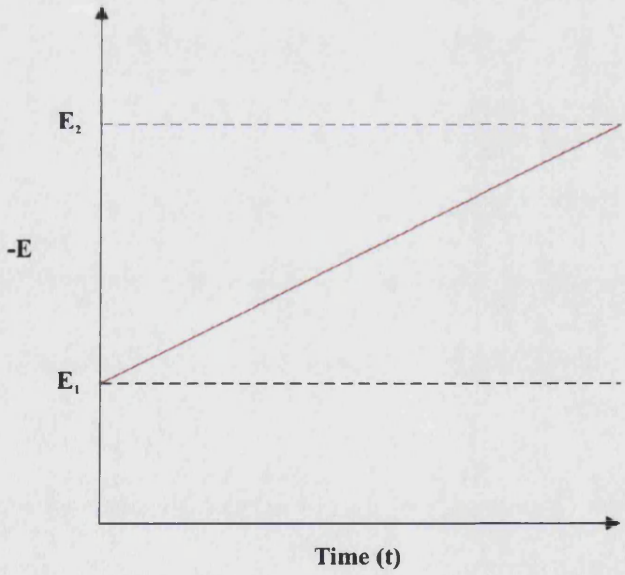

Fig. 1.4. The potential waveform employed in linear sweep voltammetry.

The potential is applied with the voltage changing at a constant rate (v), and a typical voltammogram for a single one-electron transfer reaction can be seen in Figure 1.5.

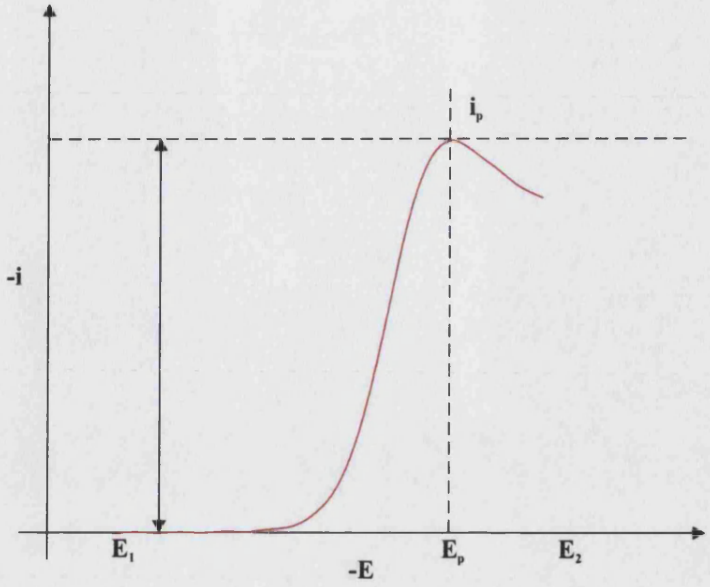

Fig. 1.5. The current voltage response of a one-electron transfer reaction performed in stagnant solution.

1.2.3. Cyclic Voltammetry

Cyclic voltammetry is very similar to linear sweep voltammetry. The potential is swept between two values at a fixed scan rate and once the potential reaches E_2, the scan is reversed and the potential is swept back to E_1.

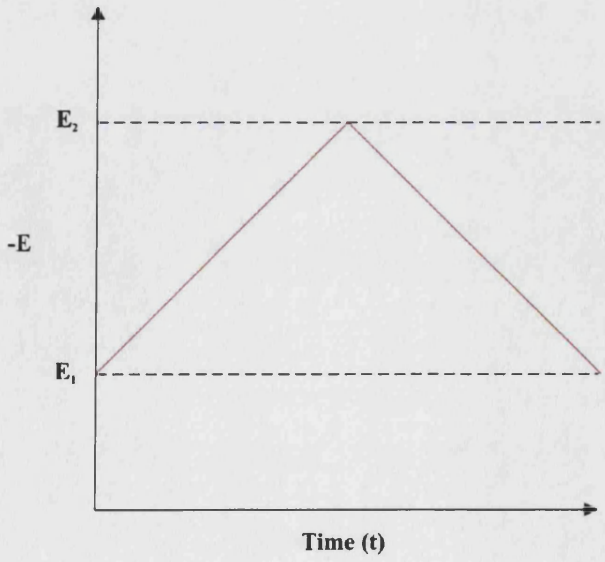

Fig. 1.6. The potential waveform employed in cyclic voltammetry.

A typical voltammogram for a single reversible electron transfer reaction is shown below

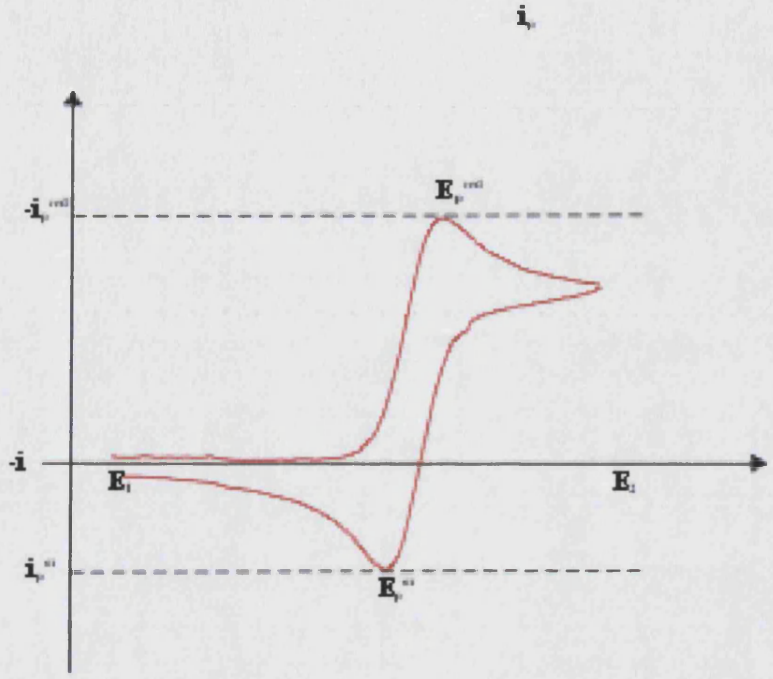

Fig. 1.7. The current voltage response of a reversible one-electron transfer reaction performed in stagnant solution.

Analysis of the voltammogram shows that the voltage separation between the current peaks for a reversible electron transfer is independent of scan rate and can be predicted using:

$$|E_p^{ox} - E_P^{red}| = 2.218\frac{RT}{nF}$$

Equ. 1.10

1.2.4. Steady-State Voltammetry

A further form of voltammetry arises where the current signal reaches a steady value after some time. This form of voltammetry is referred to as steady-state and can be performed using particular microelectrodes or hydrodynamic electrodes. In steady-state measurements the voltage is either fixed or swept at a slow rate so that the system under investigation may reach a steady-state. A typical steady-state voltammogram, which would be expected for a reversible one-electron transfer reaction using a slow potential scan rate, is shown below. The wave is seen to be considerably different to that seen for linear sweep or cyclic voltammograms experiments as discussed above. The maximum current (i_L) is called the transport limited current and arises due to the fact that a constant diffusion layer thickness is established around the electrode.

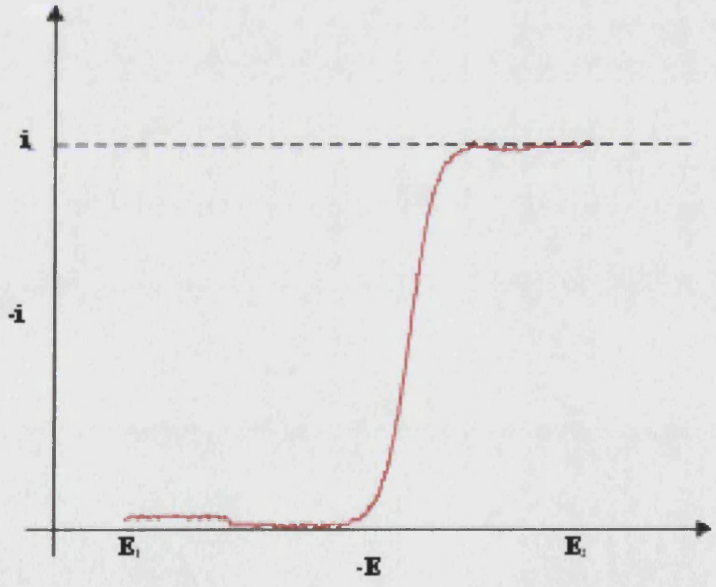

Fig. 1.8. A Steady-State Voltammogram.

In the above sections the basics of voltammetry have been outlined. The use of microelectrode and hydrodynamic electrodes are outlined in the next section.

1.3. Microelectrodes

The unusual properties of microelectrodes have opened new methods of analysing electrode processes that were not possible previously[5]. The differences in mass transport conditions in contrast to macroelectrodes brings about high current densities at the microelectrode surfaces, even though the currents themselves are very small. The concept has enabled the development of many electroanalytical applications that were not possible with conventional electrodes, such as analyses of nonpolar solvent, solids[6], gases[7] and solutions with very low electrolyte concentrations[8]. Other inherent properties of microelectrodes were also appealing, such as the change in experimental time scale at low scan rates due to the size of the electrodes and the insignificant iR effects at very high scan rates enabling the study of very fast homogeneous and heterogeneous electrode processes.

Until the development of microelectrodes in the early 1970s, little attention was given to the influence the size and geometry of the electrode surface had on electrochemical processes, apart from the direct proportionality between size and the measured signal[9,10]. It was not until the mid 1960s when current-time measurements at small stationary disc electrodes showed that the theory of planar diffusional behaviour was not apparent for microelectrodes. This phenomenon was due to edge effects caused by the small surface area, and quasi-spherical diffusion processes[11,12]. In the following years much attention was given to developing a quantitative and qualitative understanding of the processes occurring at a microelectrode[13,14]. The combination of exceptionally high current densities and low measuring currents have aided the development in the fields of analysis, sensors and scanning electrochemical microscopy.

Examples of the use of microelectrodes in steady-state voltammetry to determine rate constants of homogenous processes have since been developed[15-17]. Measurements of the diffusion limited currents as a function of varying microelectrode

sizes, the rate constant of a chemical step in a catalytic EC mechanism, can quickly be determined. Other examples include the study of ECE mechanisms and dimerisation processes, such as that of triphenylamine[18], have been reported.

In later studies, the mechanism of a whole range of industrial electrosynthesis processes have been analysed, and the main advantage of the microelectrode is the absence of iR distortion in current-voltage curves even at high concentration of the reactants. For instance, the steady-state measurements revealed experimental conditions under which hydrodymerisation of acrylonitrile to adiponitrile (Monsanto process) dominates over simple reduction of acrylonitrile to propionitrile[19]. Other examples include the catalytic mechanism to methoxylize furane by indirect anodic oxidation in the presence of bromide and methanol[19] and the reductive hydrodimerisation of formaldehyde to ethyleneglycol[20]. The use of voltammetric techniques using high scan rates have also been reported for investigating the kinetics of fast heterogeneous charge transfer reactions, such as addition[21,22], isomerisation[23] and homolytic cleavage[24].

Other applications can be seen in chemical analysis systems where illustrations of microelectrodes have been reported in trace element analysis and direct sample analysis (for example in fruit). Also, microarray electrodes have found an increasing application in the manufacture of electrochemical chemo- and bio-sensors, as their combination of small dimensions and relatively large sensitive area reduces response times and the signal to noise ratio.

Many types of designs of microelectrodes have been exploited (see Figure 1.9), and the planar microdisc electrode has traditionally been the most popular type of microelectrode in experiments. However, more recently, greater use has been made of microband[25] and microcyliner electrodes[25] as the surface areas could be enlarged by changing the length of the band or the circumference of the ring without changing the specific properties of microelectrodes. Also, the use of micro arrays have been reported to show similar properties[26,27] such as an interdigitated arrangement. In the coming

sections, details into the microdisc and microband electrodes which have been used in the studies detailed in this Thesis are given.

1.3.1. The Microdisc Electrode

Due to the dimension and shape of a microdisc, steady-state voltammetry can be observed for these electrodes. Figure 1.9 illustrate the diffusion layer at short and long time scales. Where the radial length r_a is a secondary variable contributing to the edge effect of diffusion layer at a short time scale. Where as, when the diffusion layer grows to a hemicircle in a long time scale, the radial distance in the polar co-ordinate r_p rather than a cylindrical co-ordinate represents it.

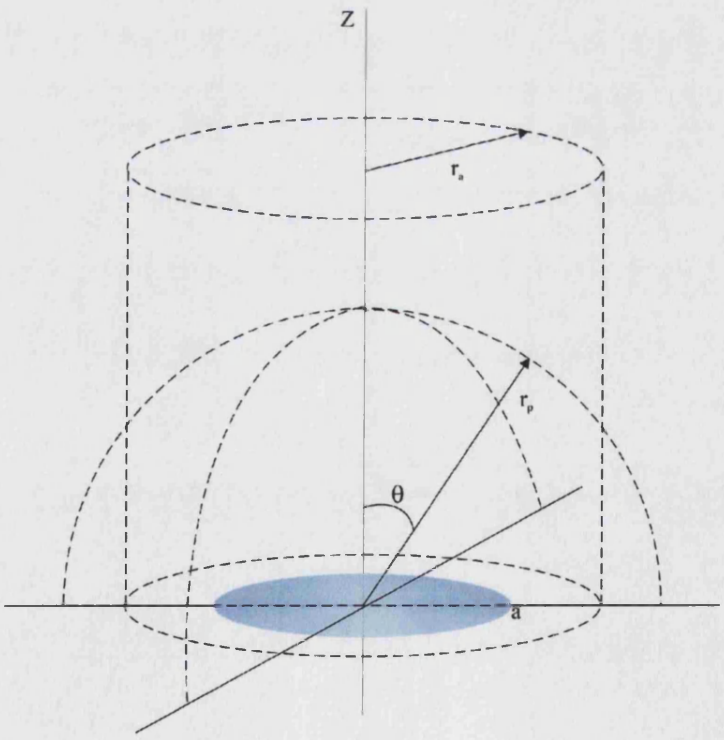

Fig. 1.9. Microdisc Electrode Geometry.

Saito has reported an analytical expression for the diffusion controlled limited current, i, under steady-state conditions, and this is given by the following equation where 'a' is the radius.

$$i = 4nF\, D_o [O]_{Bulk}\, a$$

Equ. 1.11

1.3.2. The Microband Electrode

For a microband electrode the diffusion layer develops from a plane parallel to the electrode surface into a concentric plane centred at the corresponding line electrode. The current density is non-uniform and is essentially infinite at the edge of the electrode for a stagnant system. Where r is the two-dimensional cylindrical distance of the diffusional distance.

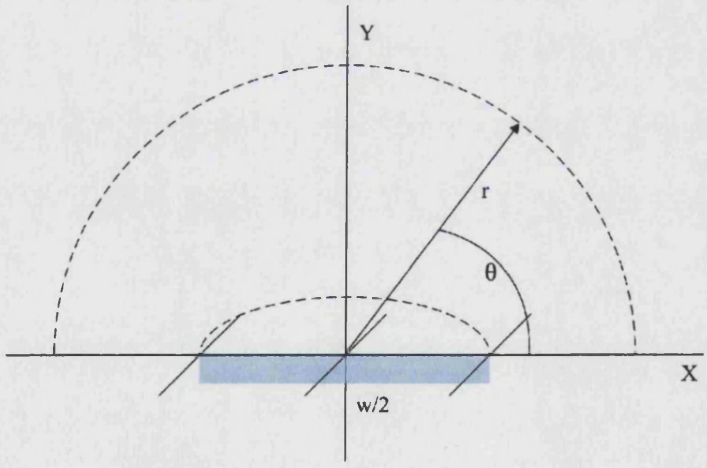

Fig. 1.10. Microband Electrode Geometry.

Analytical expressions for the transient behaviour for microband electrodes have been reported, and at short times is given by:

$$i = nF D_o [O]_{Bulk} b\left\{\frac{1}{\sqrt{\pi\theta}} + 1\right\}$$

Equ. 1.12

where b is the length of the band electrode. Whereas at long times the current response is given by:

$$i = 2\pi nF D_o [O]_{Bulk} b\left\{\frac{1}{ln\theta + 3} + \frac{0.577}{(ln\theta + 3)^2} - \frac{1.312}{(ln\theta + 3)^3}\right\}$$

Equ. 1.13

1.4. Hydrodynamic Electrodes

Hydrodynamic systems involve processes that have a well-defined pattern of material moving to and from an electrode surface. This is governed by forced convection, which when applied to a system dominates the mass transport, eliminates the effects of natural convection and supplements diffusion as the main transport to the electrode surface. As the rate of transport of material to and from the electrode surface is much greater than in a stagnant system, a higher sensitivity can be achieved with this approach. Forced convection can be introduced into a system in many ways. Two such methods are, the electrode may be fixed and electrolyte solution allowed to flow across the surface or the electrode may move (for example by rotation [28]) thus inducing convection in the solution. Many types of hydrodynamic electrodes have been developed in the past, such as the rotating disc electrode, wall-jet electrode and channel electrode[28]. By understanding the mass transfer occurring in these systems an evaluation of kinetic and mechanistic parameters can be achieved, as controlling the rate of convection determines the time material remains close to the electrode.

The ability to characterise electrode reactions with increasingly faster (heterogeneous and homogeneous) kinetics has become an area of interest and challenge in dynamic electrochemistry[29]. With voltammetric measurements, processes such as mass transport may occur in series with other processes such as chemical reactions, adsorption/desorption and heterogeneous electron transfer[3]. Therefore sufficiently high mass transport rates are necessary, compared to the timescales of these other processes, if chemical and/or electron transfer kinetics are to be resolved from voltammetric analysis. For these reasons the necessity of delivering high mass transport rates under well-defined and controllable conditions are of key importance. Many techniques using microelectrodes have been explored in the past to demonstrate well-defined high mass transport rates. Methods of large perturbation, such as cyclic voltammetry and potential step chronoamperometry, have been extended into the sub-microsecond time domain[3,30,31]. A method as mentioned earlier uses the relationship of the steady-state current density and electrode radius to deduce kinetic information, as small electrodes promote fast mass transport rates[32]. Also, an approach utilising the positive feedback mode of the scanning electrochemical microscope (SECM)[33-37] has been reported to show enhanced mass transport properties at a microelectrode by means of diffusional-feedback. Both heterogeneous electron transfer[36] and coupled chemical reactions[37,38] have been studied successfully in this way.

The deployment of microelectrodes in convective systems represents an alternative and attractive approach for achieving enhanced and variable mass transport rates under well-defined steady-state conditions. Microelectrodes that can be fabricated reproducibly and characterised with high precision in well-defined hydrodynamic systems have since been reported. In the coming sections a brief review is given of the some of the main systems that have been well-documented.

1.4.1. Fast-Flow Tubular and Channel Microelectrodes

One of the first techniques of high steady-state mass transport was reported using a turbulent flow tubular microelectrode[39]. The experiment relied on a re-circulating flow system to deliver electrolyte solution to a 100 μm metal ring electrode under turbulent conditions. The approach had proven to provide a study of reasonably fast heterogeneous electron transfer kinetics and the rates of homogeneous reactions coupled to heterogeneous electron transfer[39-41].

Another study of a high-speed channel electrode proved to increase the range of timescales accessible[42]. The arrangement of the cell was similar to that of a conventional channel electrode, except the flow was over a narrow microband electrode occurring at high sheer rates. Studies revealed a linear relationship between the steady-state transport limited current and the cube root of the volume flow rate, which was consistent with that observed for a conventional channel electrode under laminar flow conditions.

A quantitative description of a micro wire electrode sited in the centre of a conventional channel flow cell has also been reported[43]. Computational predictions have been demonstrated to show good agreement to the experimental observations and outline the potential use of such flow cell devices to provide a characterisation of many processes that occur at the electrode-liquid interface.

1.4.2. Micro-Dropping Mercury Electrode

A similar methodology to a dropping mercury electrode has been reported for developing a dropping mercury microelectrode[44]. Using a fine capillary tip, mercury microdrops with final radius of approximately 50 μm were made and shown to be

similar to a conventional dropping mercury electrode. Many studies of aqueous systems have been reported to successfully use this type of electrode.

1.4.3. Microjet Electrode

The concept of the microjet electrode is based on a solution containing electroactive species of interest being fired at high velocity through a fine nozzle (diameter in the range 25 – 100 μm) onto a microdisc electrode (typically 25 μm in radius). The mass transport rates from the microjet electrode configuration proved to be suitable for the investigation of electrochemical kinetics using steady-state voltammetry. Both heterogeneous electron transfer and coupled solution kinetics have been investigated with this approach successfully[45].

In this Thesis the concept outlined in the above sections of microelectrodes and hydrodynamic systems have been taken one stage further, where the technology for microfabrication has been used to integrate microelectrodes within microfluidic devices. In the following sections, analytical expressions are given for two types of hydrodynamic system and an illustration of how their well-defined behaviour can be used in quantitative description. In particular, the channel electrode will be discussed, as the studies detailed in this Thesis have focussed on developing MECRs that are based on the concept of the channel electrode.

1.4.4. The Rotating Disc Electrode

The rotating disc electrode is one of the most widely used hydrodynamic electrodes and consists of a metallic disc electrode embedded within an insulated cylindrical rod. A schematic of the experimental set up can be seen in Figure 1.11.

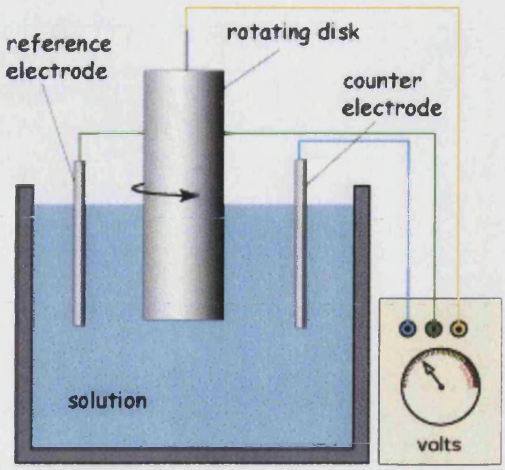

Fig. 1.11. Schematic of experimental set up for a rotating disc electrode.

Rotation of the cylindrical rod at a known speed creates a well-defined vortex around the electrode surface, where the solution adjacent to the electrode is being pulled to the surface, as illustrated in Figure 1.12.

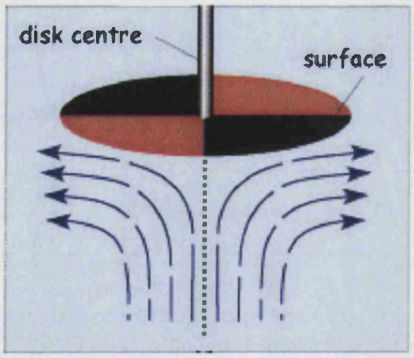

Fig. 1.12. Schematic of the solution flow profile at a rotating disc electrode.

The quantification of the transport limited current at a known rotation speed was first derived by Levich, and is given by

$$i_L = 0.62nFAD_O^{2/3}[O]_{Bulk}\nu^{-1/6}\omega^{1/2}$$

Equ. 1.14

where ν is the kinematic viscosity, ω is the rotation speed in Hz (cylces per seconds). From the equation it is seen that a linear relationship between the transport limited current and the square root of the rotation speed is apparent. Over the years the use of the rotating disc electrode has been exploited to investigate the electrode reaction mechanisms of many homogeneous and heterogeneous chemical processes coupled to electron transfer.

1.4.5. The Channel Electrode

As shown in Figure 1.14, a typical channel electrode consists of a rectangular duct which has an electrode embedded on one wall and electrolyte solution introduced through the channel under laminar flow conditions. Much work has been done on understanding laminar flow and in the early 1960s the contributions from Levich's work[46] on understanding mass transport proved to provide the insight into the development of solid hydrodynamic systems, such as the channel electrode.

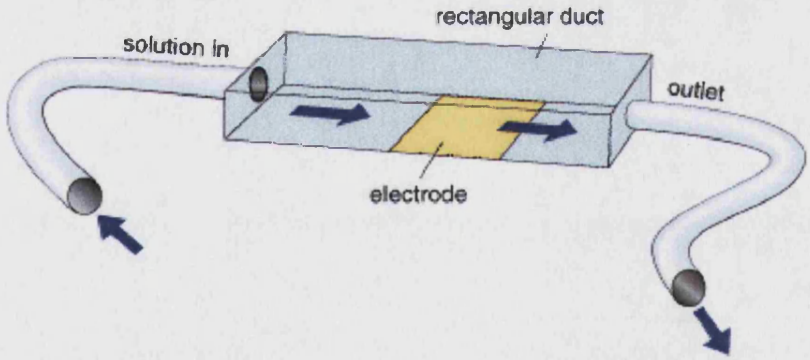

Fig. 1.14. Schematic of a channel electrode.

Laminar flow moves smoothly in layers (laminae) along constant directions (streamlines) as shown in Figure 1.15. Prediction on whether flow within a channel is turbulent or laminar can be determined using the Reynolds number (*Re*) concept. This

dimensionless parameter *Re*, relates to the cell geometry and solution velocity to provide a critical value, above which the flow changes from laminar to turbulent.

$$Re = \frac{(length) \times (velocity)}{(kinematic\ viscosity)}$$

Equ. 1.15

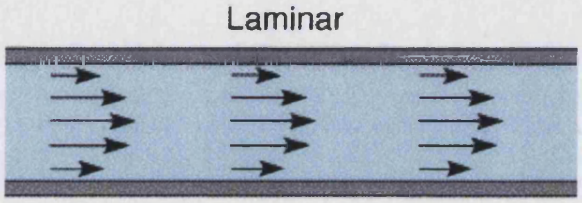

Fig. 1.15. Parabolic flow profile in a channel electrode.

Under laminar flow conditions the velocity profile can be predicted using the following mathematical equation:

$$v_x = v_o\left(1-\left(\frac{h-y}{h}\right)^2\right)$$

Equ. 1.16

where v_x is the velocity in the x direction, v_o is the centre velocity, h is the cell half height, and y is the position normal to the electrode surface. The convection-diffusion equation for the mass transport within the rectangular cavity under steady-state conditions is given by:

$$0 = D_o\frac{\partial^2[O]}{\partial y^2} - v_x\frac{\partial[O]}{\partial x}$$

Equ. 1.17

By solving the convective-diffusion equation for mass transport within the rectangular duct under steady-state conditions, the mass transport limited current (i_L) as a function of solution volume flow rate (V_{fr}) can be defined as:

$$i_L = 0.925nFwD_o^{2/3}[O]_{Bulk}x_e^{2/3}\left(\frac{V_{fr}}{h^2 d}\right)^{1/3}$$

Equ. 1.18

Where x_e is the electrode length, h the cell half-height, d the width of the cell, w the electrode width, D_o the diffusion coefficient of the electroactive material, n the number of electrons being transferred resulting in the current and F the faraday constant. This equation holds that when the flow rate is sufficiently fast, the diffusion layer thickness is much smaller than the depth of the cell.

From the expression it can be predicted that i_L varies with the cube root of the volume flow rate and an increase in the volume flow rate would cause an increase in the transport limited current. The behaviour of the current-voltage curves in the presence of coupled convection and diffusional transport can be explained by the movement of material over the surface of the electrode. Due to the laminar flow profile of solution flow in channel electrodes, the delivery of electroactive material to the electrode surface occurs in a well-defined pattern. An increase in volume flow rate causes an increase in transport of material to the electrode surface, resulting in an increase of turnover of material giving rise to a higher transport limited current. Usually measurements of this kind are carried out at a slow scan rate, approximately 5mV/s, and no peak is observed for the current-voltage curves as the thickness of the diffusion layer over the electrode surface is relatively thin and is established fairly rapidly. It is also interesting to note that the current is maintained at the potential where electrolysis occurs due to the presence of a convective flow supplementing the supply of electroactive material to the

electrode surface. Figure 1.16 shows a set of typical current-voltage curves that could be observed in a channel electrode.

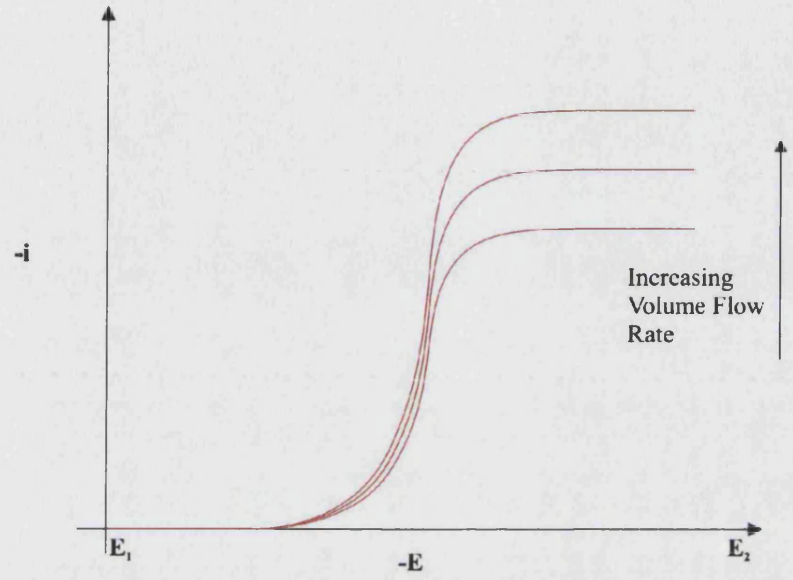

Fig. 1.16. Typical Current-Voltage curves observed for a channel electrode with varying volume flow rates.

In this Thesis the work has been expanded to explore how electrochemical techniques outlined above could be utilised to explore new avenues of innovative science and to develop a new range of micro sensors. In the next section a brief description on microtechnology is given and a review of the work reported in this area is provided.

1.5. Microtechnology

"There is Plenty of Room at the Bottom"

Quoted: R. Feynman, December 29th 1959, Annual Meeting of the American Physical Society.

A famous quotation from Richard Feynman given at the American Physical Society Annual Meeting in 1959, raised concepts of a small world where information could be stored on media with small dimensions and mechanical systems would be on the atomic scale. Whilst the main area of focus that was envisaged by Feynman was nanotechnology, many of his ideas for small machines have been taken into the field of microtechnology. The aim of this section is to provide an insight to some of the concepts within microtechnology and the fields of applications where it has been developed successfully.

Microfluidic devices are miniaturised continuous flow systems or reaction vessels with typical channel or chamber widths in the range of 10 – 500 μm, Figure 1.17 shows an image of a typical microreactor.

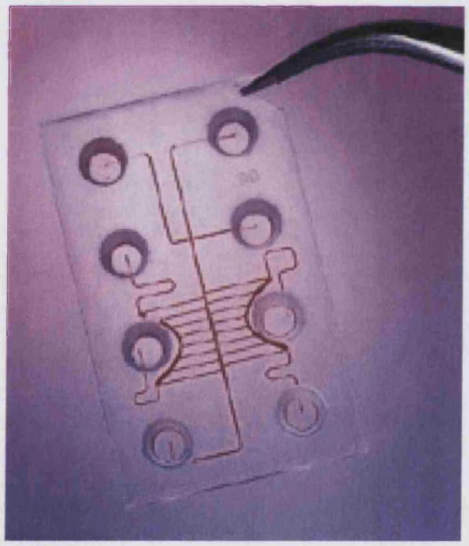

Fig. 1.17. An example of a microreactor

More than 25 years ago the first analytical miniaturised device fabricated from silicon, a gas chromatographic analyzer, was reported[47]. The device was able to separate a simple mixture of compounds in a matter of seconds. Since then much research work has been done on miniaturisation on silicon, and micropumps[48], microvalves and chemical sensors[49,50] have been developed. However, it was not until the early 1990s that a

miniaturised total chemical analysis system was proposed by Manz et al[51]. From this point onwards the concept of analytical chemistry has been brought forward to carry out more precise and efficient analysis using an automotive approach[52]. It was recognised that a small size device presented the advantage of a smaller consumption of chemical reagents. Moreover, the concept of miniaturisation enabled an integration of many techniques within a single device. The capability of sample handling, analysis and detection occurring within one unit over a short time scale began to appeal to many areas of industry.

The following sections provide a review of the most common microfabrication techniques that have been reported until now, as well as applications where microfluidic devices have been used.

1.5.1. Fabrication Techniques

Micromachining technologies have primarily been silicon-based, due to the traditional role of this semiconductor in electronics industry and its excellent mechanical properties[53,54]. However, recent developments into micro fabrication procedures to achieve high precision, has led to the application in the patterning of materials other than silicon. Thus, ceramics, plastics, quartz and glass are gradually becoming accepted complementary materials to silicon, widening the potential range of applications of microfabricated components and systems. In the next few sections, some examples of microfabrication methods that have been used for the manufacture of microfluidic devices in various substrates are presented.

1.5.1.1. Microchannels in Silicon

Many microchannel fabrication techniques have been reported using silicon, with the four most common being wet isotropic, wet anisotropic, dry isotropic and dry anisotropic[54]. Isotropic methods work by etching the silicon wafer equally in all directions, whereas anisotropic methods work by having an etch rate which is significantly faster in one or more directions. Most of the wet etching techniques involve dipping the silicon wafer into a solution of etchant. Depending on the crystal structure of the silicon, the etchant either consists of KOH and tetramethylammonium hydroxide or a solution known as HNA, which contains hydrofluoric acid (HF), nitric acid (HNO_3) and acetic acid.

With dry etching techniques silicon wafers are placed in front of a beam of reactive ions (RIE)[53,54], and left to etch for a certain time. One type of RIE, termed deep reactive ion beam etching (DRIE), has gained much interest in recent years, as it is a very high aspect ratio etching method for silicon, giving aspect ratios up to 30:1 (height:width).

Using photolithographic techniques, as detailed later in Chapter 2 and 3, regions of a silicon wafer can be masked away to leave revealed patterns of the channels that need to be etched out, and using any of the above techniques, the required microchannel can be fabricated. Channels made from silicon are usually sealed with a glass cover plate using field assisted or anodic bonding[53,54]. An illustration of the various processes involved in manufacturing a silicon microchannel can be seen in Figure 1.18.

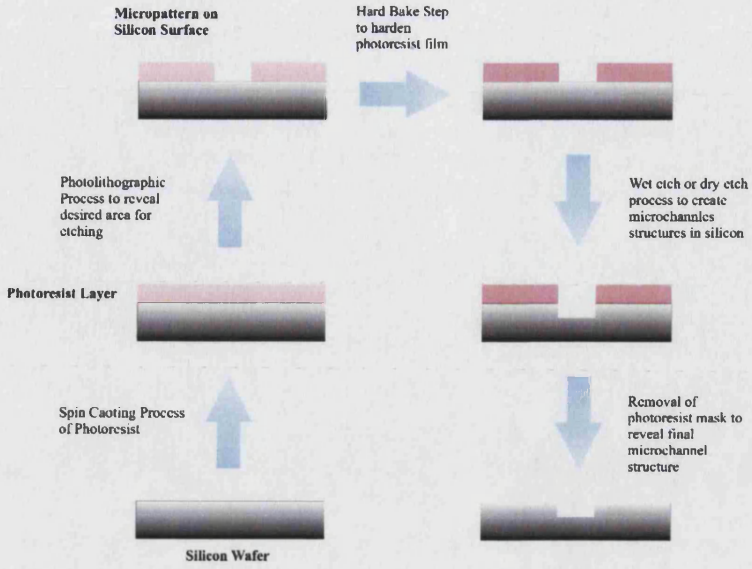

Fig. 1.18. Illustration of the various fabrication steps involved in manufacturing a silicon microchannel

Some of the first microfluidic devices were made using silicon, and much literature has been reported where microfluidic systems were used to develop electrokinetic separation procedures. Studies into free flow electrophoresis of amino acids and proteins[55], and DNA analysis synchronised cyclic capillary electrophoresis[56] and gel electrophoresis[57] have been reported. Pressure driven flow applications have also been shown in silicon microfluidic devices, and applications in liquid and gas chromatography[58], optical detection cells[59], microreactors[60] and miniaturised flow injection analysis systems[61] have been demonstrated.

1.5.1.2. Microchannels in Glass or Quartz

The use of glass as a substrate to fabricate microfluidic devices has become more favourable and common due to its optical transparent properties. Also, devices made from fused silica (quartz) have been considered an attractive material due to being UV-transparent. Photolithographic procedures, which are detailed later on in Chapters 2 and 3, have been combined with either wet or dry etching techniques to fabricate

structures in glass. Etched glass microchannels are usually sealed using thermal bonding techniques or by clamping the cell together. Figure 1.19 illustrates the various stages involved in the fabrication procedure.

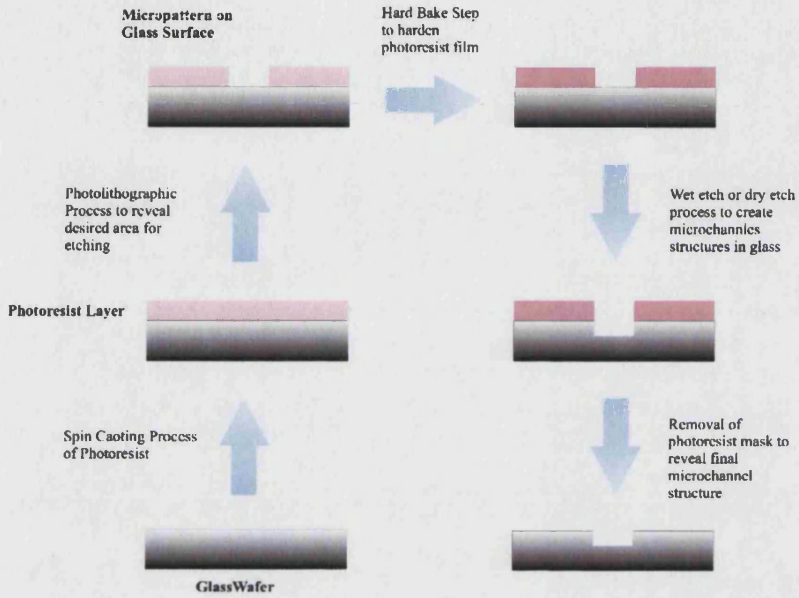

Fig. 1.19. Fabrication stages involved with manufacturing a glass microchannel.

The use of RIE of quartz has also been demonstrated to produce liquid chromatography microfluidic devices[62], and DRIE of pyrex has been reported to give deeper channels[63] for applications in chromatography as well as others that were described for silicon based channels.

Photostructurable glass such as Foturan have also been reported to be used for making microfluidic devices[64]. The inherent photosensitive property of this substrate subsequently results in microcrystallites being formed due to the glass being exposed to UV light. Etching in HF removes these crystalline regions to reveal microchannels of minimum depth 25 μm (see Section 3.1.1.3 and Figure 1.20 for details). Recently a microfluidic device fabricated using Foturan was reported to be used in electrophoresis separation of fluorescently labelled amino acids in channels which were 500 μm in depth and 200 μm in width[65].

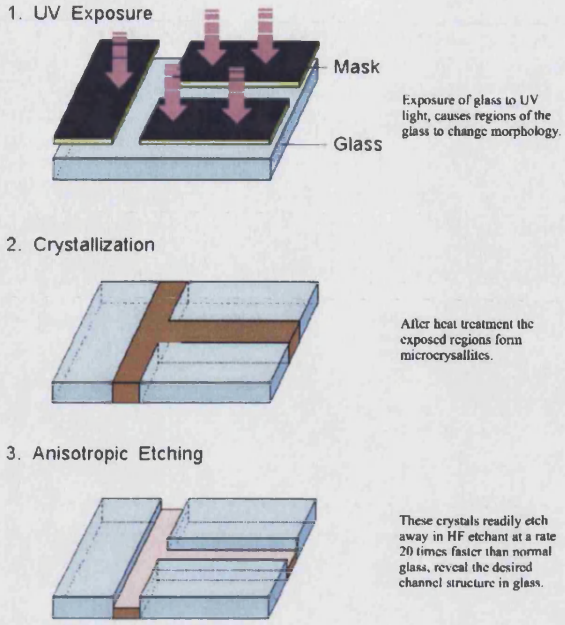

Fig. 1.20. Fabrication stages involved with manufacturing microchannels using Foturan Glass.

1.5.1.3. Microchannels by Replication in Poly(Dimethylsiloxane) (PDMS)

Due to the inexpensive fabrication procedure of working with Poly(dimtheylsiloxane) (PDMS), it is becoming an increasingly popular material to work in. The special properties of this elastomer, and its use in soft lithography to obtain micrometer sized structures, are described in several reviews[66,67]. Fabrication of microchannels involves casting a solution of the PDMS prepolymer onto a master stamp whose surface has been structured to yield a topography or surface relief of some kind. When cured, the PDMS replicates with nm resolution the surfaces with which it has been in contact to reveal the desired channel structure. These microchannels can then be bonded with glass, silicon or PDMS by treating the surface to be bonded using an oxygen plasma[68,69]. Figure 1.21 details the various stages involved.

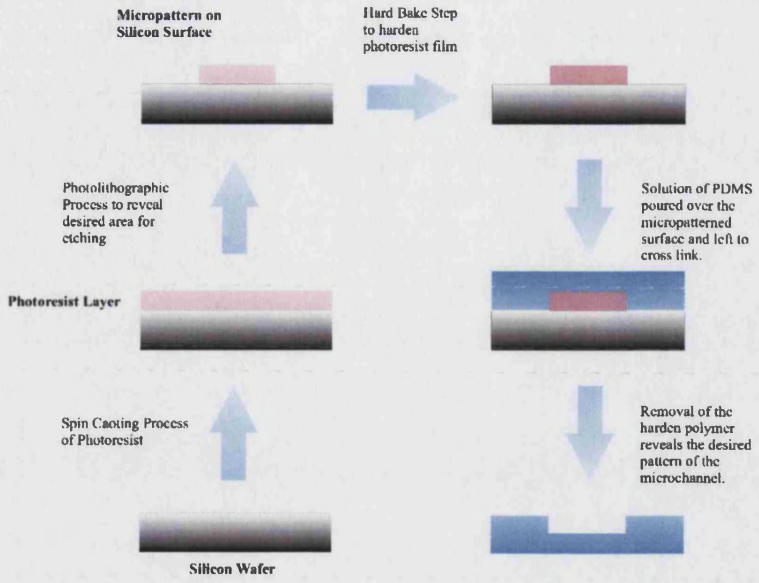

Fig. 1.21. Illustration of microchannel fabrication procedure using PDMS.

The use of microfluidic devices replicated in silicone was reported as early as 1989 by Masuda et al, for biological application involving cell fusions. Several groups have reported more recently three-dimensional structures. In one case many thin patterned PDMS layers were stacked to form three dimensional channel paths[70]. Anderson et al used a similar approach yielding thin layers with through-holes and microstructuring on both sides, which were sealed with thicker PDMS slabs[71].

1.5.1.4. Microchannels by Replication in Other Polymers

Master stamps made in silicon can also be used to imprint or hot emboss channels in hard plastic materials like Poly(methyl methacrylate) (PMMA) at temperatures close to the softening point of the plastic or, alternatively, at elevated pressure[72]. In addition an alternative approach can be used, where the silicon stamp can be used to make a Ni electroplated stamp over itself[73]. Using a positive or negative image of the desired stamp on silicon, an electroplated stamp with both impressions can

be made, and, using the two types of Ni stamps, both imprinting and injection moulding can be used to make plastic channels.

1.5.2. Applications of Microfluidic Devices

Many concepts and applications of microfluidic devices have been developed and shown to provide technological advances in many fields. In the coming sections some of the main areas of research activities where microfluidic devices have been applied will be discussed.

1.5.2.1. Sample Preparation

Many sample preparation procedures require reproducible and well-defined processes, and the use of microfluidic devices to prepare and organise samples with high efficiency has been an area of research that has been given much interest. Examples can be seen in sonication techniques that have been utilised in microsystems to perform lysis of anthrax spores by extracting DNA in order to develop short time scale detection techniques[74].

Another example can be seen in liquid-liquid extraction systems to perform multiple parallel extractions of ten separate organic fluids using a single aqueous feed[75]. Other developments in the area have led to an ion-sensing system, which involves alternating pumping of several organic phases into an aqueous phase, forming a stable aqueous-organic layer in a microchannel where ions can be selectively and sequentially extracted[76]. Further developments in the field led to microextraction systems, and Tokeshi et al described improved cobalt complex extraction systems[77,78] as well as ion pair microextraction of iron in chloroform by putting two parallel laminar flows of different phases in contact. Also the concepts of solid-phase extraction techniques have

been reported using microsystems, and an example was documented by Yu and co-workers where monolithic porous polymers within microchips channels were used to perform on-chip solid-phase extraction[79].

1.5.2.2. Reactors and Mixers

The development of micromixers has been used in many applications where efficient mixing is required for a chemical analysis technique. Many forms of micromixers have been reported using turbulent liquids flow as well as other methodologies such as laminar flow[80] and ultrasonic mixers[81]. Illustrations of the use of micromixers have been shown by Floyd et al, where a laminar flow mixer, heat exchanger and a probing region were used to perform infrared transmission kinetic studies[80].

The development of microsystems for chemical analysis has also been an active area of research, as high efficiency and sensitivity can be achieved. Microfluidic chemical analysis techniques have been used to study processes such as derivitisation of amino acids[82] and protein synthesis[83]. Also the development of enzymatic microreactors for chemical analysis has been reported for glucose detection techniques[84].

The development of immunoassay microreactors has also been illustrated and an example can be seen for the detection of acetylcholinesterase by flow injection analysis and electrophoretic separation. Other examples include a rapid diffusion competitive immunoassay based on the inter-diffusion of two fluid components and further detection down stream has described by Hatch et al, where analysis time of less than 1 min, direct analysis of blood samples and detection in sub-nanomolar range were demonstrated[85].

1.5.2.3. Detection Techniques

Many spectroscopic techniques have been used as a means of performing analysis of processes occurring within microchannels. The use of chemiluminescence and electrochemiluminescence have been demonstrated with microsystems[86], where examples can be found in detection methods of glucose and codeine in enzymatic reactors[84]. Other optical techniques, such as fluorescence, have also been documented[86] and an approach has been presented where an array of micro-lenses was used to perform on-chip fluorescence detection[87]. Other examples include the use of multi-channel laser induced fluorescence detection to quantitatively detect clinical substances[86].

Non-fluorescence optical measurements in microsystems have also been illustrated, and a detection technique based on holographic refractive index was used to follow the separation of carbohydrates, demonstrating the potential of this approach as a universal detection system for microfluidic systems[88]. The use of an online detection technique based on Raman spectroscopy has been shown, and the time-resolved resonance Raman spectroscopic technique used in a microfluidic device was used to elucidate the structure of a chromophore and changes in protein-chromophore interactions[89].

Different microfabricated devices for coupling capillary electrophoresis to an electrospray mass spectrometer have been reported by many groups to analyse proteolytic digests as well as pepetides[90]. Another example has been described where two mass spectrometer analyzers were connected separately to microfluidic devices through nanoelectrospray emitters to perform trace analysis of membrane proteins and carnites in human urine[91].

Other techniques based on single molecule detection have also been demonstrated where analysis was performed by focussing a laser beam in an area of a few micrometers and counting the fluorescent burst from each molecule. Detection

limits in the picomolar range were obtained[92]. Also, utilising a fluorescence burst counting technique, single DNA molecules were detected. A single non-fluorescent molecule detection method based on thermal lens effect was successfully demonstrated as well, and using the technique, Sato et al reported detection in the subzeptomolar range in glass devices[93].

1.6. Integration of Electrochemical Function in Microfluidic Devices

One of the unique possibilities offered by microfabrication technology is the direct integration of elements not having a fluidic function. The ability to deposit and structure thin metals or other conductive films on substrates or channel surfaces is being exploited in microfluidics for interrogating electrochemical detection techniques. Amperometric, potentiometric and conductometric techniques are subject of an increasing interest, looking at its integration into microfluidic devices[94,95]. This is mainly because of the detection limits, since output signals for electrochemical measurements depend on the electrode area, whereas for optical techniques, such as absorbance or fluorescence, depend on the amount of detectable volume available[96]. As a result, limits of detection to do not diminish as rapidly for electrochemical methods as they would for optical techniques[97]. The use of micromachining technologies to integrate electrochemical sensing elements into microfluidic devices brings unique advantages not possible in conventional systems. For instance, devices incorporating detection electrodes do not require a large amount of peripheral equipment for acquisition of detector signal. This makes the development of portable instrumentation based on microfluidic devices with ECD a realistic possibility.

Numerous approaches have been used for interrogation of electrodes into microsystems. In the simplest case grooves or channels, whose purpose was to hold metal or carbon electrodes in place, are formed in one of the surfaces. Many moulding

techniques with PDMS[98] and hot embossing techniques with PMMA have been reported[99]. Alternatively, electrode channels were formed in PDMS and filled with carbon paste, or laser ablated in polyethylene terephthalate (PET) and filled with carbon ink.

More sophisticated techniques involve deposition and patterning of metal layers using photolithographic techniques (detailed in Chapter 2). Such techniques have been used as well, and devices made from PDMS[100] and PMMA[101] have been reported to show the ability to perform electrochemical detection. However, recent advances in quantifying the electrochemical signal of microelectrodes fabricated using thin metal later deposition techniques have been reported. Studies of the behaviour of partially blocked electrodes[102,103] and micro mesh electrodes[104] fabricated from thin films of Ti/Au have illustrated good quantitative agreement with computational simulations. In this Thesis the concepts developed on microchannel fabrication and electrochemical characterisation of thin metal films have been utilised in developing a novel range of MECR devices[105-107].

1.7. Thesis Structure

The remainder of this Thesis has the following format: Chapter 2 outlines the experimental procedures used. Chapter 3 describes the development of several new methodologies for fabricating Microelectrochemical Reactors. In particular the use of a range of new materials and techniques are described. Chapter 4 details the development of a new flow visualisation technique, which utilises a voltammetric approach. Experimental results of flow images recorded for macroscopic flow cells as well as microchannels are illustrated. Chapter 5 introduces the concept of Microelectrochemical Reactors and provides details into the electrochemical characterisation of these devices using finite element modelling techniques. An outline of potential applications of these

devices is also provided. Chapter 6 expands from the knowledge and results achieved in Chapter 5 to introduce another novel range of Microelectrochemical Reactor for studying the elusive behaviour of liquid-liquid interfaces. The development and characterisation of a new range of microsystems for two and three phase flow are detailed, and an electrochemical methodology is provided to interoperate the mass transport properties occurring within the individual liquid phases.

Chapter 2

Experimental Procedures

2.0. Introduction

The techniques described in this chapter concern established fabrication and experimental procedures that were adapted to develop a novel range of Microelectrochemical Reactor (MECR) devices. An account into the photolithographic techniques that were used to engineer micro patterns and structures on a range of substrates will be given. Information into the methodology used for characterising these devices using an electrochemical approach will also be presented.

2.1. Photolithographic Procedure

A photolithographic technique, based on a projection-printing system, was used to produce photoresist patterns on substrates such as glass and silicone [108-111]. In this section, a description of the various steps involved in fabricating the desired photoresist pattern will be given.

2.1.1. Photo Mask Fabrication

The process involved using a technical drawing software package to create a scaled black and white artwork, which was enlarged by a factor of ten. The enlarged artwork was printed on acetates using a high-resolution laser printer (Cannon PS-NX 60). The images on the acetates were projected using a projection screen, which had a

camera mounted above it at a known height. After calibrating the height to give an image reduction of a factor of ten, an image was taken of the projected artwork onto a high-resolution millimask negative plate (Agfa). The projection time required varied depending on the dimensions that were photographed, but the typical range of exposure was found to be between 10 – 15 seconds. Figure 2.1 shows the setup of the projection screen and imaging equipment used.

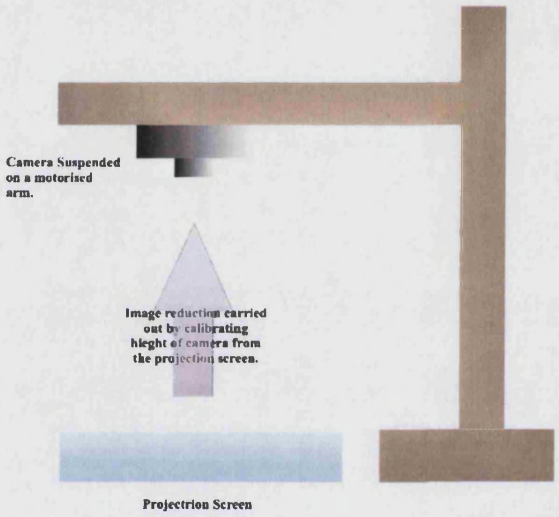

Fig. 2.1. Schematic for producing photo masks.

The exposed negative plates were developed using a solution of millimask G282c developer (Agfa), to give an opposite image of the artwork. This type of photo mask was used to make patterns as small as 10 μm and an image of a typical mask can be seen in Figure 2.2.

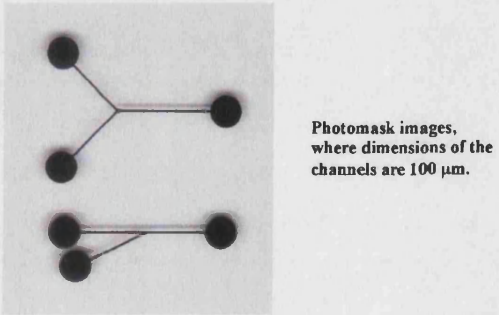

Fig. 2.2. Image of a typical photo mask.

2.1.2. Micro-patterning Photoresist

Thin films of photoresist were coated onto substrates using a spin-coater. The thickness of the film was determined by the viscosity of the photoresist and the relative speed set on the spin-coater. After coating the substrates with photoresist, films were pre-baked in a fan-assisted oven or hot plate in order to dry and harden the layer of photoresist on the surface of the substrate.

The photo masks produced from the image reduction procedure, as detailed in the previous section, were used to project an ultraviolet (UV) light source (340 nm) from a mask aligner (Karl Suss, model MJB 3) onto the substrates coated with the film of photoresist (see Figure 2.3). The exposure time to UV light varied depending on the dimensions of the artwork being transferred, as well as the intensity of the UV source. For the mask aligner used in the studies an exposure of 30 - 60 seconds was found to give the correct dosage of UV light.

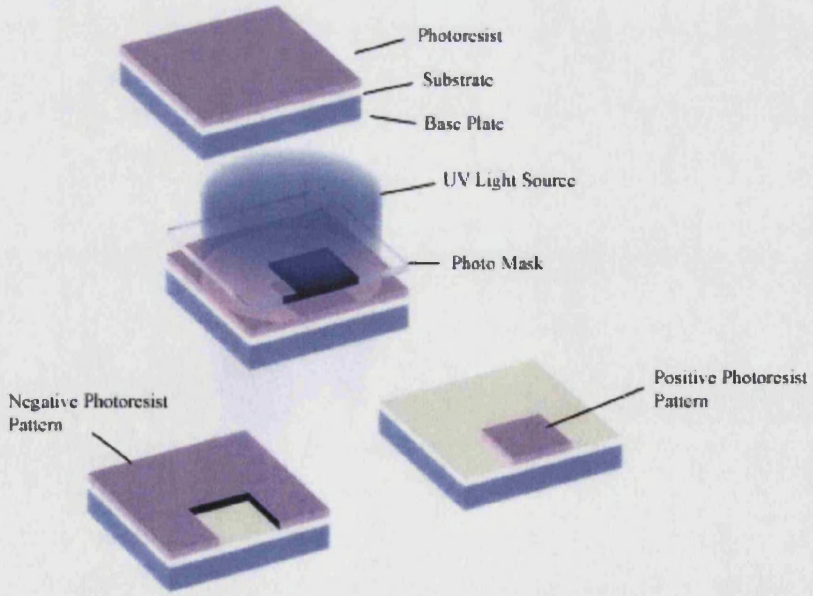

Fig. 2.3. UV exposure process.

The exposed films of photoresist were developed using a developer solution to reveal the desired photoresist micro-pattern. The development time was varied depending on the dimensions of the artwork again, but a typical length of time involved a development of approximately 1 minute or more. After the developing process, the substrates were washed with Milli-Q water thoroughly before being blow dried in a clean supply of nitrogen and post-baked in an oven or hot plate. Figure 2.4 illustrates the steps involved in fabricating the photoresist patterns.

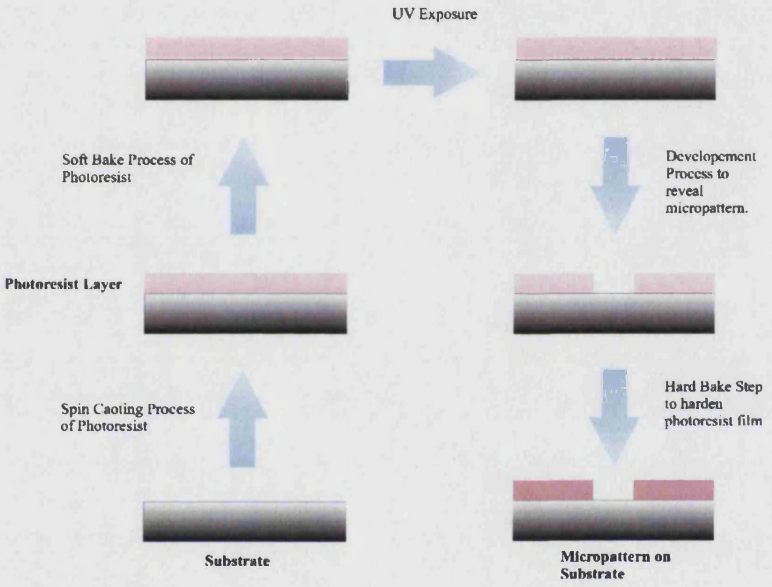

Fig. 2.4. Outline of Photoresist micro-patterning procedure.

Two different types of photoresist were used depending on the application of the fabricated artwork:

- Microposit S1828, supplied by Shipley.
- SU8 2000, supplied by MicroChem.

Detailed below are the specifications for the procedure used with the two types of photoresist.

Microposit S1828 involved a positive working process, where the image of the photo mask was directly transferred onto the photoresist film. The process involved exposing regions of the photoresist to UV light that dissolved away in a developer solution (AZ351, Shipley) to imprint the desired artwork onto a substrate. Table 1 and 2 detail the conditions used with this type of photoresist with the steps outlined in Figure 2.4.

Spin-Coater Speed (rpm)	Coating Time (s)	Film Thickness (μm)
4000	45	5

Table 1. Spin coating specification for Microposit S1828.

Pre-Exposure Bake (°C) (Using Hot Plate)	Bake Time (min)	UV Exposure (mJ/cm^2)	Post-Exposure Bake (°C) (Using Hot Plate)	Bake Time (min)
115	1	150 - 250	115	1

Table 2. Baking and exposure conditions for Microposit S1828.

The SU8 2000 had properties opposite to that of Microposit S1828, where the images produced were a result of unexposed regions of the photoresist developing away in a solution of SU8 Developer. This is known as a negative working process, and the SU8 structures produced on substrates were permanent and chemical resistant. This photoresist was used to produce micro structures that were required to remain as a permanent feature. The process required for this photoresist was slightly different to that explained above for Microposit S1828.

Various film thicknesses were fabricated by controlling the spin-coater speed and the range is detailed in Table 3. These films were then put through a two step post-exposure baking process on a hot plate first at 65°C and then at 95°C. Details of which are given in Table 4. The baked films were then exposed to UV light as outlined in Table 5 and were then further baked at 65°C and 95°C for a time interval depending on the thickness of the films, as shown in Table 6. After allowing the substrates to cool down they were then developed in a solution of SU8 Developer as described in Table 7, followed by rinsing in Milli-Q water and isopropanol before blow drying with a clean supply of nitrogen.

Spin- Coater Speed (rpm)	Coating Time (s)	Film Thickness (μm)
1000	30	75
2000	30	40
3000	30	25

Table 3. Spin coating specification for SU8.

Film Thickness (μm)	Pre-Exposure Bake at 65°C (min)	Pre-Exposure Bake at 95°C (min)
75	3	9
40	2	5
25	1	3

Table 4. Two step pre-exposure bake on a hot plate required for the different SU8 film thicknesses.

Film Thickness (μm)	UV Exposure (mJ/cm^2)
75	500 - 600
40	250 - 350
25	220 - 240

Table 5. UV Exposures required for different SU8 film thicknesses.

Film Thickness (μm)	Post-Exposure Bake at 65°C (min)	Post-Exposure Bake at 95°C (min)
75	1	7
40	1	3
25	1	3

Table 6. Post-Exposure bake on hot plates required for different SU8 film thicknesses.

Film Thickness (μm)	Development Time (min)
75	7
40	5
25	4

Table 7. Development time required with the different SU8 film thicknesses.

2.2. Microelectrode Fabrication

Glass microscope slides were adopted as a substrate, on which gold or platinum metal films where fabricated to act as electrodes. The photolithographic procedures as outlined in Section 2.1 were used to create a pattern of Microposit S1828 on the surface of the glass wafers. The patterned wafers were then put through a metal coating cycle using either an Argar Sputterer to produce a film of platinum, or an Emitech K975 metal

evaporator to give a titanium/gold film. The coated wafers were then immersed in acetone to lift off the photoresist to reveal the pattern of metal film. Figure 2.5 illustrates the steps involved.

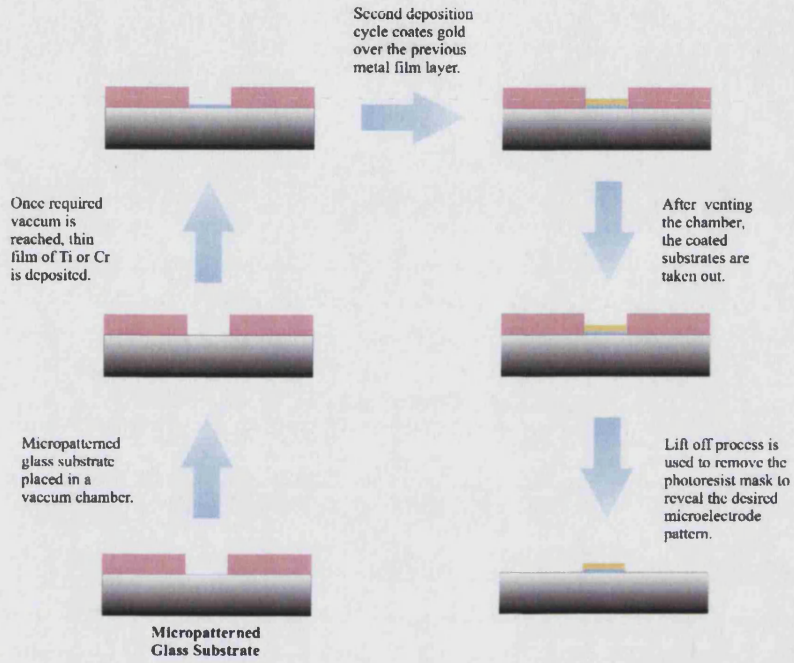

Fig. 2.5. Microelectrode metal deposition process.

Typical film thicknesses of the platinum electrodes were in the order of approximately 300 nm and were produced by sputtering for five minutes. However due to better adhesion properties of the titanium/gold films using the metal evaporator, most of the experimental work was carried out using electrodes fabricated with an evaporator.

The evaporation process involved a two-step coating cycle of the patterned glass. The chamber was pumped down to a vacuum of $1x10^{-6}$ mbar before beginning the coating process. A thin film of titanium approximately 20 nm thick was coated over the photoresist patterned glass, followed by a film of gold approximately 150 nm thick. The titanium was used to act as an adhesion layer between the glass and the gold film. Once the films had been deposited on the surface and the vacuum chamber vented, the

photoresist masks were removed using acetone to reveal the desired gold electrode pattern.

Prior to the metal coating process, the glass slides were cleaned with an acid wash of hydrogen peroxide (Aldrich) and sulphuric acid (Aldrich) solution (H_2SO_4 : $3H_2O_2$), (known as Piranha solution[112]), to remove any traces of grease and organic residue. After the acid wash the glass slides were rinsed a number of times with Milli-Q water, before being sonicated in absolute ethanol (Fisher) and dried in a clean nitrogen supply. This was found to improve the quality and adhesion of the metal films fabricated.

2.3. Microchannel Fabrication

Fabricated channel structures on substrate surfaces were used to construct a sealed microchannel unit. The process involved using a microelectrode plate, fabricated using the procedure outlined in Section 2.2, to act as a cover plate. The channel, which could be fabricated using a range of techniques, was aligned and sealed over the electrode patterned cover plate. Details of the various methods used to fabricate well-defined microchannels will be presented in Chapter 3, where a range of photolithographic as well as other techniques, were used. Figure 2.6 illustrates a schematic of the approach used to construct a channel unit.

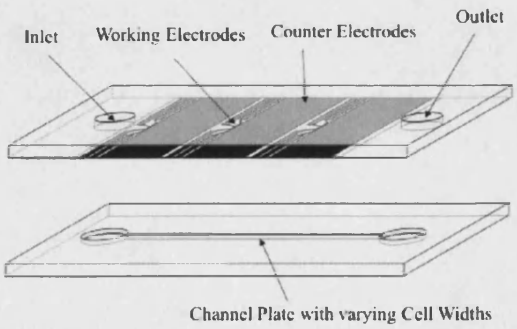

Fig. 2.6. Construction of a channel unit.

The process of sealing together the channel and cover plates was either carried out using a low melting point wax, or by clamping the plates using a rig built in-house. With both approaches an inlet and outlet region was created in the channel by drilling holes in the glass cover plates using a PCB drill (Radio Spares) and dental drill bit (Skillbond).

2.4. Flow Systems

In later chapters an account is given of the various cell geometries used for the research work. In this section a description of two methods that were used to give well-defined and reproducible fluid flow within microchannels will be presented.

2.4.1. Gravity Fed Flow System

A flow arrangement as detailed in Figure 2.7 was used to transport liquids through channels under the influence of gravity. The setup was placed within a fume cupboard as many of the solvents used were volatile.

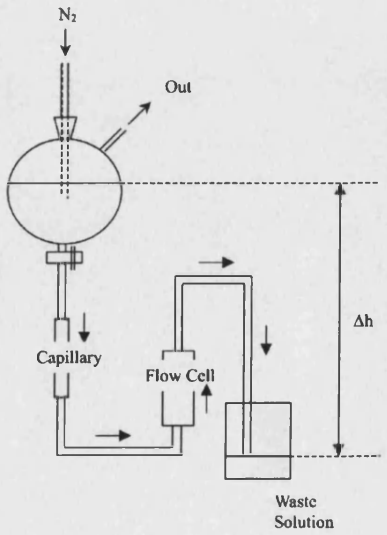

Fig. 2.7. The gravity fed flow system.

The volume flow rate through the channels was controlled by the difference in height (Δh) between the reservoir and the collection vessel. In all the experiments the volume flow rates for a range of values of Δh were calculated by measuring the total volume collected over a certain time. The use of capillaries were also explored to achieve control over volume flow rates, and capillaries ranging in different internal diameter sizes were cited as part of the flow regime in some measurements (as illustrated in Figure 2.7).

A similar setup as shown in Figure 2.7 was used to study the flow of two or three immiscible liquids, and Figure 2.8 shows the flow system used for the two phase flow measurements. The setup employs a series of reservoirs, depending on the number of liquid phases required for the analysis, and connections for cell inlets. Similar strategies were used to control and measure the volume flow rates of all the liquids involved in the analysis.

Before any electrochemical measurement all liquids were purged by degassing with nitrogen to remove any traces of oxygen.

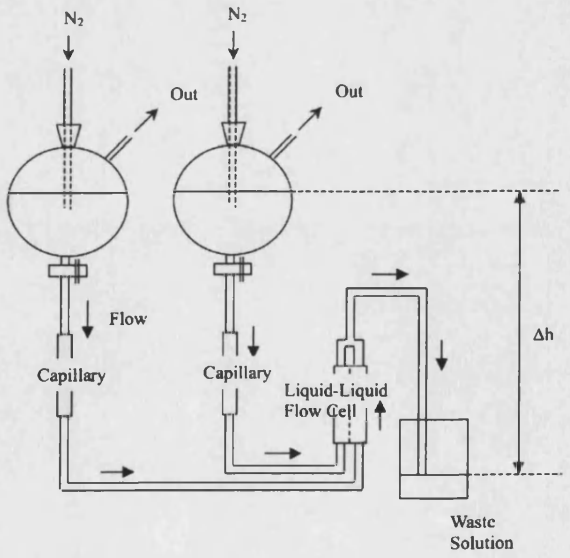

Fig. 2.8. The flow system employed for multi immiscible liquids.

2.4.2. Syringe Pumps

A Harvard Programmable PHD 2000 syringe pump was used, Figure 2.9 shows the setup employed. The pump was interfaced with a computer and programmed to apply a range of volume flow rates from µl to ml per second.

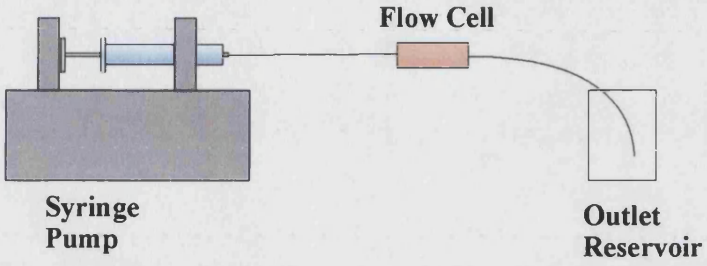

Fig. 2.9. The flow system setup using syringe pumps.

The setup was also used to interrogate multiphase flow, and additional adaptors were mounted on the pump in order to connect two or more syringes. With this setup all syringes were pushed with the same force. Figure 2.10 details the setup used.

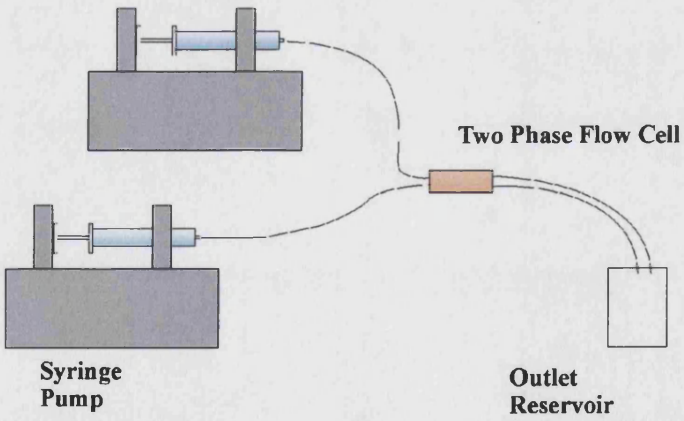

(a).

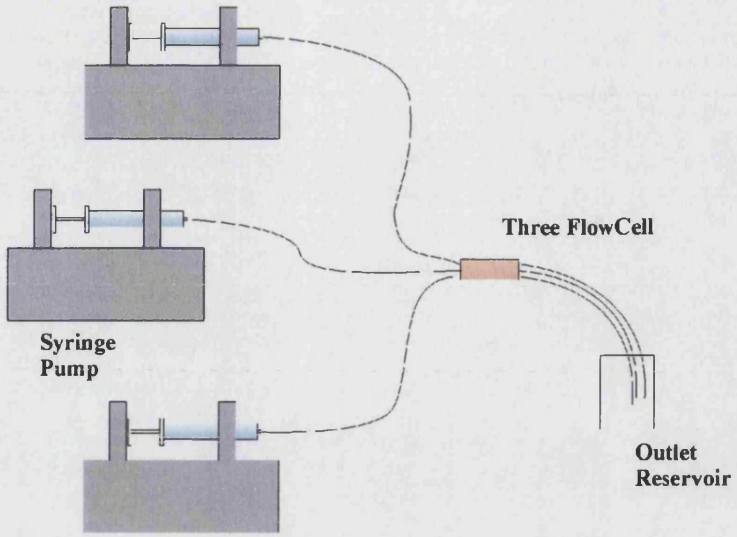

(b).

Fig. 2.10. Flow system setup using a syringe pump for multiphase flow. **(a).** Two Phase Flow, **(b).** Three Phase Flow.

2.5. Chemical Reagents

Detailed in the table below are all the chemicals used along with the supplier and grade.

Chemicals	Producer	Grade
Acetone	Aldrich	HPLC
Acetonitrile	Aldrich	HPLC
Alumina	LECO	-
AZ 351 Developer	Shipley	Clean Room Quality
1,2-Dicholoroethane	Aldrich	HPLC
Ethanol	Fisher	Absolute
Ferrocene	Aldrich	98%
Gold	Advent Materials	99.99%
Hexaaminеruthenium(III)chloride	Aldrich	98%

Hydrofluoric Acid	BDH	42%
Hydrogen Peroxide	Aldrich	35 wt. %
Isopropanol	Aldrich	99.9%
Microposit S1828	Shipley	Clean Room Quality
Millimask G282c Developer	Agfa	Clean Room Quality
Nitric Acid	Aldrich	90%
Octanol	Aldrich	99.9%
Poly(dimethylsiloxane)	Dow Corning	-
Platinum	Advent Materials	99.99%
Potassium Chloride	Aldrich	99.999%
Potassium Ferricyanide	Aldrich	99%
Potassium Ferrocyanide	Aldrich	99%
Potassium Hydroxide	Aldrich	99.99%
SU8 2000	MicroChem	Clean Room Quality
Sulphuric Acid	BDH	95%
Surlyn	DuPont	-
Titanium	Advent Materials	99.99%
Tetrabutylammonium perchlorate	Fluka	99.9%
Tris(4-bromophenyl)amine	Aldrich	98%
N,N,N',N'-Tetramethyl-1,4-phenylene diamine	Aldrich	98%

Chapter 3

Microfluidics: Introduction into the fabrication techniques.

3.0. Introduction

"Devices for handling nanolitre quantities of fluids are creating new fabrication challenges and finding new applications in biology, chemistry, and materials science."

Quoted: G.M. Whitesides, A.D. Stroock, Physics Today, 2001.

The above is a statement summarising the motivations for researching microfluidics by scientists from many disciplines. The number of processes for screening materials in fluidic environments has increased substantially, and applications such as the analysis of DNA or drugs, screening of patients, and combinatorial syntheses are becoming more demanding[113]. The need to manipulate fluids on a micro scale has become a necessity in order to keep up with the growing requirements of industry. Over the past two decades extensive research has been reported where the use of many methodologies have been exploited to fabricate microfluidic devices. However, interrogating systems on a micro volume scale can bring about many practical hurdles in analysing fluids, and an elegant approach to this problem can be found with the use of electrochemical techniques.

In the early 1990s, the first microfluidic devices reported were fabricated in silicon and glass by photolithography and etching techniques that were adapted from the microelectronics industry[114,115]. Since then, much work has been published using these techniques in which designs of sensors for certain applications have been explored[86]. More recently, polymers have also been investigated as a substrate material for

microfabrication and extensive work has been done on developing soft lithographic techniques[116].

In this chapter a brief summary on the techniques that have been reported in the past will be discussed and a description on how these techniques were used to develop a novel range of MECRs will be presented.

3.1. Development of the Microelectrochemical Reactor

The approach of the channel electrode technique and its application to study many fundamental concepts was outlined earlier in Chapter 1. In this chapter, the development of the channel electrode to probe and investigate phenomena in a microfluidic environment is outlined. A novel class of Microelectrochemical Reactors, consisting of a rectangular duct channel unit with microns dimensions and microelectrodes situated on one wall of the channel, is presented. Figure 3.1 illustrates a schematic of a MECR.

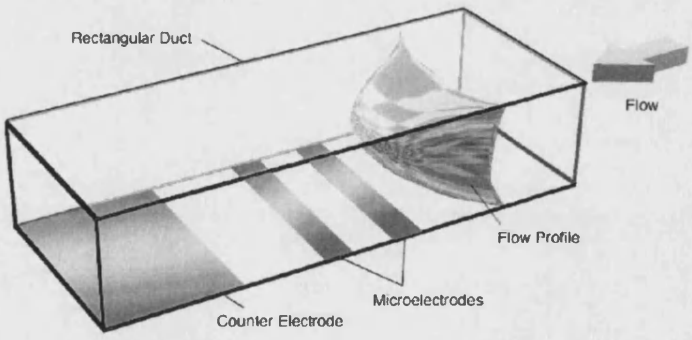

Fig. 3.1. Schematic of a Microelectrochemical Reactor.

Definitive characteristics of microchannels needed to be identified, for example the fabrication procedure had to develop well-defined structures and the substrate had to be flexible in its application as well as having chemical inertness. In the following sections a detailed description will be provided about the various methodologies used for

fabricating microchannel structures on a range of substrates. A discussion into the merits of each approach will also be presented.

3.1.1. Glass-Based Microchannels

In the past, glass has been widely used as a material to machine out microchannels[117-119], this process has proved extremely successful in developing analytical tools, such as the channel electrode[120] and applied to a range of applications, such as spectroelectrochemistry. The chemical inertness of glass provides it with the flexibility to be used in a variety of chemical systems and thus proved to be a favourable substrate to fabricate MECR devices.

In this section the different methods that were used to construct glass based microchannels will be illustrated. A description of the approach used to place microelectrodes within the channel unit is also provided.

3.1.1.1. Thin Glass Channel Electrodes

As a first approach, a practical method based on constructing a channel using glass slides was developed. Using this technique it was possible to fabricate channels down to the dimensions of 100 μm in width, 100 μm in height and a length of up to 7 cm. Figure 3.2 shows a schematic to illustrate the procedure used.

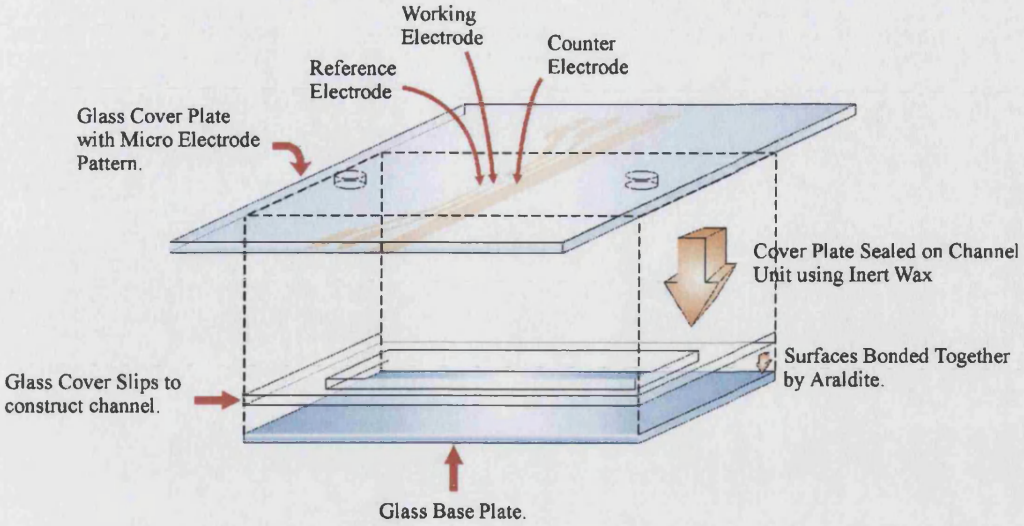

Fig. 3.2. Schematic for a channel cell built using glass slides.

The device, as shown in Figure 3.2, consisted of a channel unit and a cover plate with microelectrodes and contact pads. The two sections were sealed together with an inert low-melting point wax[121].

The channel unit was made of a glass microscope slide (Fisher) with the cavity created by building thin glass cover slips (Fisher) around the sides. All the cover slips were cemented to the microscope slide using araldite (BDH). The desired height of the channel was obtained by using a range of glass cover slip thicknesses, and the width by placing a separator of known width between the cover slips before cementing them in place. A typical range of channels fabricated with this approach had a height of between 100 – 300 μm and width of between 100 μm – 10 mm. Holes of 1mm in diameter were drilled in the cover plate using a PCB drill (Radio Spares) and dental drill bits (Skillbond), in order to provide inlet and outlet openings in the channel. Glass pipette ends (BDH) used as inlet/outlet tubes, which had a diameter of approximately 1mm, were fed into the holes and cemented to the glass surface using araldite. Figure 3.3 shows an image of a typical fabricated MECR, where the dimensions of the channel were: width 1mm, height 100 μm and length 7 cm.

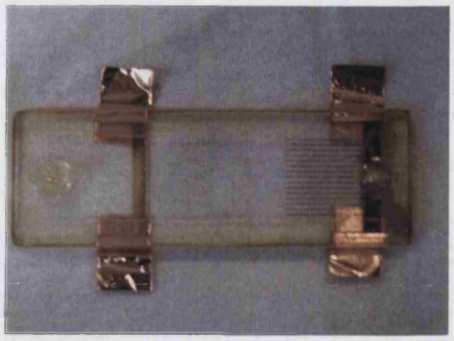

Fig. 3.3. Image of typical MECR made with thin glass slides.

A computer-generated mask was exploited to produce a photoresist (Microposit S1828) image of the desired electrode configuration on the glass cover plate, as detailed in Section 2.1. Gold films were then evaporated onto the glass through the photoresist mask as described in Section 2.2. When sealing the channel units, the microelectrodes were positioned after an inlet length l_e, which according to Schlichting[122], is necessary to establish Poiseuille flow and is given by:

$$l_e = 0.11\left[v_0 \frac{h}{v}\right]$$

Equ. 3.1.

The above methodology demonstrated the capability of fabricating glass channel structures down to dimensions of a 100 μm with relative ease and simplicity. However, even though the approach used photolithographic techniques to produce well-defined structures as small as 10 μm for the microelectrodes, the channel fabrication procedure detailed in this section was limited to dimensions of 100 μm and the precision of the channels was not to the same level as that of the microelectrodes. Much work has been published in the past where photolithographic techniques have been used to fabricate well-defined structures on glass[117-119] substrates,in the following sections a description of the processes adopted will be given.

3.1.1.2. Ion Beam Etching

Deep reactive ion beam etching of quartz glass where the ion beam source is used to etch away a substrate has been reported[123]. The reactive ions used in this process increase the etch rate of the unmasked regions of quartz glass.

A similar methodology was adopted to create well-defined glass channels. However, due to limitation of equipment, the use of reactive ions could not be adopted and only dry ion beam etching (Edwards, model 306) was possible. This limited the ability to produce channels with a depth of less than 10 μm.

The method involved spin coating a thick layer of positive photoresist (Microposit S1828) using a rotation speed of 1000 rpm to yield a film thickness of 20 μm on a glass wafer. Using photolithographic procedures as described in Section 2.1, a photoresist mask of the desired channel arrangement was produced. Due to a thicker film of photoresist, the UV exposure time was increased to 60 seconds. The substrate was placed in the ion beam chamber and the exposed regions of the glass were allowed to etch along with the photoresist mask. After the photoresist mask was almost etched away, the process was stopped and the glass wafer was cleaned and examined (see Figure 3.4 for details of the process).

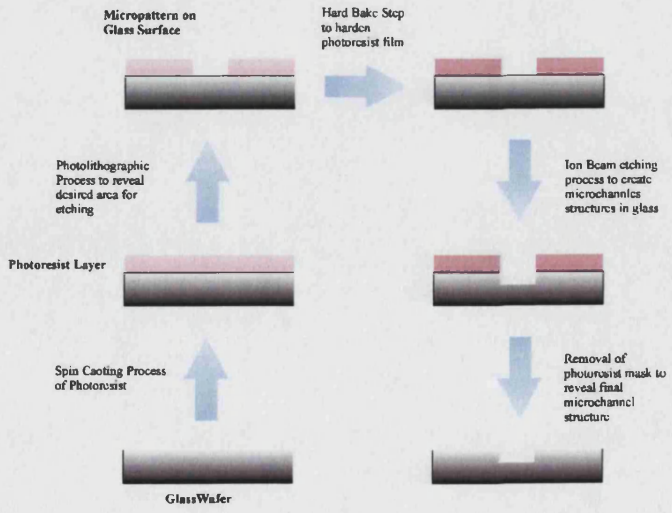

Fig. 3.4. Fabrication process for glass channels using ion beam etching.

Although this method provided a good level of precision, the process was very complex, costly and required long time scales due to the slow etch rate. The process was therefore poorly suited for exploratory work.

3.1.1.3. Photoetchable Glass - Foturan

Much development work has been reported on fabrication techniques, which involve wet etching of glass or silicon, or dry etching processes such as reactive ion beam etching. Some research work has concentrated on exploring different types of materials in order to achieve precision, as well as having a more cost effective process, which is more suited for exploratory work.

Fabrication techniques utilising photoetchable glass were reported by Dietrich et al.[64], where a new range of glass substrates known as Foturan (Schott) were developed. These glass substrates achieved high aspect ratio microstructures at low fabrication costs. The glass was designed to be sensitive to short wavelength UV light and using this property it was possible to fabricate microstructures. Photoresist patterns were utilised for creating reverse patterns of titanium metal films on the Foturan glass (see Section 2.1). These titanium patterns were used to act as a mask to allow exposure of certain regions of the glass to yield the desired channel. When exposing to UV light it was important that the wavelength was approximately 310 nm or lower and the energy density was approximately 2 J/cm^2. After exposure to UV light, the glass had to be heat-treated, which involved heating the glass up to 500°C at a rate of 1°C/minute, and then leaving at that temperature for the duration of one hour. After this period, the glass was heated to 600°C at a rate of 1°C/minute, and left at that temperature for another hour before cooling down to room temperature, at a rate of 1°C/minute. (Figure 3.5 details the process.)

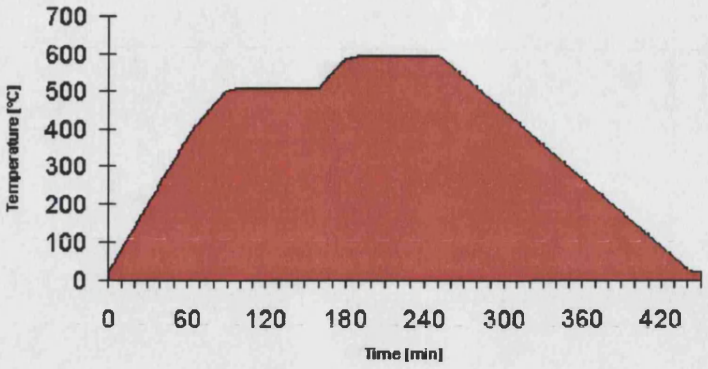

Fig. 3.5. Heat treatment procedure.

A programmable furnace was used (Carbolite) for the heat treatment cycle and once complete, the regions of glass exposed to UV light became crystallised and had a distinctive dark pink colour. These crystals had a diameter of between 1 - 10 μm and etched away at a rate of 10 μm/minute, using a solution of 10% HF, to reveal the desired channel structures. Figure 3.6 details the processes involved in fabricating channels in Foturan glass.

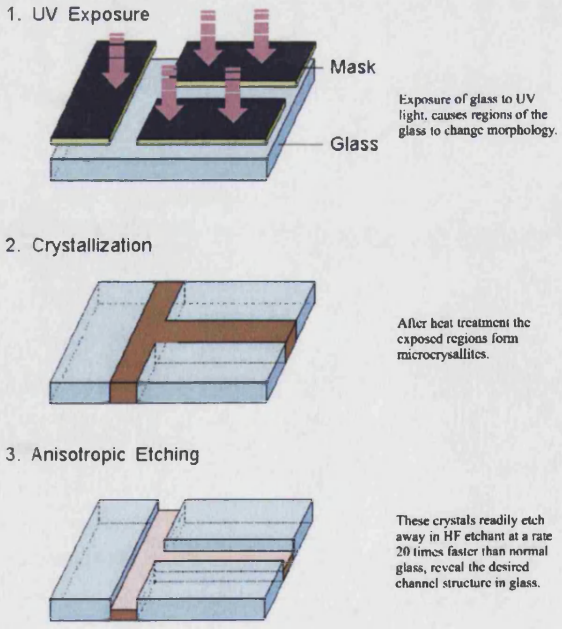

Fig. 3.6. Fabrication process for channels in Foturan Glass.

This method proved to be the most effective approach in comparison to the other two techniques for glass channel fabrication described earlier. The method allowed for the possibilities of fabricating on a glass substrate a well-defined structure, as well as providing flexibility in utilising the MECR devices in exploring a range of applications. Figure 3.7 shows images of examples where the precision of the structures achieved has been illustrated[124].

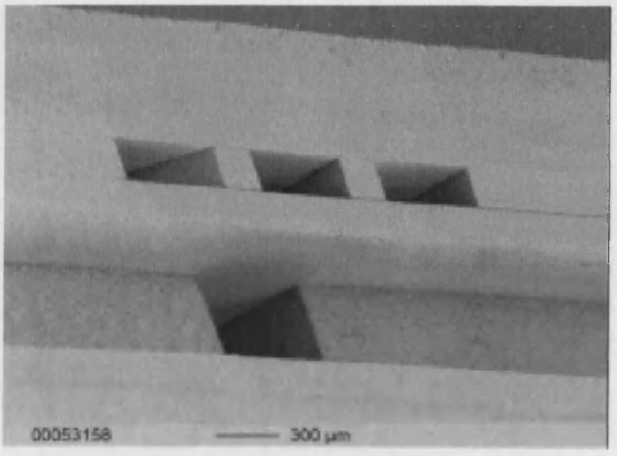

Cross Sectinal View of a Mixing Chamber.

(a).

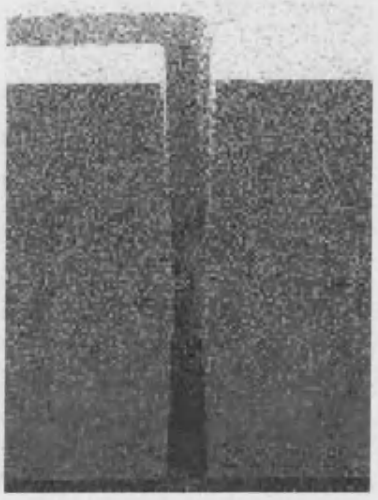

Image showing ecth profile where the width of the channel is 100 µm, and the channel has been etched through to a depth of 1 mm. From the image it can be seen that the slope of the wall is about 1°, showing that Foturan glass can be use to give high aspect ratios with good definition.

(b).

Fig. 3.7. Etched profiles of Foturan glass. **(a).** Cross section profile of a microchannel. **(b).** Edge profile of a microchannel.

A similar strategy, as outlined in Sections 2.1 - 2.3, was used to create the microelectrode cover plates, to introduce inlet and outlet openings and to seal using inert low-melting wax. Figure 3.8 shows a schematic outlining the construction process for the MECR, as well as an image of a complete device.

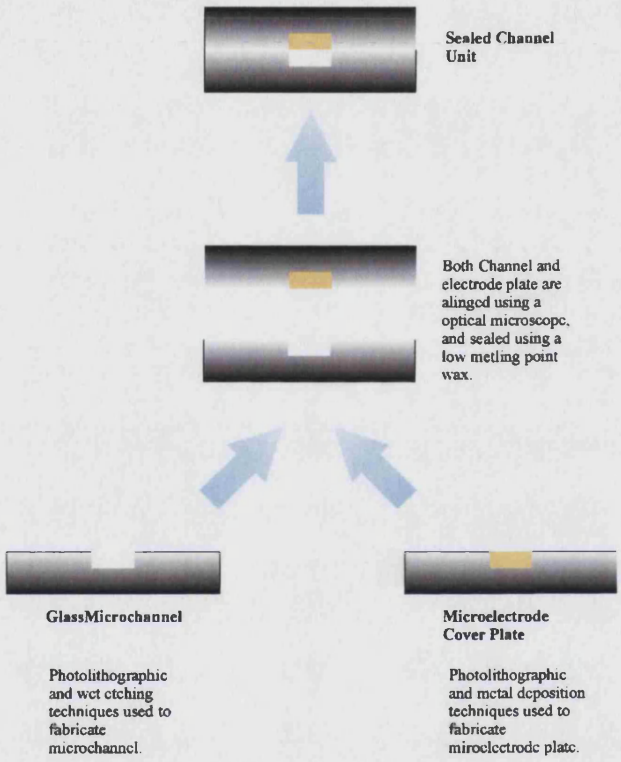

(a).

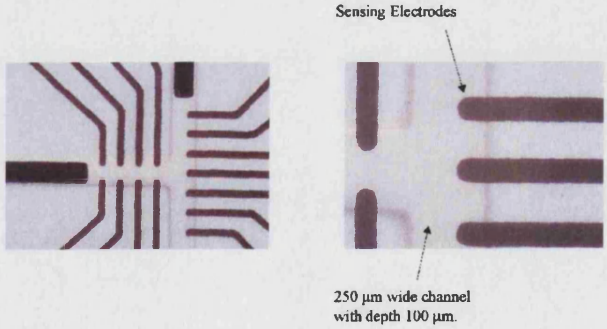

(b).

Fig. 3.8. (a). Schematic outlining the process involved in constructing MECRs. **(b).** Image of a MECR device fabricated using Foturan Glass.

As outlined in this section the Foturan Glass proved to be an effective and efficient way to fabricate well-defined MECR devices. However, even though the technique had the ability to make structures out of glass as small as 10 μm, the process to seal these channel units for dimensions less than 50 μm in height and width proved to be challenging. In the coming sections a discussion into a range of alternative techniques to fabricate and seal channel units with dimensions not achievable with Foturan Glass will be presented.

3.1.2. Silicon Based Microchannels

Wet etching of silicon is another well-documented technique[58,86] and due to silicon having a single crystal structure the anisotropic etching process can produce highly resolved micro structures. Figure 3.9 shows some cross sectional images of two etched silicon channels[125]. These unique etching properties of silicon were used to identify a strategy to fabricate and seal microchannels, with dimensions less than that established for Foturan Glass. Procedures detailed in Section 2.1 were used to create photoresist masks that exposed regions of the silicon wafer to a solution of etchant. A solution of hydrofluoric acid and nitric acid were used to make the etchant solution, and details of the process can be seen in Figure 3.10.

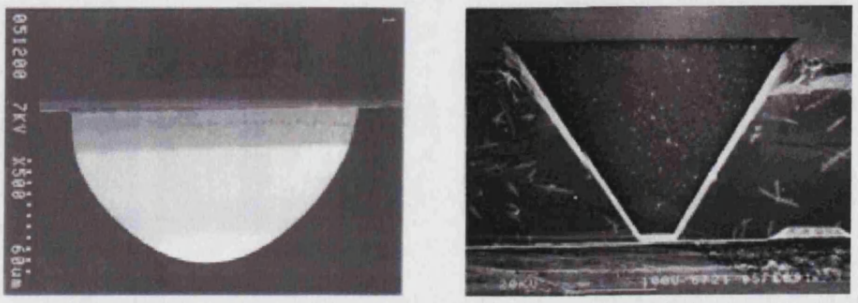

Isotropic Etching **Anisotropic Etching**

Fig. 3.9. Image of a silicon channel profile using wet etching techniques.

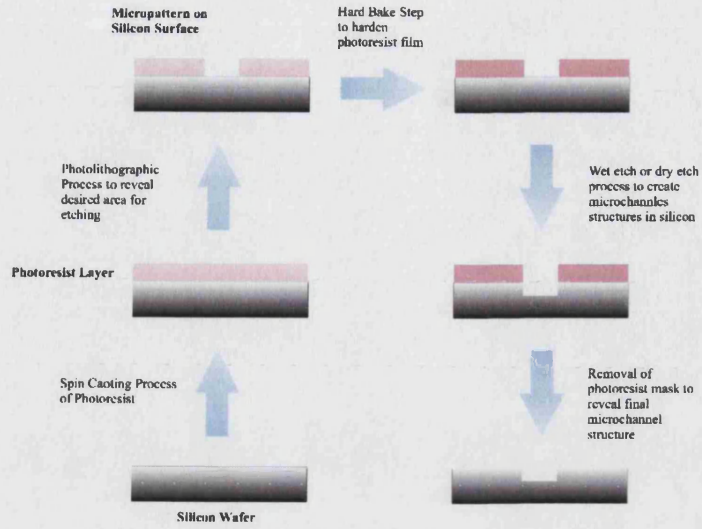

Fig. 3.10. Fabrication process for silicon channels using wet etching techniques.

As an alternative method, a similar approach of ion beam etching, as detailed in Section 3.1.1.2, was used to produce well-defined microchannels in silicon wafers. Images of the channels can be seen in Figure 3.11 where the dimensions of the channels were: width 50 μm and depth 3 μm.

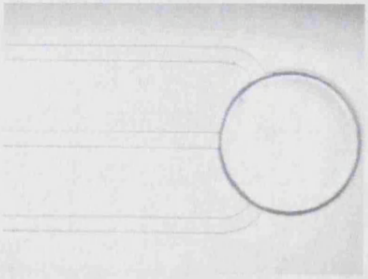

Image taken of a microchannel made from ion beam ecthing silicon. The dimensions of the channels were: width 100 μm and height 5 μm.

Fig. 3.11. Images of silicone channels fabricated using ion beam etching.

From the images it can be seen that well-defined microstructures can be produced using this process, and that the etch rate of silicon was faster than that of glass fabricated microstructures. Nevertheless, added complications needed to be tackled in relation to sealing the channel units and isolating the microelectrode contact regions from the silicon wafer. In addition, one of the key long term motivations for developing

the MECR was the ability to combine electrochemical techniques with optical techniques - silicon was not ideal with due to its flexibility for use in these applications.

3.1.3. Soft Lithography

Many methods have demonstrated different approaches to fabricating micro, and in some cases nano structures, using alternative substrates such a polymers[113]. Micromoulding techniques currently being explored, which form the basis of soft lithography include; microcontact printing (μCP)[126], replica moulding (REM)[127], microtransfer moulding (μTM)[128], micromoulding in capillaries (MIMIC)[129] and solvent-assisted moulding (SAMIM)[130]. In this section, the use of some of these methods will be discussed in attempting to develop a process for rapid prototyping of MECR devices, as well as outlining a strategy of constructing microchannels with dimensions smaller than that reported so far.

3.1.3.1. Micromoulding

The approach of using moulding can present many advantages. For example, the use of REM has been demonstrated in mass production of surface relief structures such as diffraction gratings[131], compact discs[132] and microtools[133]. Much literature has been published on the various techniques using polymer substrates and Figure 3.12 summarises various processes that have been reported.

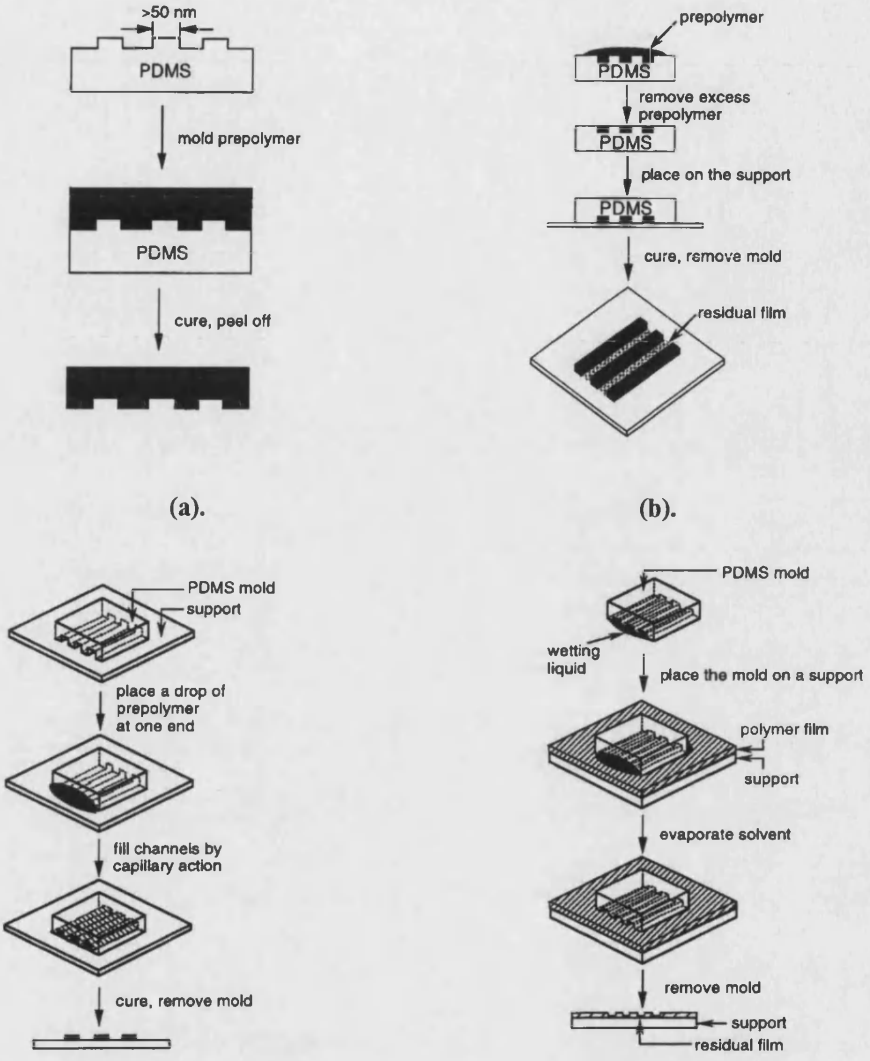

Fig. 3.12. Schematic illustration of procedures for **(a).** replica moulding, **(b).** microtransfer moulding, **(c).** micromoulding in capillaries, **(d).** solvent-assisted micromoulding.

A similar strategy, as outlined in Figure 3.12, was used to produce poly(dimethylsiloxane) (PDMS) microchannels sourced from Dow Corning (Sylgard 184). The photolithographic procedure, as outlined in Section 2.1, was used to fabricate a photoresist pattern of the desired microchannel on a silicon wafer. PDMS was poured onto the silicon wafer to cover the photoresist and allowed to cross-link (a procedure that is similar to that outline in Figure 3.12(a)). Once the polymer had hardened it was carefully peeled away to reveal an imprinted channel. The dimensions of the channel

could be controlled using the photoresist mask and the method allowed for the possibilities of creating channels in the range: width as low as 10 μm, height 80 - 5 μm, and length up to 6 cm.

However, PDMS had poor inertness to organic solvents and swelling of the polymer would cause leaks in the final MECR device. Therefore, the scheme was taken one stage further, where the use of other materials, which exhibited better chemical inertness as well as being transparent, was investigated.

The use of sodium silicate solution to bond glass surfaces has been reported[134]. The structural properties of the solution when dried have been studied and demonstrate that when solidified the solution forms a stable inert solid[135]. Hence the sodium silicate solution was used as molten to create microchannels. Similar procedures as outlined above were used to create PDMS moulds where the mould was designed to be a reverse image of the final microchannel design. A sodium silicate solution (Aldrich) was poured into the PDMS mould and left to set at 90°C for 1 hour (Figure 3.13 details the process). Analysis after retrieving the sodium silicate structure from the PDMS mould showed that well-defined channel structures could be made. The technique proved to be a useful way of fabricating microchannels, as the PDMS stamps were not damaged in the process, they could be re-used to make more channels. Large volumes of sodium silicate solution proved to contract substantially when solidifying, which in turn created poorly formed microchannels. For these reasons, the wafers of hardened silicate were thin and delicate and proved difficult to handle when trying to seal over an electrode cover plate.

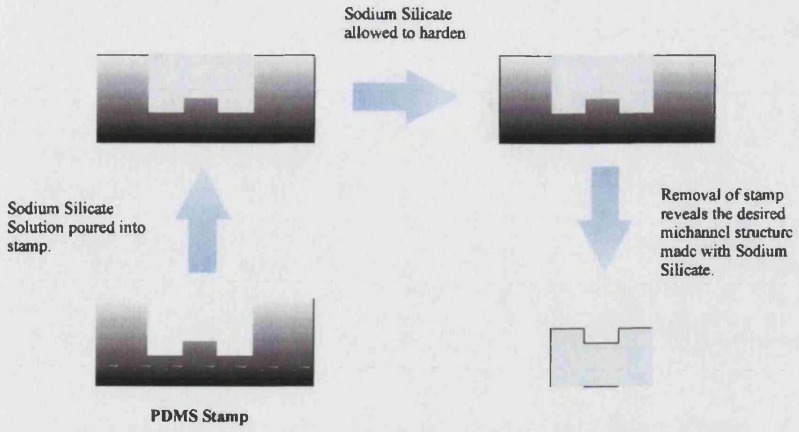

Fig. 3.13. Fabrication process for channels using sodium silicate.

Another method, which adopted a similar ideology as the SAMIM method where sodium silicate solution was poured directly over a photoresist pattern on glass, was used. Once the sodium silicate had hardened, inlet and outlet openings were introduced into the glass and an attempt to dissolve the photoresist pattern was made. However, dissolving the photoresist proved to be difficult and sonification was used to try to agitate and remove the pattern. This caused similar issues with regards to the material contracting, and showed poor results as the definition of the structure became distorted.

From the studies documented above it was apparent that micromoulding showed potential merits towards fabricating well-defined microstructures. However, a substance that showed good chemical resistance and high aspect ratios of forming microstructures needed to be identified. In the next two sections a description of two types of polymers, which showed these characteristics, will be given.

3.1.4. Micromoulding Surlyn – Polymer Microchannels

Further investigations into alternative materials revealed the possible use of a food packaging resin, Surlyn (Du Pont), which had good chemically inert properties.

The polymer could be sourced commercially in two forms, either in its raw form of beads or in pre-pressed sheets with a range of thicknesses (20 – 250 μm).

Initial studies focussed on the polymer sheets acting as a gasket and the design illustrated in Figure 3.14 was used.

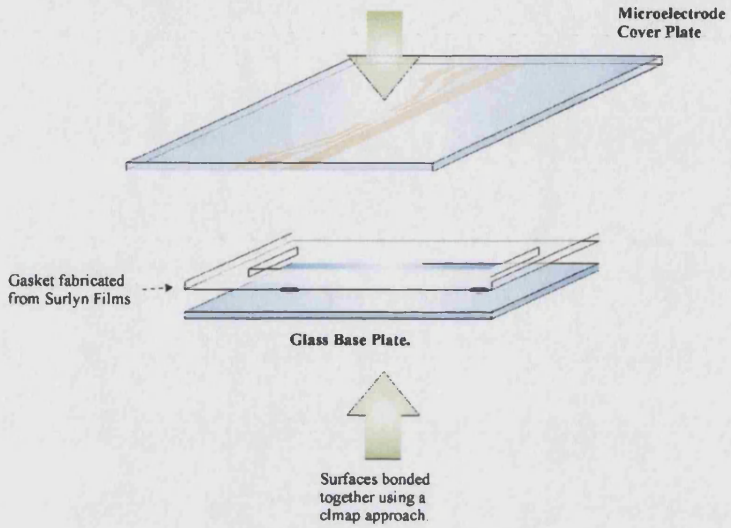

Fig. 3.14. Schematic outlining the process involved in constructing MECR device using Surlyn Sheets.

Surlyn polymer sheets of known thicknesses were cut to create channel stencils with the dimensions in the range: width as small as 100 μm, height 20 – 250 μm. The sheets were carefully cut using a sharp scalpel knife to reveal the channel stencil that was then used as a gasket. The Surlyn gasket was carefully aligned on top of a microelectrode plate (prepared as outlined in Section 2.2.), using an optical microscope (Olympus), after which another glass cover plate with inlets and outlets holes was placed over the films. The sandwiched channel was then clamped between two perspex blocks to give a sealed MECR device.

The fabrication process outlined in the above paragraph was limited to only producing straight channels, with dimensions to a precision of 100 μm. Ion beam etching was studied to achieve a higher level of control to produce complex

microchannels geometries, as well as smaller dimensions. Polymer films were melted on glass substrates to produce rigid polymer surfaces. Using photolithographic procedures as outlined in Section 2.1, photoresist was patterned to mask regions of the polymer film. The exposed regions were then etched to give the desired channel patterns on the surface of the polymer films. The polymer films were allowed to etch under an ion beam source in a similar way as outlined in Section 3.1.1.2. The process proved to yield well-defined and precision microchannels, which had the dimensions in the range: width as small as 10 μm, height no more than 10 μm and length no more than 1cm. Figure 3.15 outlines the processes involved. The fabricated channels were sealed using a clamp approach similar to the process described above.

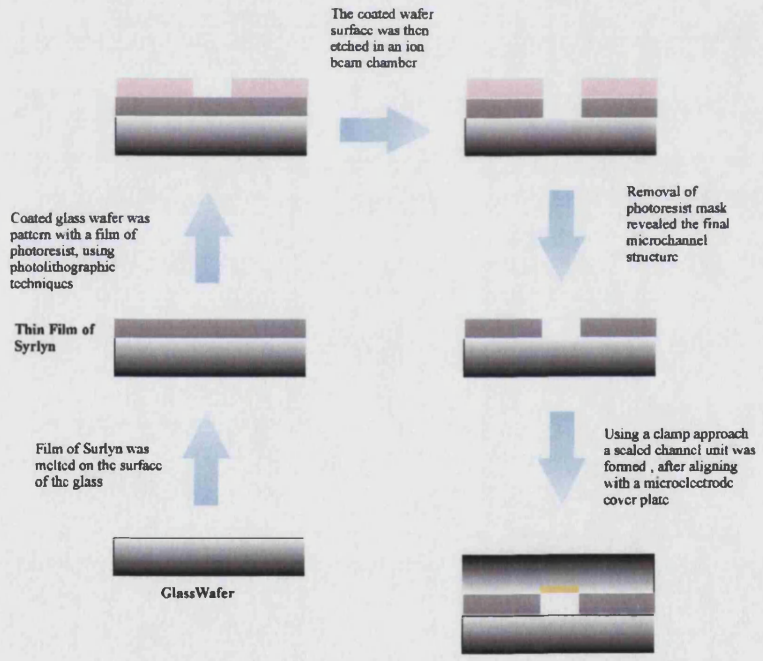

Fig. 3.15. (a). Schematic outlining the process involved in fabricating complex microchannels using Surlyn films.

The polymer sheets were found to be an effective way of making simple channel geometries and proved to give a cost effective approach to fabricating microchannels similar to that demonstrated for the approach which utilised thin glass cover slips in

Section 3.1.1.1. Conversely, the approach using ion beam etching to make more complex channel geometries proved to be an expensive and time consuming technique. As one of the motivations for working with polymer channels was to develop the ability for rapid prototyping, an approach using the polymer beads to micromould channels was investigated as an alternative means of fabricating complex microchannels.

A hot embossing strategy was employed to create polymer microchannels made from Surlyn. Photolithographic and wet etching techniques, as detailed earlier, were used to create raised microchannel imprints on the surface of silicon or Foturan Glass. The microstamps were then secured on glass backing plates using araldite and heated on a hot plate to 115°C. A thick polymer film of Surlyn (5 mm), made before hand using the beads, was rolled over the surface of the hot stamp and the pattern of the microchannel was imprinted on the surface of the thick film. The edges of the film were then trimmed to give a microchannel that was made completely from Surlyn. The channel was aligned on the surface of a microelectrode cover plate, which had inlet and outlet holes drilled in it, and clamped using the perspex blocks, as described earlier, to give a sealed MECR device.

So far, all the techniques described in this chapter have given alternative means of fabricating microchannels on glass, silicon or polymer substrates. Using these methodologies it was possible to create channels which could have well-defined and reproducible structures with dimensions as small as: width 100 μm, height 20 μm and length up to 10 cm. However, none of the approaches showed potential in making microchannels that had dimensions which were less than this. In the final part of this chapter a fabrication approach that allowed microchannels with dimensions: width 10 μm, height 5 μm and length 5 cm, to be fabricated, will be presented.

3.1.5. Microchannels Made From SU8 2000

Much literature has been published on the use of SU8 and recently a methodology that used this material to create microchannels has been reported. In this section, this technique has been utilised to create a range of MECR devices.

Microelectrode plates were fabricated as outlined in Section 2.2 and used as the substrate on which SU8 microchannels were fabricated. Using the Mask Aligner, a photo mask of the desired channel design was aligned over the electrode plate coated with a film of SU8 as outlined in Section 2.1.2. After exposing and developing the SU8 film, a pattern of a microchannel was fabricated over the surface of the microelectrodes. Figure 3.16 shows an illustration of the fabrication process as well as images of a typical device fabricated with this approach.

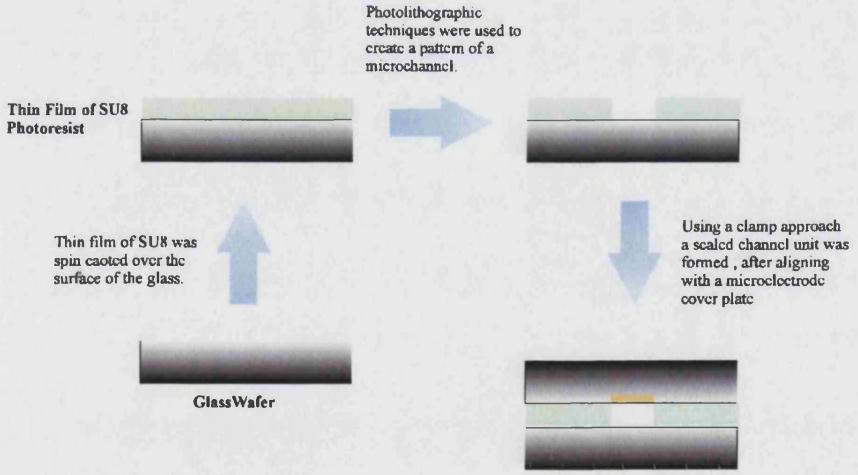

(a).

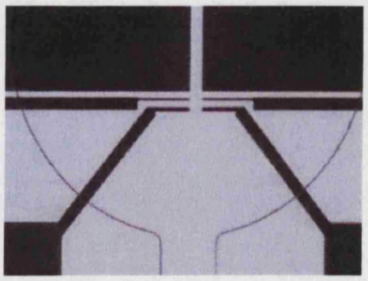

Image of a channel fabricated using SU8 with dimensions: width 500 μm opening into a circular chamber of 5 mm diameter, and height of 25 μm.

Fig. 3.16. (a). Illustration of the process used to fabricate SU8 MECR devices. **(b).** Microscope image of a SU8 MECR device.

Inlet and outlet openings were drilled into a glass cover plate and placed over the SU8 channel unit. A clamp approach, as outlined for the Surlyn microchannels, was used to seal the glass cover plate over the channel unit.

In this chapter various techniques were shown to be a useful for to designing and fabricating a range of novel MECRs. In particular, an approach using glass slides, as described in Section 3.1.1.1, which gave well-defined channels with dimensions down to 100 μm, has been outlined. In addition, photolithographic techniques have been demonstrated to fabricate a range of MECR devices with precise structures and complex channel designs. Furthermore, alternative materials such as sodium silicate, Surlyn and SU8 have been used with soft lithographic and photolithographic techniques to produce channel structures that are cost effective and require less time to manufacture.

Overall, using a combination of the techniques outlined in this chapter, the potential of MECRs in many applications can be explored. In the coming chapters a description and quantification of MECRs fabricated with the techniques outlined above is presented.

Chapter 4

Flow Visualisation: A Voltammetric Approach

4.0. Introduction

Flow profiling is of great academic and commercial interest. The potential to address fluid flow behaviour can provide a great deal of insight into collision and reactions that occur in a fluid environment. The capability to monitor these processes could provide an insight into the pathway of flow, and how the interaction of liquids could govern reactions. The property of liquid flow patterns is a critical aspect of microscopic devices, ranging from surgical endoscopes and microelectromechanical systems to the commercial 'lab on a chip'. These devices allow chemical analysis and synthesis on scales unimaginable a decade ago and interest in developing methods that monitor liquid flow patterns has become an active area of research.

Flow visualisation techniques have been successfully employed by researchers to gain a comprehensive understanding of the properties of liquids in flow fields. Many methods have been utilised and used in combination with numerical modelling to provide a quantitative model of processes occurring within cells[136-138]. Particle streak velocimetry (PSV)[139,140] and particle imaging velocimetry (PIV)[141-145] have been employed widely to aid in flow characterisation[146-150] due their simplicity and ease of application.

PSV utilises small particles that may be imaged in space. An exposure is recorded for a time interval such that the particle travels more than its own diameter, creating a streaked image on a photographic plate. Analysis of the trace length on the

image permits the displacement of the particle to be determined and the velocity then calculated from the exposure time.

The related PIV technique employs a pulsed light source to illuminate fine particles injected into fluid. This approach produces single spot images of the individual particles on the flow image[151,152]. By identifying and tracking each particle as a function of time, the velocity field within the device may be revealed. These methods can provide useful information regarding the bulk fluid characteristics. However, properties close to an interface prove more challenging. To address this limitation a number of approaches have been developed. One example is the use of a chemisorption approach[153]. A dye chemisorbed onto a cell surface is arranged such that a colour intensity distribution is generated. The distribution is determined by remission photometry and the remission data can be related to the local surface mass density via a calibration procedure. The approach yields information regarding the local mass transfer coefficients close to the interface of interest.

Increasingly sophisticated approaches are also appearing that permit the three dimensional analysis of information obtained from measurements such as that above. One example is computer tomography (CT)[154,155], which is an advanced computer-aided visualisation technique that enables a cross sectional view of the fluid flow to be obtained. An emission source is rotated around the object on a fixed plane. The projection data is then processed from a range of directions to gain a three dimensional view of the flow profiles. This approach has been used with a range of electromagnetic radiation techniques, including X-ray and gamma-ray[156] and UV/Vis via high intensity laser sources[157].

For bulk fluid analysis, the majority of techniques employed require the external injection of a tracer into the system. An inherent problem with such techniques is that the injection of a tracer can alter the fluid flow behaviour and provide misleading results. An alternative strategy based on electrochemical methods electrolyses a reagent within a fluid and in the process creates a tracer which may then be monitored in a similar

manner to those noted above. One popular approach is the hydrogen bubble method[158] where small bubbles of hydrogen are generated from an aqueous solution by electrolysis and traced through the cell. Flow lines and time lines can thus be created by the use of suitable electrode geometries and voltammetric conditions. Applications of this technique include the investigation of two-dimensional impulsively started jet flow commonly used for hydraulic power applications[159]. A further application of an electrochemical approach is the 'electrolytic precipitation method'[158]. In this arrangement, metal (typically a tin alloy) is plated onto a cell wall, or a fine wire is introduced into the stream. The metal act as an anode and the electrolysis reaction generates small white particles that can be traced through the cell using similar strategies to those noted above. Although successful, both techniques are limited to aqueous electrolytes and prove difficult to quantify due to the complexity of the coupled electrolysis processes.

In this chapter, an electrochemical approach is demonstrated that can be extended to a range of media. The merits of this approach are discussed and the potential of numerical modelling to provide quantitative analysis is highlighted. The design and development of this novel approach will be presented and the results achieved will be discussed for application in macro and micro flow systems.

4.1. Electrochemical Approach to Flow Visualisation

An approach to the visualisation and quantification of mass transfer in liquid flow has been studied where the technique utilises an array of microstrip electrodes situated within a duct through which electrolyte solution is flowed. The concept is based on the electrolyte solution containing a reagent that may be electrolysed and in the process undergoing a colour change. The electrolysis products can then be swept through the cell and the pathway imaged via digital video. Results are presented for

experimental geometries where a range of obstructions are deliberately introduced into the duct. Figure 4.1 provides a schematic of the design.

Transport rates within the cell were restricted such that Stokes flow conditions can be maintained throughout and the streamlines generated from the electrolysis used to map the flow profiles through the devices.

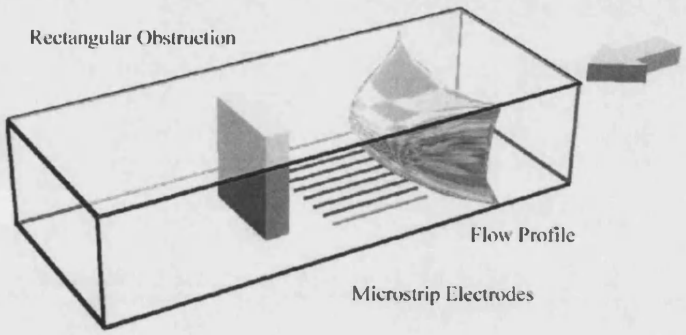

Fig. 4.1. Schematic design for an electrochemical flow visualisation device

4.1.1. Macro Flow Visualisation

In this section, a strategy is demonstrated for examining the streamlines produced from an electrolysis reaction occurring at a series of microstrip electrodes fabricated onto glass walls of flow cells with typical dimensions of 1-2cm wide and 100μm high. The fabrication processes used and conditions to obtain a series of data for a range of different macroscopic cell designs are detailed below. An electrolyte solution containing a colourless reagent, tetramethyl phenylene diamine (TMPD), was used. The reversible one electron oxidation of TMPD to form a blue cation was induced at a series of microstrips electrodes while flowing through a range of differently designed cells. Real time images of the evolving coloured streams were recorded using a digital video camera.

4.1.1.1. Experimental Procedure

The cells employed for the measurements were composed of two glass microscope slides sandwiched together with 100μm thick glass separators, as illustrated in Figure 4.2. A range of different cell designs were constructed using a similar methodology as outlined in Section 3.1.1.1. Figure 4.3 shows schematics of the various designs flow cells that were used in the analysis.

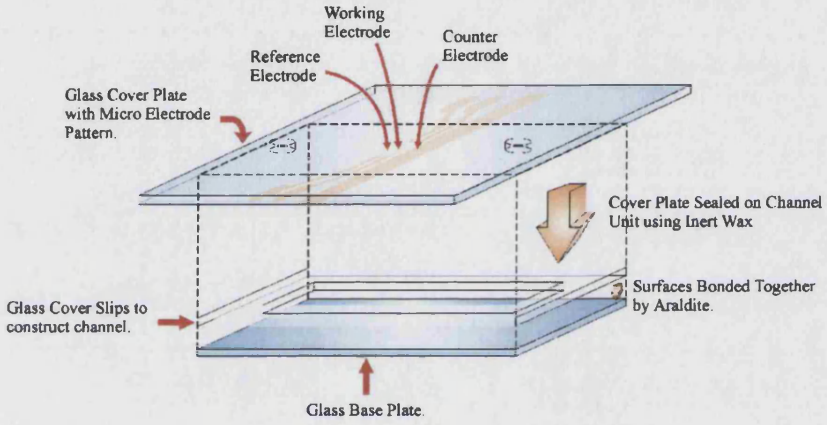

Fig. 4.2. Typical schematic of cell construction.

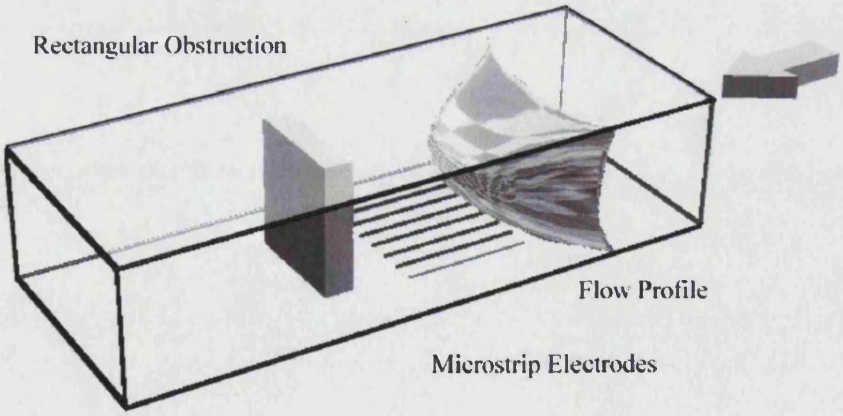

(a).

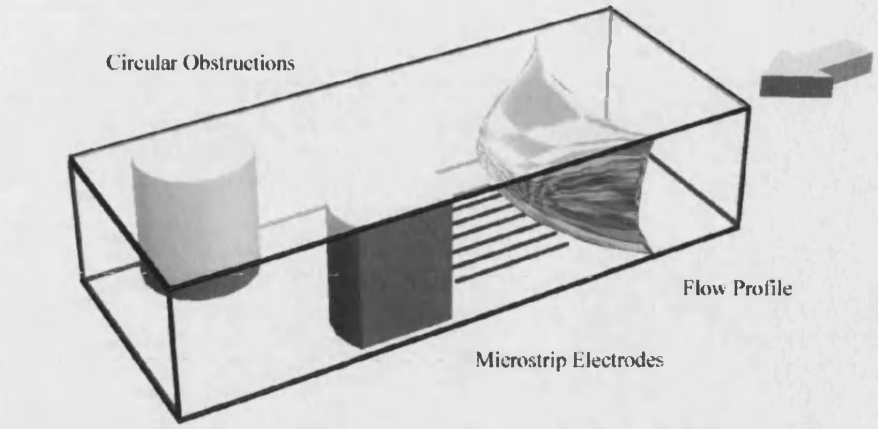

(b).

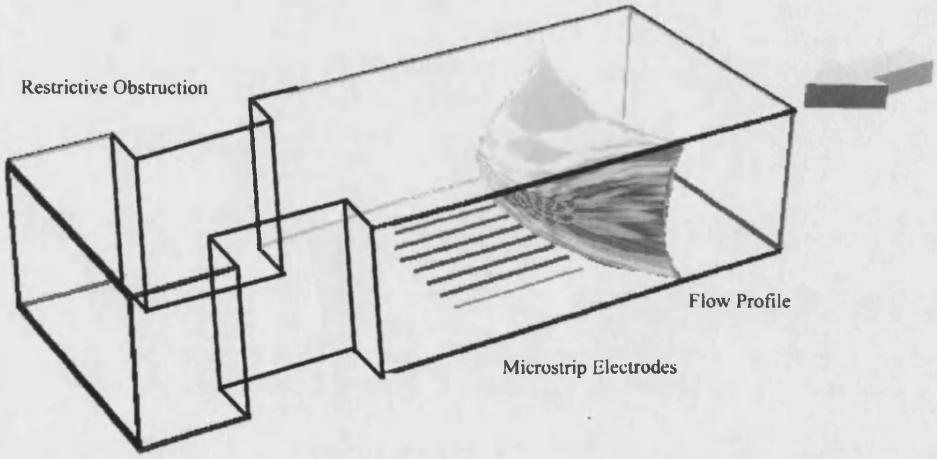

(c).

Fig. 4.3. Illustration of various cell designs used for analysing flow behaviour in macroscopic flow cells, **(a).** rectangular obstruction, **(b).** circular obstruction, **(c).** restrictive volume pathway.

Fabricated cells were situated within a gravity fed flow system as detailed in Section 2.4.1[160,161]. Pt microstrip electrodes of approximate dimension (length: 4 cm, width 100 μm) were fabricated from a mask generated using a photolithography[108,162-164] approach as detailed in Sections 2.1 and 2.2 and an argon sputter (Argar Scientific). Photoresist approximately 1μm thick, were also used to mask regions of the Pt films that acted as contact lines for the microstrip electrodes. A platinum gauze acted as the counter electrode and this was located downstream of the working electrode in order to minimise interference from side products that could be produced at this electrode.

Reagent solutions were prepared using pre-dried acetonitrile, tetramethylphenylene diamine and dried tetrabutyl ammonium perchorate. In all measurements solutions were purged with nitrogen for 15 minutes prior to electrolysis.

All electrochemical measurements were controlled using a home built potentiostat and images were recorded in real time using a digital video facility (Sony PC100) and downloaded using standard graphical procedures.

4.1.1.2. Results and Discussion

Experimental measurements were performed using the geometries shown in Figure 4.3. The cells possessed approximate dimensions of: width 1.8cm, height 100 μm and length 7 cm. The obstructions had dimensions as detailed in Figure 4.3 and were situated approximately 1cm from the end of the microstrip electrodes.

Degassed acetonitrile solutions containing 0.1 mol dm^{-3} TBAP and $5x10^{-3}$ mol dm^{-3} TMPD were introduced in the cells via a gravity fed flow system, as detailed in Section 2.4.1, and electrolysis measurements performed at a range of fixed flow rates. Each of the microstrip electrodes were set to +0.5V (vs pseudo Pt reference) that corresponded to the transport limited one electron oxidation of TMPD to the subsequent radical cation.

Figure 4.4 shows an image recorded using a digital video for a volume flow rate of $1.04x10^{-2}$ cm^3s^{-1}, under steady-state conditions for the cell design with a rectangular obstruction (see Figure 4.3a). It is apparent from the image that each line of electrolysis product generates a streamline trace through the cell.

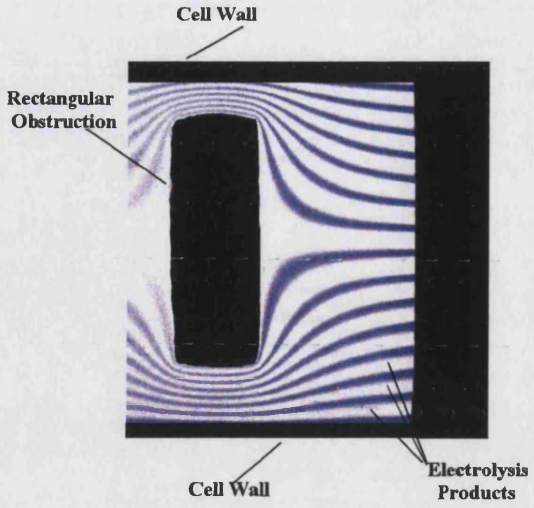

Fig. 4.4. Streamline image recorded using a digital video camera at a volume flow rate of 1.04×10^{-2} cm^3s^{-1}, under steady-state conditions.

Inspection of the region close to the obstruction reveals a thinning of the streamlines. This is caused by the acceleration of the fluid through the small gap and the velocity profile that acts to push the product into a finer stream. This behaviour can be visualised by examination of Figure 4.5, which reveals the predicted profile of a streamline generated using finite element simulations. Experimental measurements were repeated for a range of flow rates (10^{-2} – 10^{-4} cm^3s^{-1}) and similar data obtained.

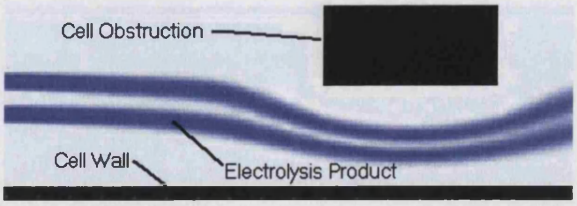

Fig. 4.5. Numerical prediction of two streamlines using a finite element simulation[1].

[1] Simulated results achieved from calculations by I. E. Henley.

Next the evolution of the streamlines was examined as a function of time. In these measurements a potential step experiment was performed from 0V to 0.5V (vs pseudo Pt reference). These limits correspond to no oxidation of TMPD (0V) and the transport limited one electron oxidation of TMPD (0.5V) to the corresponding radical cation. Figure 4.6a reveals an image taken one second following the potential step. Clearly, the electrolysis product has begun to be swept from the electrode and the resulting streamline begun to reveal the obstruction ahead. Figure 4.6b was then taken a further second later with the streamline now further advanced along the cell. Eventually the profile returns to that noted in Figure 4.4 under steady-state conditions.

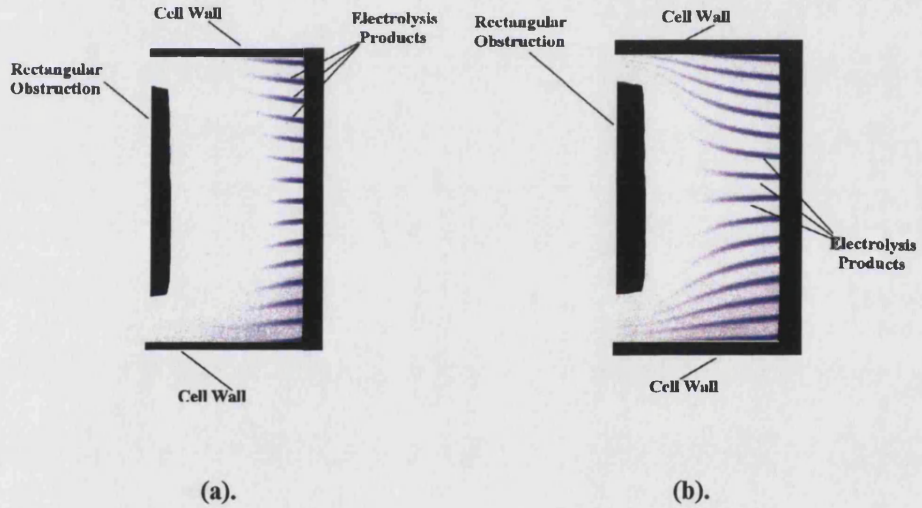

Fig. 4.6. Streamline images recorded, **(a).** one second and **(b).** two seconds following the potential step.

A similar approach using circular obstructions as detailed in Figure 4.3b was used to study the transient periods of coloured streams produced by pulsing the potential on and off at the microstrip electrodes. Figure 4.7 shows the images recorded, which show the broadening of the streams due to diffusion can be pinned and controlled by the volume flow rate of the solution. Using this technique it is possible to visualise and

determine displacement of material in a flow regime and to develop an understanding of how it can be controlled relative to the volume flow rate.

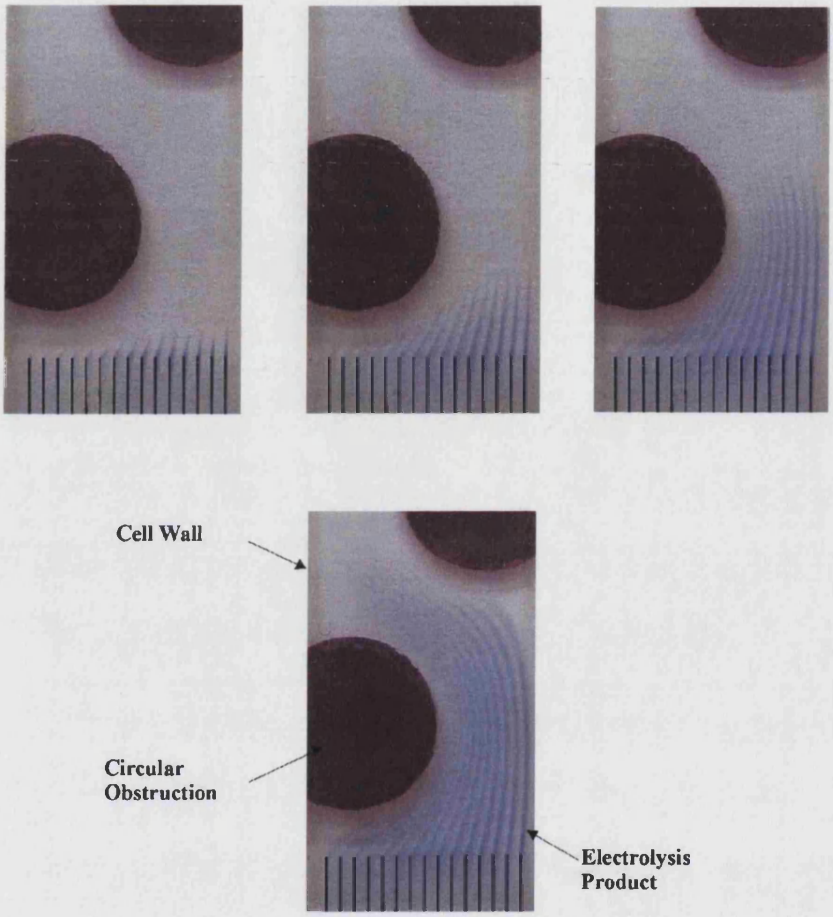

Fig. 4.7. Streamline images recorded using a circular obstruction, showing the evolution of coloured streams through the cell at short time intervals.

Using the design detailed in Figure 4.3c it was possible to gain an insight into the velocities at various points along the cell width. The flow cell was fabricated in such a way that the microstrip electrodes were spaced at various points along the width of the cell. Figure 4.8 details the results achieved.

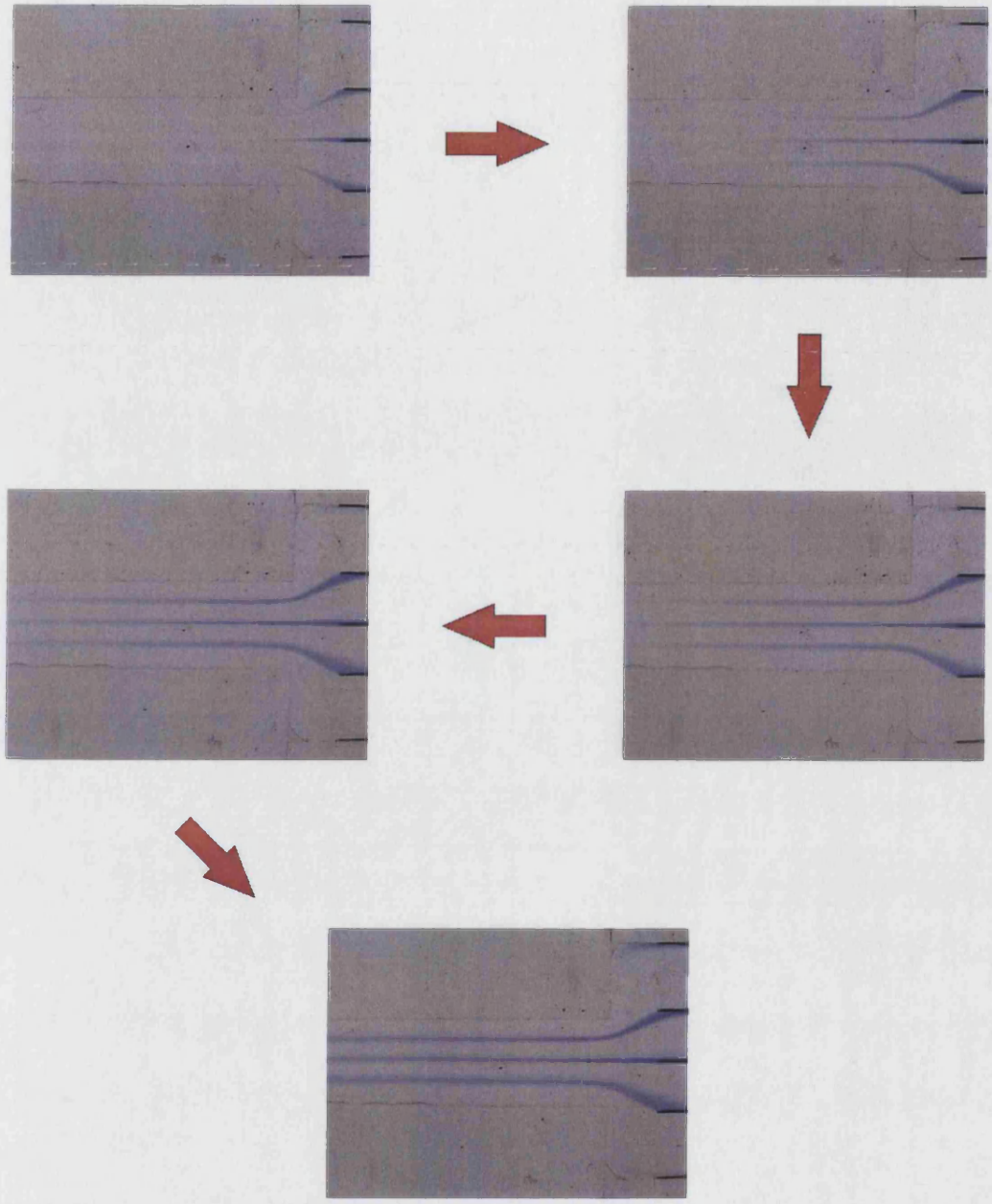

Fig. 4.8. Streamline images recorded showing the evolution of coloured streams at various points along the width of a cell.

Moments after the potential was stepped to begin the electrolysis reaction it became apparent that the central stream travels faster than the others either side of it (see Figure 4.8a). This was due to a laminar fluid flow caused by a drag force being exerted on the cell walls by the fluid where the velocity at the walls is zero. On examining the images recorded after a length of time, this observation becomes even more apparent

and it is possible to acquire an image of the flow profile, as marked out in Figure 4.8b. It is also interesting to note how the streams produced at either edges of the cell wall have a time lag in comparison to the central three streams, which correspond to the transport rates at the cell walls being extremely slow relative to the centre of the cell. A final analysis of the central streams shows thinning of the streams when passing through the restricted channel pathway. This again is caused by the accelerating central velocity of the solution as the restricted volume in the narrowing cell width has a higher pressure being exerted in the flow system.

The above measurements highlight the ability to monitor the transport of material through flow cells using a non-invasive voltammetric approach. In particular, the simplicity of the approach to alter the voltammetric conditions, and therefore monitor the real time evolution of the streamlines, offers possible benefits over traditional visualisation strategies. Whilst the technique does not have a commercial impact, it does act as a precursor for developing an approach on a micro scale. The ability to shrink the width of the microstrip electrodes to sub-micro dimensions using routine photolithography strategies offers the possibility of using this type of strategy to image the flow and reaction profiles within micro reactor devices.

The next section of this chapter deals with the description of how an electrochemical approach has been developed to carry out flow visualisation analysis on a micro scale.

4.1.2. Micro Flow Visualisation

A similar strategy was adopted as in the previous section, where the streamlines produced from an electrolysis reaction occurring at a series of microstrip electrodes were examined. Glass microchannels were used with typical dimensions of 100 – 500 μm in width, 50 – 100 μm in height and 3 – 6 cm in length. A similar imaging setup was

employed where a digital video camera was set up to image through an optical microscope. An electrolyte solution with the same chemical reagents as detailed above was flowed through the microchannels and the blue cation streams were imaged. Details of the fabrication, experimental conditions used in the studies, and results achieved, are given for a range of different microscopic cell designs.

4.1.2.1. Experimental Procedure

Measurements were carried out using cell designs as illustrated in Figure 4.9.

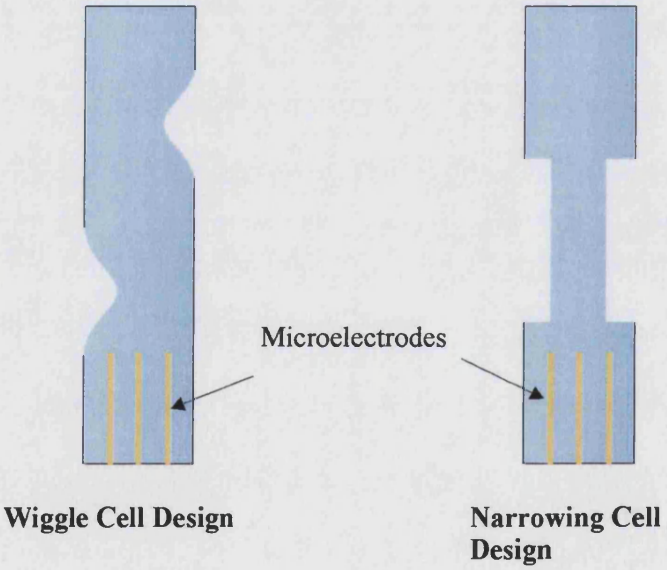

Fig. 4.9. Illustration of micro flow visualisation cell designs.

The cells were fabricated using Foturan Glass and details of the procedure can be found in Section 3.1.1.3. Gold microstrip electrodes with dimensions: length 3 mm and width 20 μm with spacing of 20 μm between each strip were fabricated using similar techniques as outlined in Sections 2.2 and 4.1.1.1. The microelectrode plate was sealed using a low-melting point wax to the microchannel structures. Images of two cells with channel dimensions can be seen in Figure 4.10.

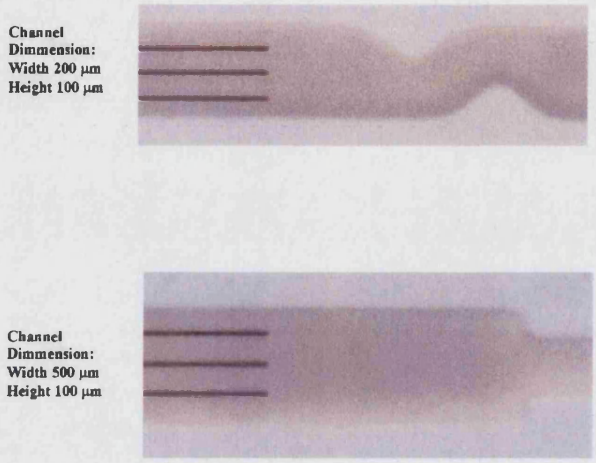

Fig. 4.10. Images of two micro flow cells used for flow visualisation measurements.

A gravity fed flow system, similar to that reported in the earlier section, was used to pump electrolyte solution through the micro cells. Reagents as detailed for the macro flow visualisation measurements were used and all electrochemical measurements were controlled using a built in-house potentiostat. The evolution of streams of electrolysed product were imaged through a microscope and recorded on a digital video camera (Sony PC100).

4.1.2.2. Results and Discussion

Experimental measurements were carried out using the two geometries shown in Figure 4.10. A solution of acetonitrile purged with nitrogen, containing 0.1 mol dm^{-3} TBAP and $1x10^{-2}$ mol dm^{-3} TMPD, was flowed through under the influence of gravity. Electrolysis measurements were performed at fixed volume flow rates similar to the analysis detailed above for the macro cell designs. Figure 4.11 shows the images

recorded for one of the micro cells using a volume flow rate of 1.25×10^{-4} $cm^3 s^{-1}$, under steady-state conditions. It was apparent from the results that a similar behaviour analogous to the macro cells was seen when examining the behaviour of the streamlines. Comparable thinning of the streams was observed as the streams evolved through the narrowing region of the channel.

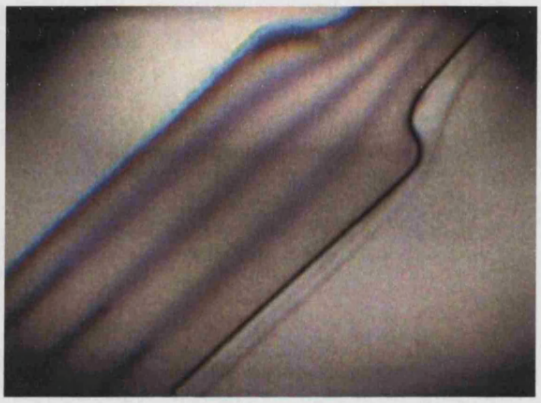

Fig. 4.11. Streamline images recorded at a volume flow rate of 1.25×10^{-4} $cm^3 s^{-1}$, under steady-state conditions.

A quantitative modelling approach to examine the diffusional broadening of the streams within the micro cells at various flow rates was analysed and compared with results achieved experimentally. The experimental images and the finite element calculations showed a similar behaviour of the streams. Figure 4.12 shows the results achieved by the cell design depicted in Figure 4.10(b), using the same experimental conditions employed in the measurements in Figure 4.11. An attempt to record the progress of the streamlines at various time intervals proved difficult, as the central velocity through the micro cells was very high (approximately 1 - 2 ms^{-1}), and the digital camera could not process the images within the time scale of the transport rates. However, an analysis concentrating on how a single stream observed for the experimental results compared to that seen for the simulations was carried out.

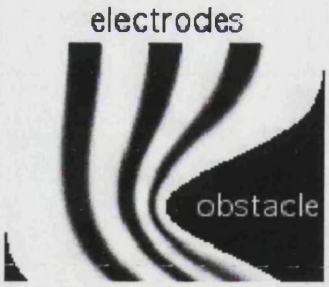

(a).

Image taken just after setting the potential distribution accross the central microstrip electrode.

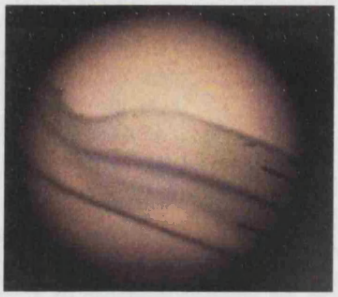

Image frame recorded after a time scale less than a millisecond.

(b).

Fig. 4.12. Flow visualisation results for a micro flow cell with a wiggle obstruction. **(a).** Results achieved using finite element simulations[2]. **(b).** Image observed from experimental analysis.

The results showed that an electrochemical approach to image flow within a micro environment was possible. However, due to the roughness of the Foturan Glass, images recorded during measurements were difficult to resolve, and only after careful construction of the flow cells could a reasonable image be seen and documented.

In this chapter, the ability to monitor fluid behaviour and transport of material within a micro volume was demonstrated using an electrochemical approach. A novel range of electrochemical flow visualisation techniques were introduced and the concept was able to prove that a subtle approach of imaging flow, without perturbing the fluid is possible.

---

[2] Simulated results achieved from calculations by I. E. Henley.

Chapter 5

Microelectrochemical Reactors (MECRs)

5.0. Introduction

Microelectrode sensors have recently been combined with hydrodynamic techniques to permit the development of new diagnostic tools in the field of electrochemistry[45]. The use of hydrodynamic electrodes brings considerable simplicity to experimental measurements made under steady-state or quasi-steady-state conditions. Their well-defined hydrodynamics permit the quantitative analysis of kinetic and mechanistic parameters of electrode processes, and electroanalysis can provide an optimal tool for combined spectroscopic/voltammetric sensing[28,165-168].

Many forms of hydrodynamic electrodes have been exploited in the past[169-172] and are detailed in Chapter 1. One versatile and highly successful hydrodynamic configuration exploited previously for voltammetric measurements is the channel flow cell[173,174]. In this arrangement a rectangular duct permits well-defined and predictable mass transport control to be achieved using a sensing electrode embedded smoothly in one wall of the duct through which electrolyte solution flows. Figure 5.1 depicts a typical channel flow cell setup.

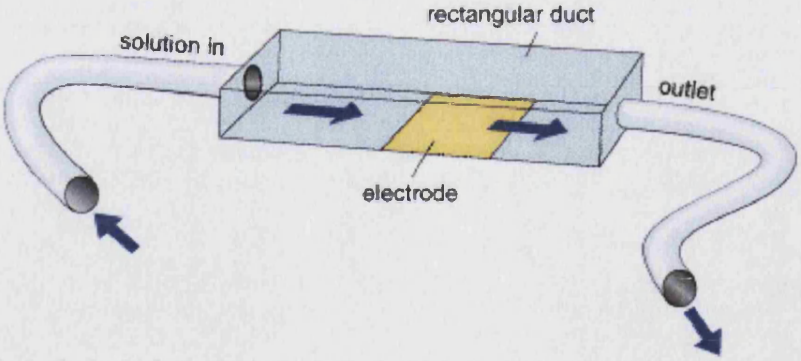

Fig. 5.1. Typical channel flow cell setup.

These electrodes offer much potential as they have the capacity to be applied in many applications. Illustrations exist in systems where analytical procedures that have a flow-through nature can be facilitated by these electrodes, for example following chromatographic separations[175,176]. They also can be used in spectroelectrochemistry with little adaptation, and have been exploited for electrochemical studies in conjunction with infra red (IR), UV/Visible, Electron Spin Resonance (ESR) and fluorescence spectroscopy[177-180]. Furthermore, the possibilities of irradiating electrode surfaces through solutions to learn of photoelectrochemical processes have been explored and much reported using the channel electrodes[174,181-186]. The methodology has also been exploited to interrogate processes occurring at insulator/electrolyte surfaces[187-192]. The recent application of channel electrodes for determining the mechanistic phenomena of processes such as two phase synthesis, phase transfer catalysis, metal extraction and colloid science in liquid/liquid systems will be detailed in the coming chapter.

During this period of development of hydrodynamic voltammetric strategies, the miniaturisation of reactors and cell designs for lab-on-a-chip applications has developed rapidly. This is largely due to the possibility of developing new analytical and synthetic approaches[193-195]. Much research has demonstrated a vast field of applications that include biochemical analysis, chemical synthesis, multiphase flow and high throughput screening.

A Recent approach that unites the benefits of these two significant research topics has been reported. In this approach a computer aided design has been utilised to predict the microfluidic behaviour around a microwire electrode sited within a narrow rectangular duct. The velocity profiles predicted by the calculations were used to solve the mass transport expressions for an electrochemically active material undergoing a transport limited reaction at the electrode/solution interface. Predictions of the variation of the transport limited current as a function of volume flow were found to be in good agreement to those obtained experimentally.

The above approach demonstrates the possibility of studying electrochemical measurements under microfluidic control in a well-defined and quantifiable method. In this chapter studies broaden to a novel class of Microelectrochemical Reactors (MECRs) will be presented.

5.1. The Development of MECRs

The above section provided an insight into hydrodynamic electrodes and the diversity of the channel electrode. In the next part of this chapter, the various fabrication techniques described in Chapter 3 will be utilised to develop a new electrochemical methodology for a range of MECR devices. The iterative procedure involved in developing these novel devices requires an understanding of how the materials used to fabricate the devices had a profound effect on the electrochemical response.

A quantitative description will be presented to give an insight into the electrochemical response seen and how designing of microelectrodes could optimise the response observed in MECR devices. Also, discussions of potential applications of MECRs will be illustrated to show promising techniques for mechanistic and kinetic analysis, as well as possible commercial relevance.

5.1.1. Development of Microelectrode Metal Films

There has been much literature published on the use of metal deposition techniques on a range of substrates and over the years this has been combined with photolithographic procedures to fabricate well-defined metal film patterns on substrates. Detailed in Sections 2.1 and 2.2 are the techniques adopted to produce well-defined microelectrodes for use in MECRs. These electrodes have demonstrated very good adhesive properties to glass as well as good continuity and conductivity. It was found that the use of a thin film of titanium before coating the glass with gold or platinum proved to give the adhesive properties of the metal films to glass surfaces. However, even though the technology allowed the capability of fabricating a vast range of electrodes, an understanding into how the electrode designs could have an effect on the electrochemical response inside a microchannel had to be established. This was of particular significance when the electrode would be in an environment where it would address micro litre volumes of electrolyte solution.

An analysis of the electrode design and geometry revealed that the contact lines to the microelectrodes sited within the channels were a critical aspect. To ensure reproducible electrochemical measurements, it was important to achieve a uniform potential across the whole microelectrode surface. As the metal films had a thickness in the order of nanometers, the resistivity was relatively high. To minimise any ohmic drop across regions of the electrode the contact lines were made as wide as possible and designed to contact the whole length of the electrode.

It was also found that the positions of the reference and counter electrode relative to the working electrode were critical, as this would affect the uniformity of the potential distribution across the working electrode during measurements within MECR devices. The electrode arrangement used in measurements depended on the application of the MECR device, but for most cases it was found that by placing all three electrodes

as close to one another improved the electrochemical signal. Figure 5.2 gives an image of a typical microelectrode design used.

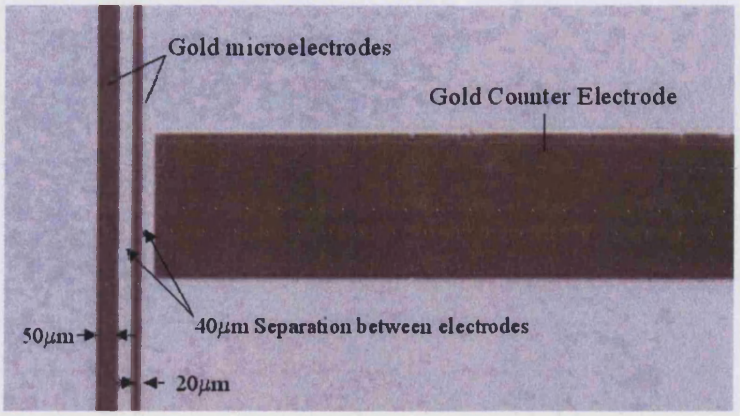

Fig. 5.2. Typical microelectrode design.

The necessity to understand the theoretical behaviour of microelectrodes and the mass transport that occurs at these electrode surfaces was critical[196]. As an electrode is miniaturised, the following phenomena are observed:

- Mass transport of electroactive species is varied from the linear diffusion normal to the electrode surface to the two or three dimensional diffusion.
- The current becomes smaller but is not proportional to the electrode area.
- The current density increases.

Sufficient work has been done in stagnant solutions to show the electrochemical response of microelectrodes[5,196], in this section a quantitative analysis observed for microband electrodes fabricated using the approach outlined in Sections 2.1 and 2.2 is presented. An analytical expression relating the peak current observed during a linear sweep voltammogram, at a microband electrode, to the scan rate has been used to interrogate the electrochemical response observed for the metal films. A plot of the normalised peak current density (j_p) against p which is the ratio of the potential scan rate

and diffusion rate has been reported by Aoki[196], and can be defined by the following equations:

$$Normalised\ Peak\ Current = \frac{j_p x_e}{2nF[O]D_o}$$

$$where\ j_p = \frac{i_p}{wx_e}$$

Equ. 5.1.

$$p = \sqrt{\frac{nFa^2 v}{RTD_o}}$$

$$where\ a = \frac{x_e}{2}$$

Equ. 5.2.

where *Ip* is the peak current, *w* is the electrode width, x_e the electrode length, *n* the number of electrons involved in the measurements, *F* the Faraday constant, *v* the scan rate in V/s, *R* the gas constant, *T* the temperature, and D_o the diffusion coefficient.

A solution of acetonitrile containing 1.126×10^{-3} mol dm^{-3} TMPD and 0.1 mol dm^{-3} TBAP as background electrolyte was prepared and purged with pre-dried nitrogen before use. Two microbands were fabricated of length 20 and 40 μm and both had a width of 500 μm, (see Figure 5.3 for images). The electrodes had a glass well built around them in which the electrolyte solution was poured into. A platinum counter electrode was immersed in the solution and clamped in place. Figure 5.4 details the setup used for the measurement.

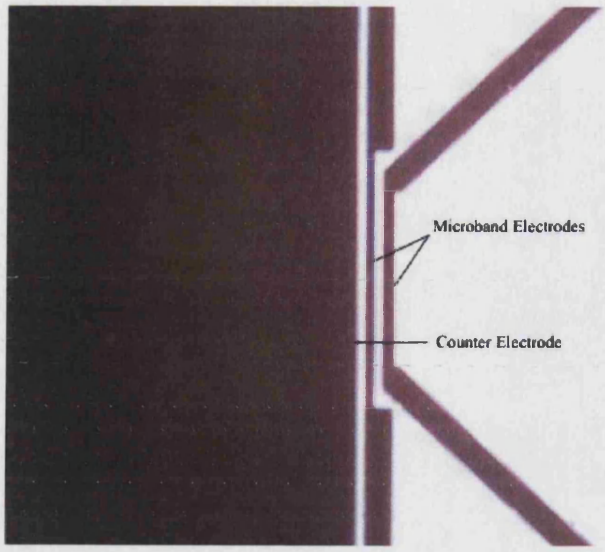

Fig. 5.3. Image of microband electrodes.

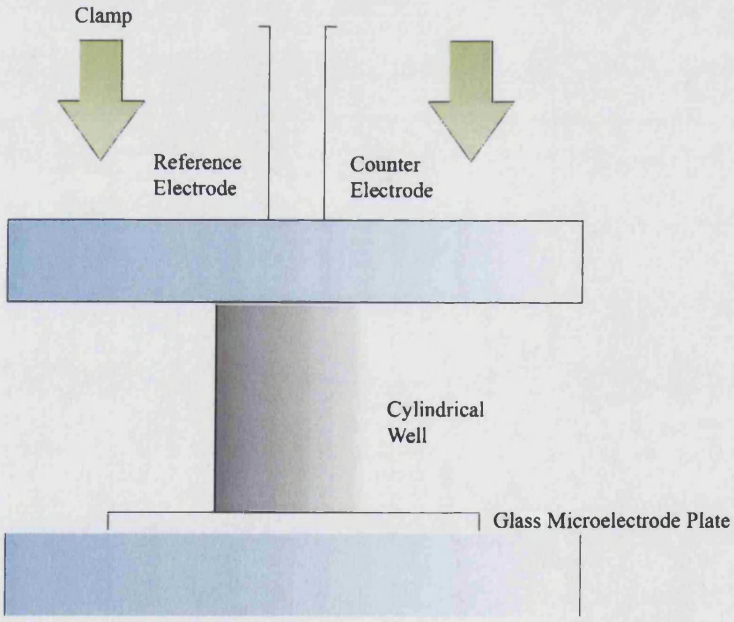

Fig. 5.4. Experimental setup for microband peak current analysis.

A series of linear sweep voltammograms were recorded at various voltage scan rates ranging between 5 – 500 mVs^{-1}. Figure 5.5 shows the typical response observed for the two microbands. For a stagnant system, the variation of the peak current density (j_p) as a

function of dimensionless potential scan rate (p) should obey the analytical expression predicted for a microband electrode as stated by Aoki et al[196]. Figure 5.6 describes the dimensionless analysis plot and good agreement can be seen between the values predicted and those recorded experimentally.

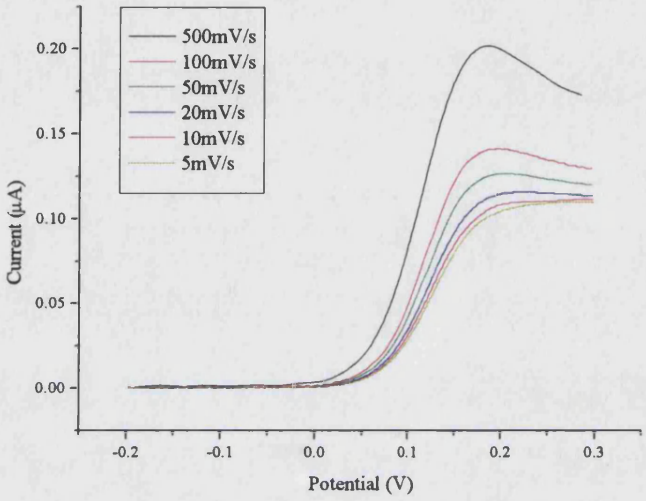

(a).

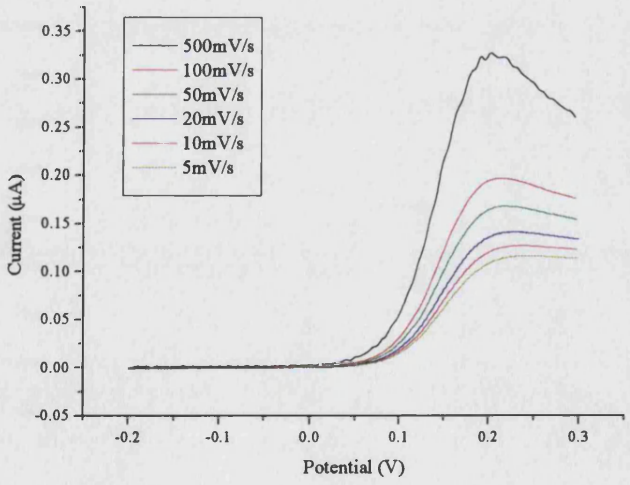

(b).

Fig. 5.5. Linear sweep voltammograms recorded varying potential scan rates, using a solution of acetonitrile containing 1.126 x 10^{-3}M TMPD and 01.M TBAP as background electrolyte, **(a).** 20 μm working electrode, **(b).** 40 μm working electrode.

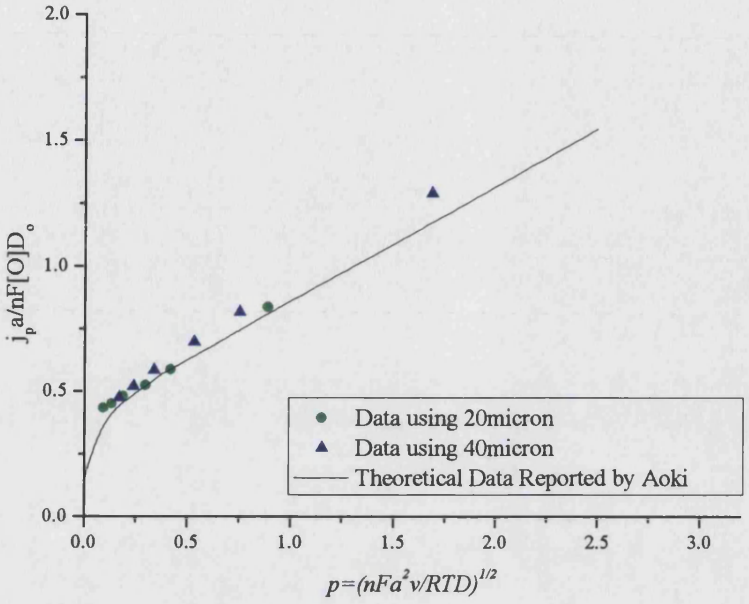

Fig. 5.6. Dependence of peak current density, j_p, of linear sweep voltammograms on the dimensionless variable p at a microband electrode.

The analysis showed that the electrodes being fabricated via this method behaved towards an electrochemical measurement, in accordance with the theory for a microelectrode. In the coming sections, the developed approach for making these microelectrodes will be combined with a series of microchannels to develop a novel range of Microelectrochemical Reactor devices.

5.1.2. Thin glass Microchannel Electrodes

An initial approach was adopted to fabricate a range of glass channel electrodes, as detailed in Section 3.1.1. The construction involved cementing a series of cover plates on a glass base plate to create a cavity which had dimensions in the range of: width 10 mm – 100 μm, height 300 – 100 μm and length 3 – 7 cm. Figure 5.7 details a schematic of the cell design.

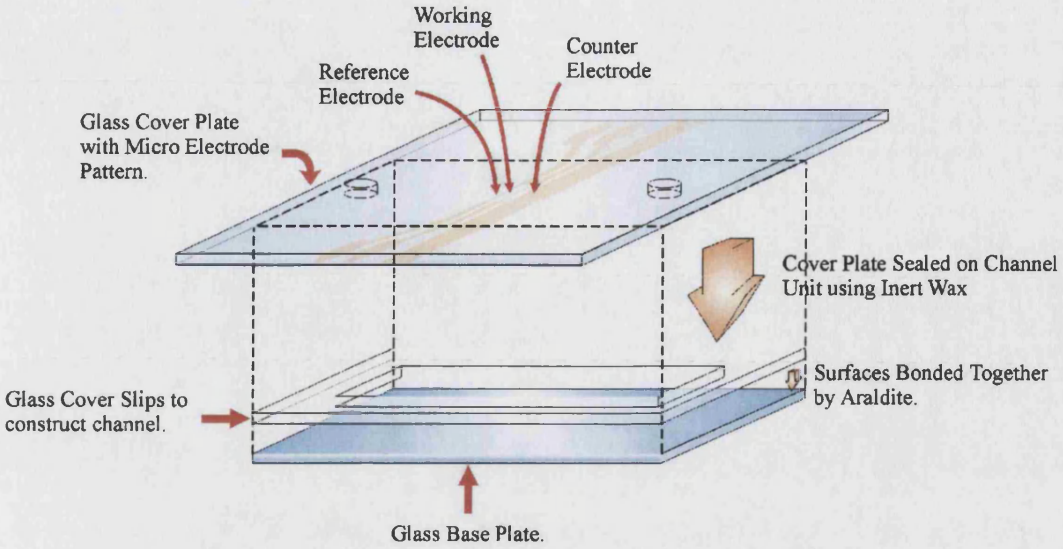

Fig. 5.7. Schematic of a thin glass channel electrode.

This methodology was found to be a cost effective and simple way to fabricate a vast range of designs rapidly. The technique also allowed a pragmatic means of screening a vast range of channel electrode dimensions. An image of a channel fabricated using this methodology is shown in Figure 5.8, where the dimensions of the channel are: width 100 μm, height 100 μm and length 5 cm.

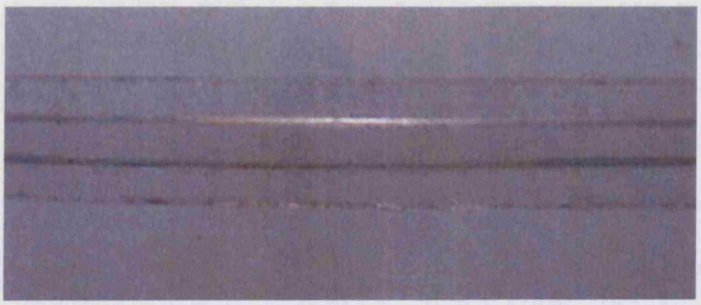

Fig. 5.8. Image of a typical channel electrode fabricated using thin glass cover slips.

Detailed in Table 8 are the range of channel electrode dimensions, the chemical reagents and experimental conditions used. All electrodes were fabricated from platinum using an Argar Sputterer, as detailed in Sections 2.1 and 2.2.

Solution of TMPD in ACN (mol dm^3)	Working Electrode Length/Width (mm)	Cell Height (μm)	Cell Width (mm)	Flow Rate Range (cm^3/s)
0.0005	2/10	200	10	0.1 – 0.001
	2/5		5	0.1 – 0.001
	2/2		2	0.1 – 0.001
	2/1		1	0.1 – 0.001
0.001	2/10	200	10	0.1 – 0.001
	2/5		5	0.1 – 0.001
	2/2		2	0.1 – 0.001
	2/1		1	0.1 – 0.001
0.0005	3/10	200	10	0.1 – 0.001
	3/5		5	0.1 – 0.001
	3/2		2	0.1 – 0.001
	3/1		1	0.1 – 0.001
0.001	3/10	200	10	0.1 – 0.001
	3/5		5	0.1 – 0.001
	3/2		2	0.1 – 0.001
	3/1		1	0.1 – 0.001

Table 8. Experimental conditions and cell dimensions used with thin glass channel electrodes.

Measurements were carried out using solutions of acetonitrile with 0.1 mol dm^{-3} TBAP and a range of concentrations of TMPD as detailed in Table 8. Prior to beginning measurements the solutions were degassed with nitrogen. The electrolyte solutions were then flowed through the channels under the influence of gravity and a potentiostat built in-house was used to investigate the electrochemical response for these channel electrodes.

Analysis of the current-voltage curves, at a voltage scan rate of 10 mVs^{-1} and their change in magnitude relative to volume flow rates were studied. From the current-

voltage curves an expected change in the transport limited current as a function of volume flow was observed. Measurements were carried out to determine the transport limited current for a wide range of volume flow rates to determine whether the cells showed an analogous behaviour to the analytical prediction described in the Levich Equation.

$$i = 0.925nFwD_o^{2/3}[O]_{Bulk}x_e^{2/3}\left(\frac{V_{fr}}{h^2 d}\right)^{1/3}$$

Equ. 5.3.

Figure 5.9 shows the results achieved using an electrode with a 2 mm length and a range of cell dimensions as detailed in Table 8. From the results a linear relationship between the transport limited current and the cube root of volume flow rate can be seen.

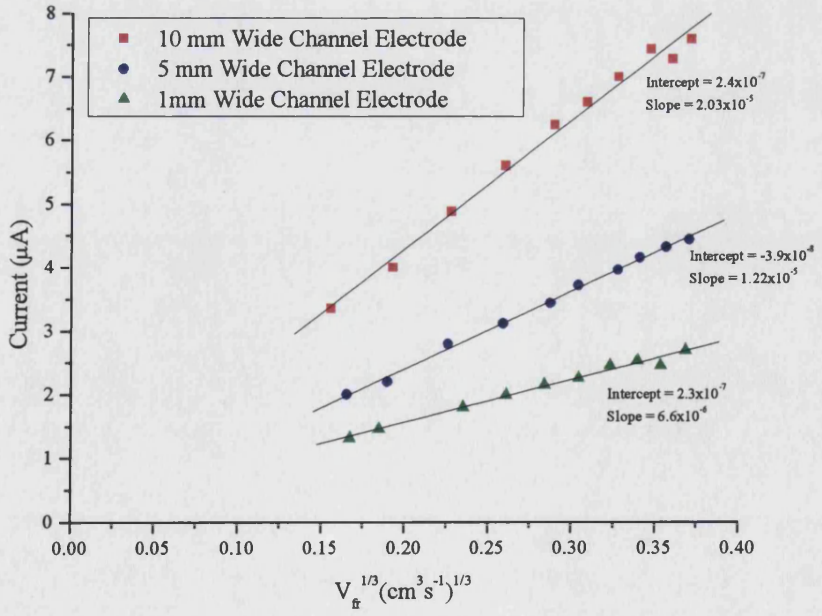

(a).

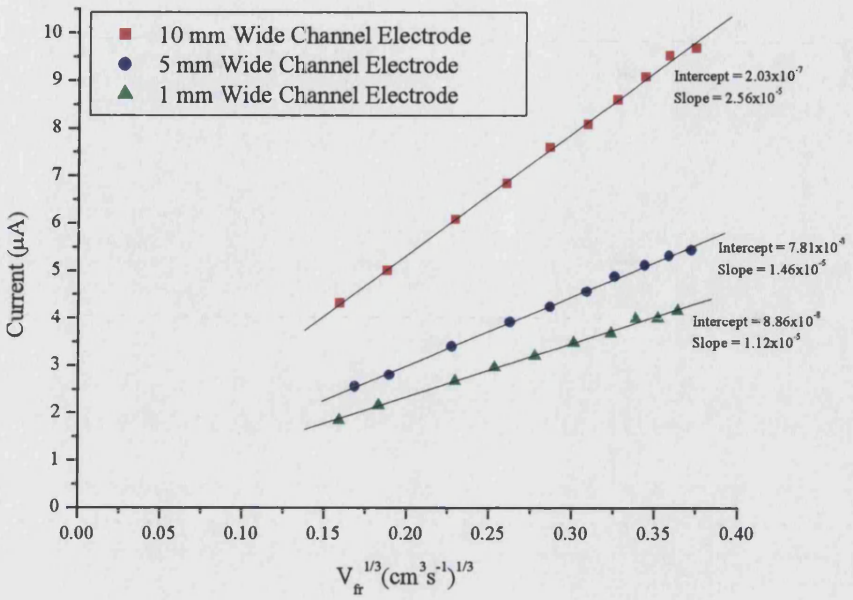

(b).

Fig. 5.9. Levich plots recorded at a range of thin glass channel electrodes widths, **(a).** 0.5mM TMPD in Acetonitrile, **(b).** 1mM TMPD in Acetonitrile.

The above approach demonstrated the possibilities of fabricating and screening a vast range of channel electrode geometries. However, due to the bonding process and the channel fabrication technique, there was some limitation to the feasibility of making the cells with dimensions less than 100 μm. Nevertheless, the cells still proved to show a good agreement to reported behaviour seen in channel electrodes[120].

In the next section, an approach to overcome the limitations of the dimensions fabricated with this technique was developed, and the use of Foturan Glass to fabricate precise dimensions of the microchannels was used. A discussion of the electrochemical response that was observed will also be given.

5.1.3. Foturan Glass Microchannel Electrodes

Having established an electrochemical response for microelectrodes under stagnant conditions to show quantitative agreement, as detailed in Section 5.1.1, experiments were conducted to interrogate the behaviour of the electrodes within a microchannel under steady flow conditions. The MECR devices were fabricated as reported previously in Section 3.1.1.2 using Foturan Glass, and a practical design is shown in Figure 5.10.

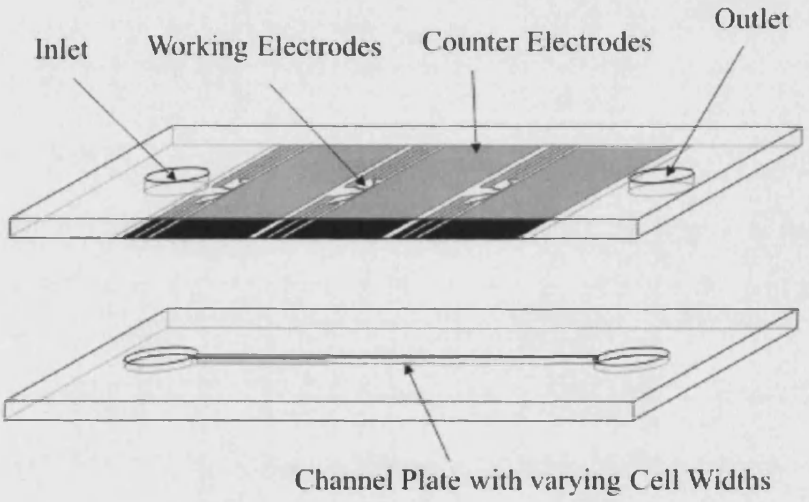

Fig. 5.10. Schematic design of MECR device made from Foturan Glass

Initial measurements were carried out using rectangular ducts, which were etched into Foturan Glass plates to yield a range of channel dimensions: height 80 – 200μm, width 100 – 500μm and length 1 – 3 cm. The same approach of sealing the cells with wax was used as discussed above. A solution of acetonitrile containing 0.1 mol dm^{-3} TBAP and a range of concentrations of TMPD were flowed through the cells under the influence of gravity. Electrochemical measurements were again carried out using a built in-house potentiostat.

Linear sweep voltammograms were recorded using a similar strategy as detailed in the previous section, and Figure 5.11 shows the current-voltage curves achieved using

$1x10^{-3}$ mol dm^{-3} TMPD, at a voltage scan rate of 10 mVs^{-1}. The results shown were recorded using were two channel dimensions; (a). width 500 μm, height 100 μm and length 3cm, and electrode dimensions: width 500 μm and length 20 μm, (b). width 125 μm, height 100 μm and length 3cm, and electrode dimensions: width 125 μm and length 20 μm. It can be seen that a change in the transport-limited current was observed for the different volume flow rates.

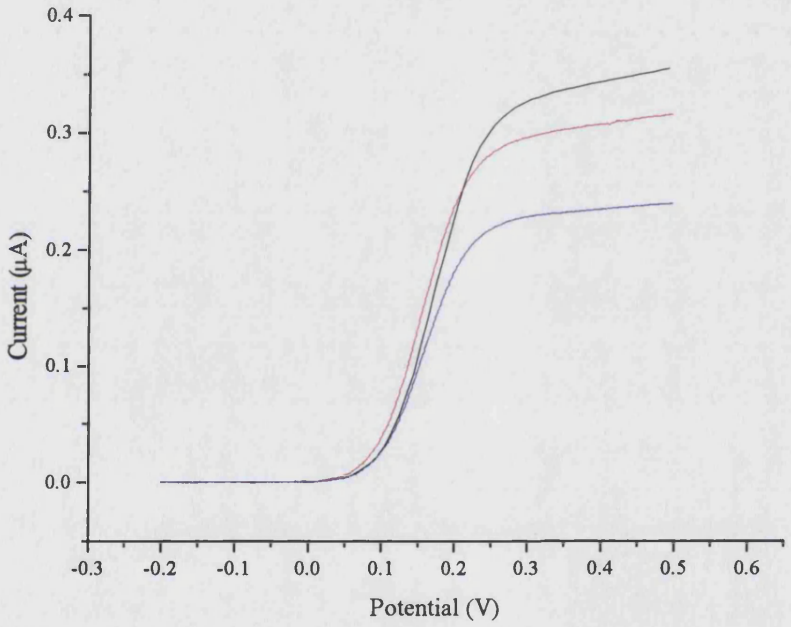

(a).

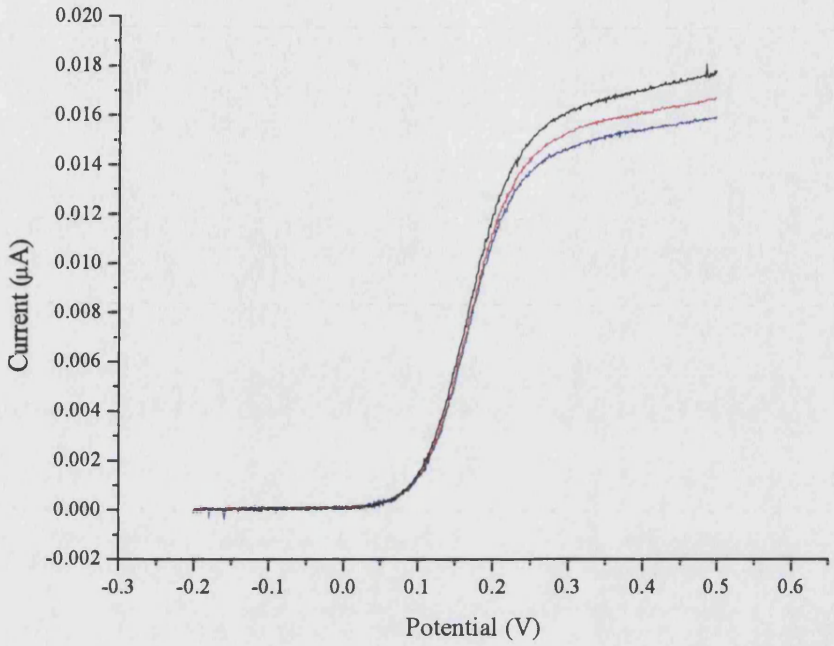

(b).

Fig. 5.11. Current-Voltage curves recorded at a range of volume flow rates, using a solution of $1x10^{-3}$ mol dm^{-3} of TMPD in acetonitrile. **(a).** 500 wide channel, **(b).** 125 mm wide channel.

Further analysis of the transport limited current relative to the cube root of volume flow rate showed that there was a linear relationship analogous to that predicted by the Levich Equation. Figure 5.12 shows the results achieved for a range of channel widths with a height of 100 μm and length 3cm. The working electrode had a width that varied with the channel width and a length of 20 μm. The data shown were recorded using a solution of acetonitrile with a $1x10^{-3}$ mol dm^{-3} concentration of TMPD.

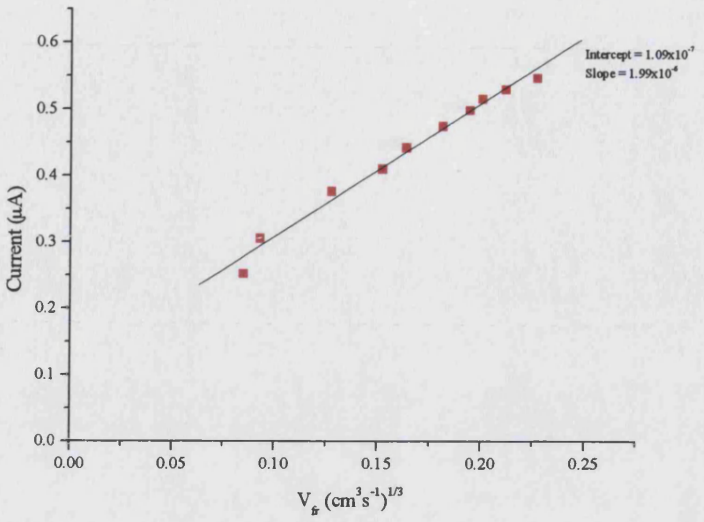

(a).

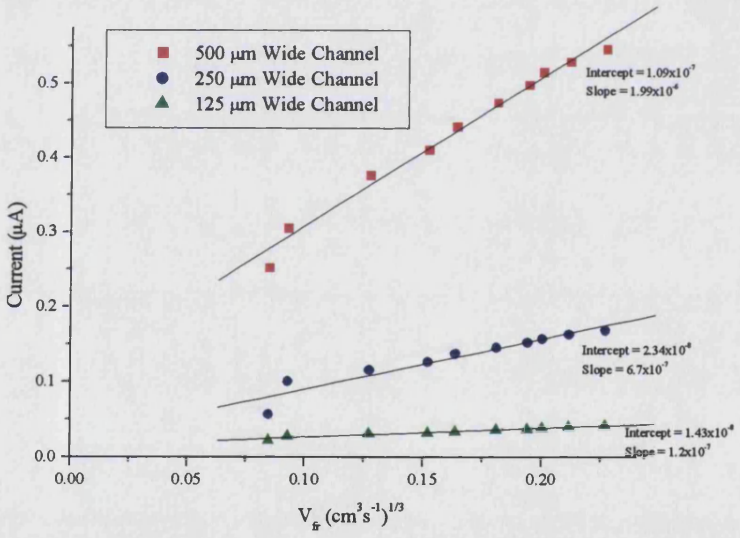

(b).

Fig. 5.12. Levich plot observed for a range of MECRs fabricated from Foturan Glass. The measures were carried out using a solution of acetonitrile containing $1x10^{-3}$ mol dm^{-3} TMPD and a microband electrode with a length of 20 μm. **(a).** Measurements observed for a microchannel with dimensions: width 500 μm, height 100 μm and length 3 cm. **(b).** Measurements observed for a range of channel widths.

The electrochemical response seen for the MECRs produced with Foturan Glass demonstrated an electrochemical behaviour that was equivalent to that of the channel electrode reported previously[120]. The technique demonstrated the capability of fabricating the devices with precision to give desired dimensions, which was not possible when using the approach reported in the previous section. However, due to the roughness of the cell walls of the microchannels caused by the wet etching process, a quantitative description of the mass transport occurring within these devices was not carried out.

In the next section a description of the process used to make Surlyn microchannels will be presented. As the channels made using this approach gave well-defined and uniform channel profiles, a quantitative description of the cells is also given.

5.1.4. Surlyn Microchannel Electrodes

The fabrication of microchannels from Surlyn thin films was described in Section 3.1.4, where the technique was utilised to make channels with dimensions: width 100 μm –1 mm, height 20 – 250 μm. Measurements and experimental conditions, as outlined in the previous two sections, were used to study the mass transport properties in the microchannels made with this approach.

A range of microband electrode lengths were fabricated: 20 – 100μm using the methodology outlined in Sections 2.1 and 2.2, and a typical image of a set of microband electrodes is shown in Figure 5.13.

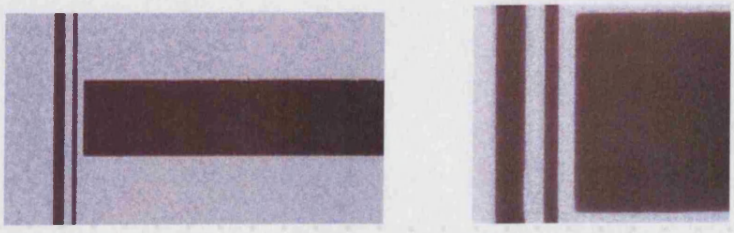

Fig. 5.13. Image of microband electrodes.

All the microband electrodes were positioned in the MECR devices after a lead in length from the inlet, in order to establish Poiseuille flow[122]. Surlyn films were aligned over the microelectrode plates and a glass cover plate with inlet and outlet openings was clamped to sandwich the Surlyn film between the two glass plates and create a sealed channel unit. The reagents employed in the studies were acetonitrile, TMPD and TBAP. In all cases, the solutions were degassed with pre-dried nitrogen[48] for 15 minutes, before flowing under gravity[197,198] through the microchannels. Voltammetric measurements at the microband electrodes were carried out using a potentiostat built in-house.

The electrolysis reaction of TMPD in acetonitrile was studied with a range of microband electrodes and was used to evaluate the variation of the transport-limited current as a function of volume flow rate. Figure 5.14 shows typical steady-state voltammograms recorded at a voltage scan rate of 10mV/s, for a microband electrode of length 50μm and width 100μm.

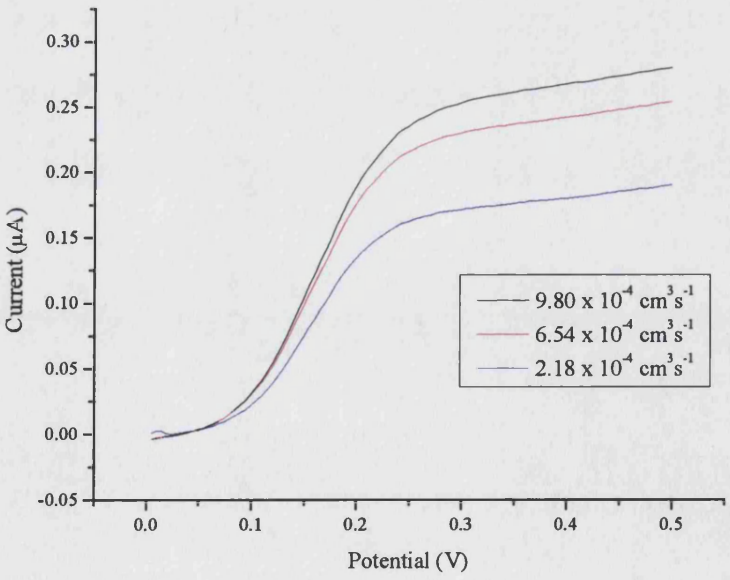

Fig. 5.14. Steady-state voltammograms recorded for 0.472mmol TMPD solution, at different flow rates for a MECR of the dimensions: height 40μm, width 100μm and length 3cm. The microband used in this measurement had the dimensions: length 50μm and width 100μm.

The microchannel had the dimensions: height 40μm, width 100μm and length 3cm. The volume flow rates used were in the range 1 x 10^{-4} to 1 x 10^{-3} cm^3s^{-1}, and the solution contained 0.472mmol of TMPD and 0.1M TBAP as a background electrolyte. It can be seen that the transport limited current depends strongly on the transport rate through the cell and this behaviour is analogous to that observed in the simulations reported for Microelectrochemical Reactors[107], as well as to that reported for macroscopic channel electrodes[46,198].

A series of voltammetric measurements was conducted using a wide range of MECR dimensions to determine and quantify the variation of transport limited current as a function of volume flow rate. Figure 5.15 and 5.16 reveal a typical set of data recorded for two different MECR devices. The data shown in Figure 5.15 were obtained using a MECR device with the following dimensions: height 40μm, width 100μm and length 3cm. In the case of Figure 5.16, the analysis was carried out using a MECR device that had the following dimensions: height 40μm, width 200μm and length 3cm. Both Figures show sets of data recorded using two microband electrode lengths, which were 27.5 μm and 35 μm.

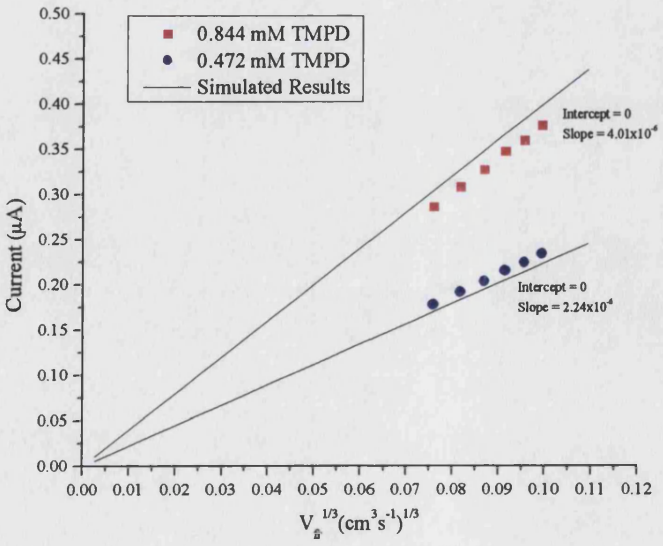

(a).

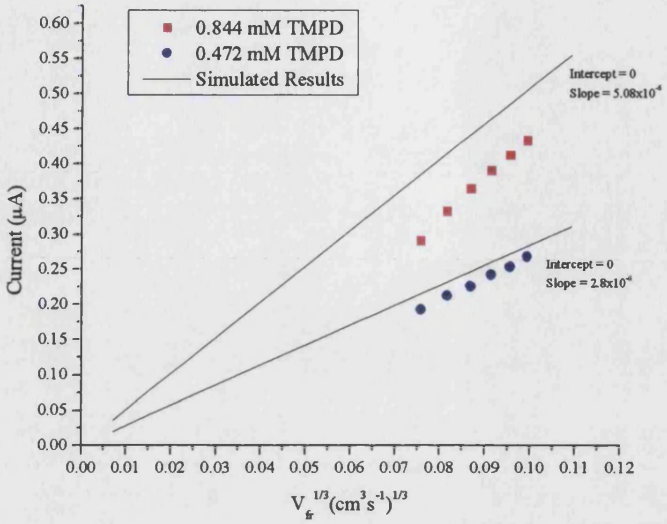

(b).

Fig. 5.15. Experimental and theoretical behaviour for the transport limited current as a function of flow rate in a MECR of dimensions: height 40 μm, width 100 μm and length 3cm. The microband electrode used in this measurement had the dimensions: **(a).** length 27.5 μm and width 100 μm, **(b).** length 35 μm and width 100 μm.[3]

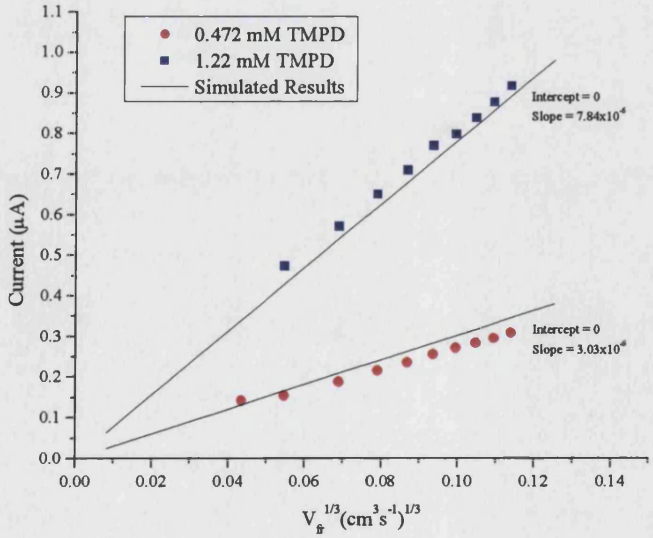

[3] Simulated results achieved from calculations by I. E. Henley.

(a).

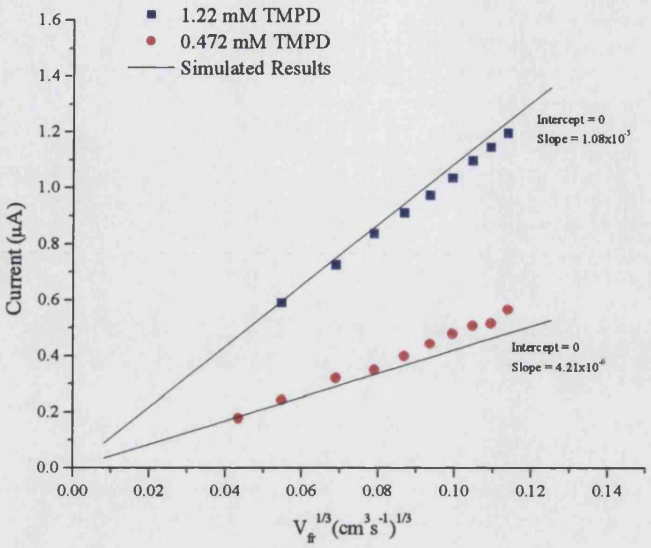

(b).

Fig. 5.16. Experimental and theoretical behaviour for the transport limited current as a function of flow rate in a MECR of dimensions: height 40 μm, width 200 μm and length 3cm. The microband electrode used in this measurement had the dimensions: **(a).** length 27.5 μm and width 200 μm, **(b).** length 35 μm and width 200 μm.[4]

In all the measurements linear sweep voltammograms were recorded at a voltage scan rate of 10mV/s to establish the transport limited current at varying volume flow rates. Both devices show a variation of the transport limited current as a function of the cube root of the volume flow rate and, in both configurations, the transport-limited current is seen to be proportional to the cube root of the volume flow rate. The relationship of the transport limited current to the concentration of TMPD solution is also illustrated in Figures 5.16 and 5.17 and is proportional as expected. This was observed for all the different MECR dimensions for a range of microband lengths.

[4] Simulated results achieved from calculations by I. E. Henley.

The results shown in Figure 5.15 and 5.16 have been overlaid with the three dimensional finite element simulated results to show good agreement. It is interesting to note that the response observed is in accordance to the Levich analysis[46], which predicts the response for a macro channel electrode that assumes only a two dimensional velocity profile due to cells having a much larger width than height. This is valid for electrodes cited centrally on the bottom wall of the macroduct where the current density across the electrode is considered to be constant.

In the case of the MECR configuration, the electrode is stretched across the whole cell width, where the hydrodynamic boundary layer would significantly influence the transport properties and current flow at the electrode. Even though the electrode is stretched across the whole width of the device a response due to the edge effects is not noticed as predicted by the simulations. This can be understood when examining the current density across the electrode. Figure 5.17 illustrates the finite element simulations results reported[107], that show the calculated current density across an electrode for various cell widths for a know volume flow rate. The data only show the current density across half the electrode width as the effect is considered to be symmetrical.

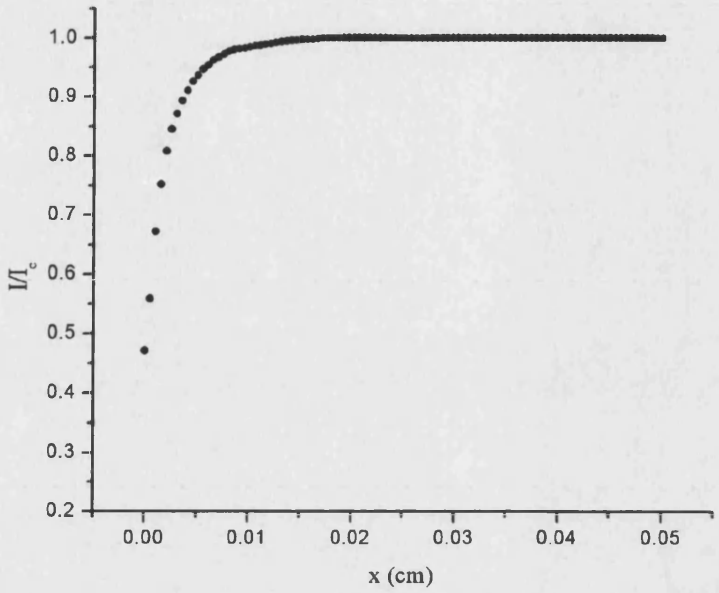
1.0
0.9
0.8
0.7
0.6
0.5
0.4
0.3
0.2
I/I_c
0.00
0.01
0.02
0.03
0.04
0.05
x (cm)

(a).

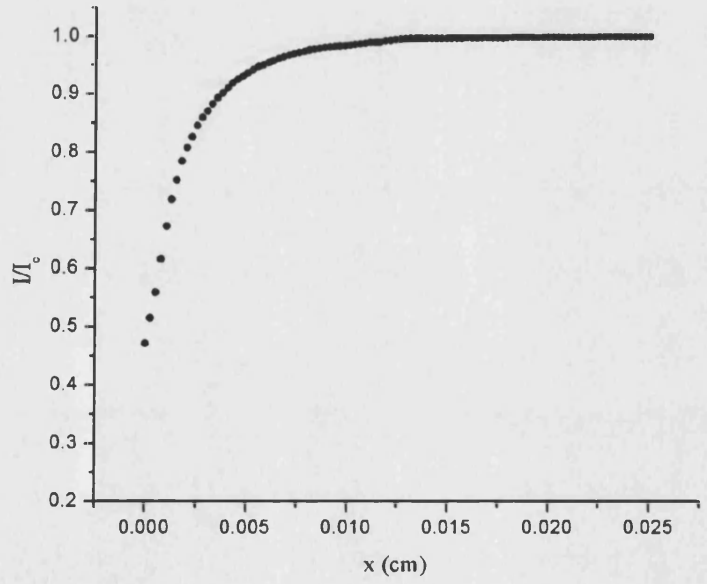
1.0
0.9
0.8
0.7
0.6
0.5
0.4
0.3
0.2
I/I_c
0.000
0.005
0.010
0.015
0.020
0.025
x (cm)

(b).

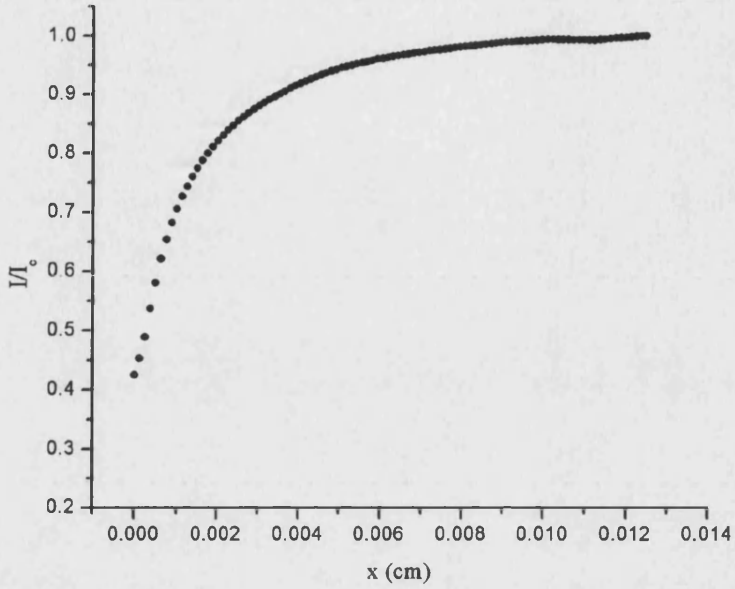

(c).

Fig. 5.17. Normalised current density plots integrated across an electrode in **(a).** 1000μm, **(b).** 500μm and **(c).** 250μm wide channels with volume flow rates of 2.6×10^{-3}, 1.2×10^{-3} and 5.0×10^{-3} cm^3/s respectively.[5]

From the above data, it can be seen that decreasing the cell width has a profound effect on the current density profile across the electrode, where the smaller the channel width, the greater the importance of the edge effect. An initial interpretation would suggest that smaller channel widths would have greater edge effects leading to a deviation from the Levich prediction[46]. The assumption of constant current density across the whole electrode width is no longer valid. However, it was found that even though transport of material at the edges of the channel is slower than that at the centre, giving rise to the current density profile, the mass transport relative to the volume flow rate still obeys a cube root relationship across the whole channel width. This meant that at any given point across the channel width, the transport-limited current would be

[5] Simulated results achieved from calculations by I. E. Henley.

proportional to the cube root of the volume flow rate. As a result the predicted and measured behaviour was found to agree with the Levich equation[28,46].

In this section, detailed analysis of the electrochemical response observed in MECR devices has been discussed. The fluid dynamics and convective-diffusional behaviour of mass transport has been proven to show good agreement with theoretical finite element calculations. Overall the development of this novel range of MECR devices has shown to be an effective means of detection in microfluidic environments and has proven to provide an optimum response to electrochemical analysis. In the next section, the methodology of MECR technology has been taken one stage further to demonstrate possible applications.

5.2. MECR Applications

The ongoing development of the lab-on-a-chip concept has had a profound effect on today's outlook into the technological advances it potentially holds. The motivation behind the development of MECRs was to bring about a novel technique that allows the possibilities of detecting and probing processes occurring in microfluidic environments. The potential benefits in advancing the field of electrochemistry towards a highly sensitive and versatile methodology can bring about interesting studies that until now could not have been carried out with such ease, accuracy and sensitivity[28]. In this next section, a discussion into some of the potential applications where MECRs can prove to be useful will be discussed and preliminary data will be presented.

5.2.1. Generator/Collector Measurements in MECRs

The kinetic studies of chemical reactions progressing through intermediate states have been given much attention[28]. Double electrode systems are particularly useful for

this purpose and have been reported to yield useful mechanistic information[28,120]. The adaptation within a channel electrode has been a well-researched area, where intermediates produced at a generator (upstream) electrode are transported to the downstream electrode where they react further. This approach has been used in the past to study short-lived species where the quantity reaching the second electrode depends on any homogenous reactions or decomposition occurring in solution. The prospects of developing this methodology towards MECRs can bring about many advantages. Due to the nature of micro devices, the transport rates within the cells have been calculated to be extremely high, where in some instances a central velocity of about 1-2 m/s can be achieved. The resolution of studying time resolved measurements, for short-lived species, could be taken to another level, where the possibilities of probing intermediates state that have not been previously reported could be possible.

An approach to develop MECR devices to carry out electrochemical measurements using two electrodes will be discussed in this section. Similar strategies as reported in the previous section for developing micro channels and microelectrodes were employed. As the measurement consists of two working electrodes rather than just one, more studies had to be carried out to determine the optimum electrode geometry to achieve a sensible electrochemical signal.

Micro channels were fabricated using techniques outlined in Sections 3.1.1.3 & 3.1.4 to yield a range of dimensions: width 100 – 500 μm, height 20 – 150 μm and length 1 - 3cm. A series of two working electrode designs was fabricated with varying electrode lengths and separations between the two working electrodes. Measurements were performed using a bipotentiostat which was either built in-house, or an ECO CHEMI PGSTAT 100. The upstream microband electrode (WE1) acted as a generator and the downstream microband electrode (WE2) as a collector electrode which were analogous to measurements reported at devices such as the rotating disc electrode and double channel electrode[28]. A typical schematic of the design can be seen in Figure 5.18.

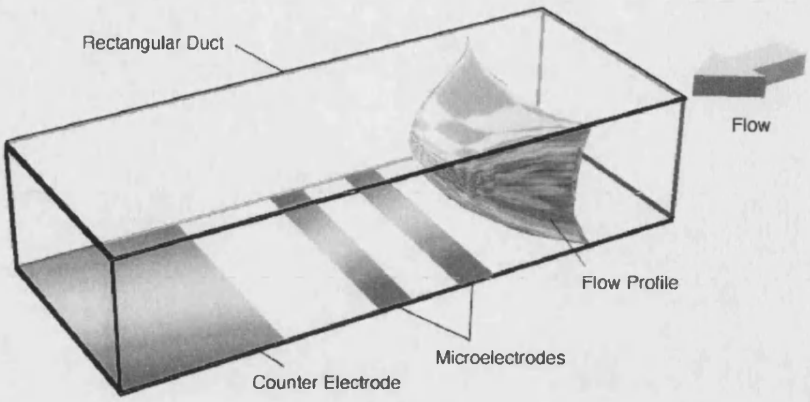

Fig. 5.18. Schematic of Double Electrode MECR.

Finite element models have been reported to show that the voltammetric response seen in a two-electrode system can be influenced by the offset potential of the downstream (collector) electrode. The results observed from the modelling, where an effect on the behaviour of the generator and collector electrode was compared for various offset potentials. The data reveal that at small offset potentials, an oxidation will be performed on both electrodes and the opposite process at the collector electrode can only be achieved if a sufficiently high offset potential is chosen. This is because the potential difference between the solution and the collector electrode can be influenced by the solution's distribution of potential, which can vary across the length of the channel between the reference and the counter electrode.

From the above simulations it was apparent that care needed to be taken with regards to choosing offset potentials while investigating double electrode voltammetric responses. Preliminary measurements were performed using a 250 μm wide and 80 μm high channel electrode that used microband electrodes with dimensions: 250 μm wide and 20 μm long generator electrode, 250 μm wide and 60 μm long collector electrode. The two working electrodes had a separation of approximately 50 μm. An acetonitrile solution containing 0.1 mol dm^{-3} TBAP and $1x10^{-4}$ mol dm^{-3} TMPD was used for the measurements. The solution was degassed with pre-dried nitrogen[199] for 15 minutes,

before flowing under gravity[200,201] through the MECR device. Measurements were performed under the following potentiostatic conditions:

WE1	TMPD	$TMPD^+ + e$
WE2	$TMPD^+ + e$	TMPD

The generator electrode (WE1) was cycled to a potential of 0.45V at 10mV/s and the collector was offset to hold at a potential of -0.2V. These correspond to the transport limited oxidation of TMPD and reduction of $TMPD^+$ at WE1 and WE2 respectively. Figure 5.19 illustrates the cyclic voltammograms recorded at three different volume flow rates, using a solution of acetonitrile containing $1x10^{-4}$ mol dm^{-3} TMPD and 0.1 mol dm^{-3} TBAP. The response observed was in accordance with larger devices (where the transport is approximated by a two dimensional model) that have been predicted to behave in a similar way to several theoretical and numerical studies.

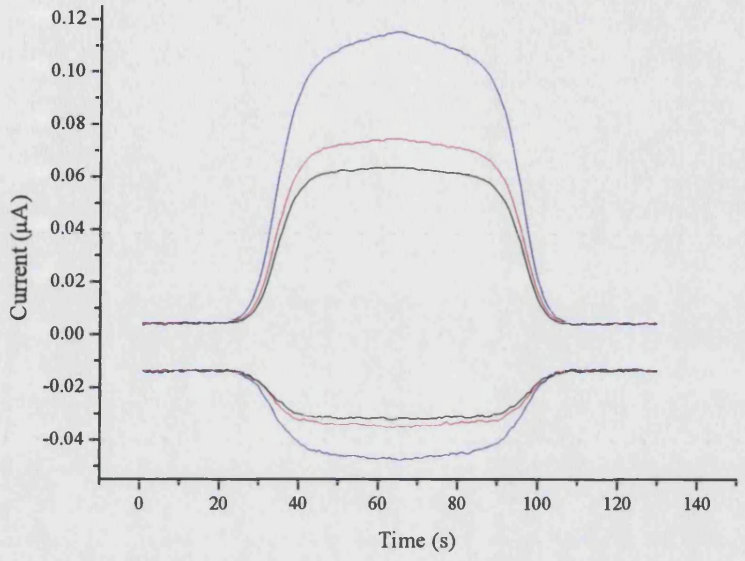

Fig. 5.19. Current variation at the generator and collector electrodes in a 250 μm wide channel using electrolyte solution containing $1x10^{-4}$M TMPD at three different volume flow rates. Working electrodes had a separation of 50 μm and dimensions: for WE1, width 250 μm and length 20 μm, for WE2, width 250 μm and length 60 μm.

Several measurements were repeated in the same manner as mentioned above for a range of volume flow rates and the collection efficiency (C_e) was measured as a function of volume flow rate through the cell.

$$C_e = \frac{Current\ WE2}{Current\ WE1}$$

Equ. 5.4.

It was found from Figure 5.20 that the collection efficiency was dependent on the volume flow rate, where an increase in collection efficiency was observed as the volume flow rate decreased. This observation can be explained in terms of mass transport, where at the high flow rates generated products are given much less time to diffuse away

into bulk solution before being addressed by the collector electrode. The collection current is still being limited, as the time that a given volume of solution remains over the electrode surface is being limited by the high volume flow rates. However, the opposite is true for relatively slow volume flow rates where material is been given more time to diffuse out into bulk solution before reaching the collector electrode. Nonetheless, because a given volume of solution is allowed more time whilst passing over the second electrode, material is given time to diffuse back in from bulk solution. Thus more material is collected and regenerated to TMPD giving rise to an increase in the collection efficiency.

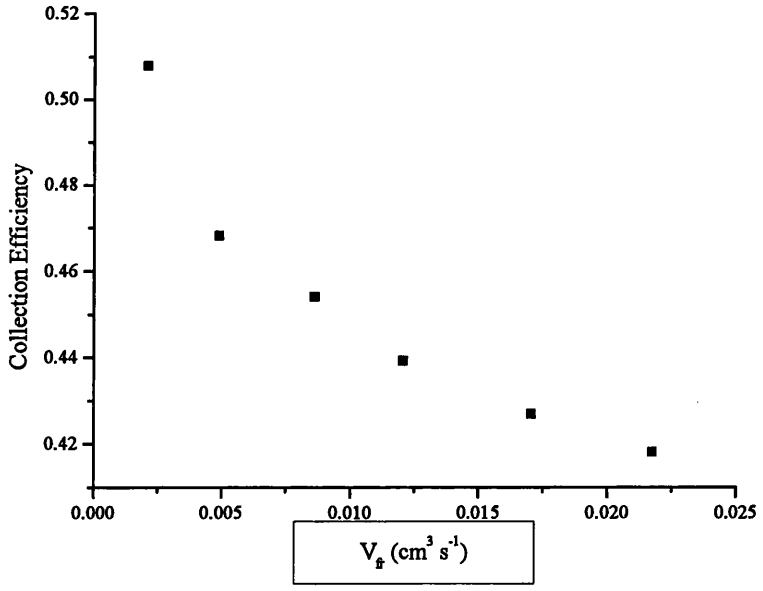

Fig. 5.20. Variation of collection efficiency as a function of volume flow rate for a 250 μm wide cell using $1x10^{-4}$M TMPD.

5.2.1.1. Voltammetric Manipulation for signal Enhancement.

Interrogating systems on a micro volume scale can bring about many practical hurdles in sensing materials in solution. In the above section, the concept of the channel

electrode and its application on a micro scale has been exploited. The use of MECRs will be discussed to illustrate the development work that has been done to broaden its application for use in enhancing electrochemical signals with the use of a series of microband array electrodes.

The concept of regeneration of material can show considerable benefits in applications where this can lead to amplifying a signal which is being monitored in solution. Figure 5.18 details a schematic of the proposed MECR design which incorporate a double electrode system. As detailed in the Figure, microband electrodes are placed on one wall of the device where the first electrode is set at a potential to electrolyse a species and the other to regenerate the electroactive material. By placing a series of these pairs of electrodes along the device it should be possible increase the turn over of material being electrolysed and regenerated. This can in turn optimise the conditions to determine the amount of electroactive species present in a given solution down to trace amounts.

Fingered sets of five-microband electrode arrays at varying separations were fabricated using standard photolithographic techniques and by evaporating titanium/gold films onto glass wafers (as detailed in Section 2.2). Images of the actual micro arrays can be seen below.

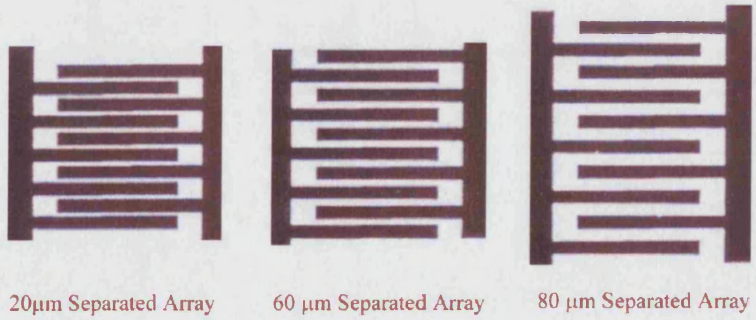

Fig. 5.21. Images of microband electrode arrays.

Initial measurements were carried out with all three arrays in a stagnant system, to determine how the response of 1mM ferrocene in acetonitrile would vary due to the separation between the microband electrodes. Figure 5.22 shows a typical linear sweep voltammogram recorded using one side of an array with a separation of 80 μm, in a cell with the dimensions: width 500 μm wide and height approximately 100 μm. As expected, a well-defined response is observed and both sides of the array were tested for all three array separations and showed similar results.

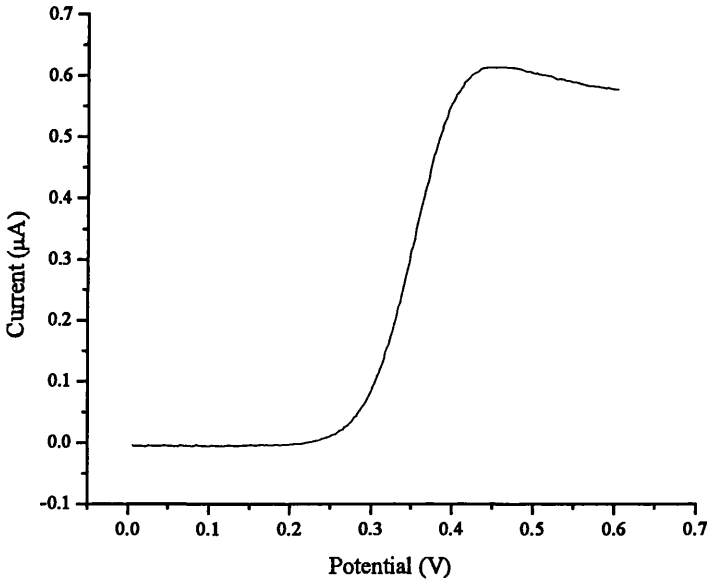

Fig. 5.22. Linear Sweep Voltammogram observed for a one half of a microband electrode array

Next, an analysis was carried out to compare the response in a stagnant system where one side of the array was set to oxidise the ferrocene and the other to regenerate (i.e. carry out a reduction). Linear sweep voltammograms were recorded for all three separations and are detailed in Figure 5.23. It can be seen that the regeneration (collection efficiency) of ferrocene increases the over all sensitivity of the arrays. Also the separation of the microband electrodes shows a significant effect on the overall response. This is due to the collection efficiency increasing with decreasing separation,

which is evident from the results where the 20 μm separated array shows the greatest sensitivity.

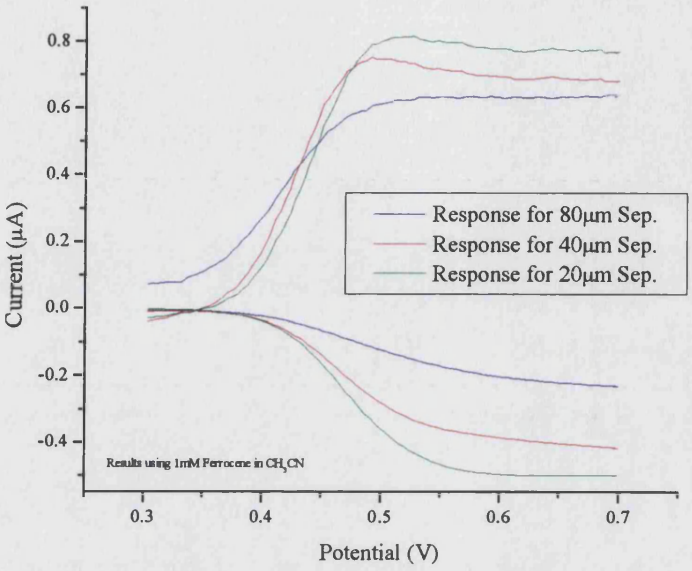

Fig. 5.23. Linear Sweep Voltammogram observed for different microband electrode array separations.

As the measurements conducted in the stagnant system showed that out of the three geometries the array with a 20μm separation gave the highest response, this geometry was used to analyse the response seen when solution was flowed through the cell under the influence of gravity[200,201]. It is important to note that there will be a considerable difference in response due to the convective force being introduced in the system and thus causing an increase of mass transport to and from the electrode surface. Due to this effect, the response that should be observed in the MECR would be higher than that observed so far and will be dependent on the transport rate through the cell (i.e. volume flow rate). Figure 5.24 shows a typical set of results observed using 1mM ferrocene in acetonitrile, for a cell with the dimensions: width 400μm, height 45μm and length 3cm. A considerable change in the response is observed when both sides of the

array were used, and where one side is detecting the ferrocene and the other side is regenerating the complex.

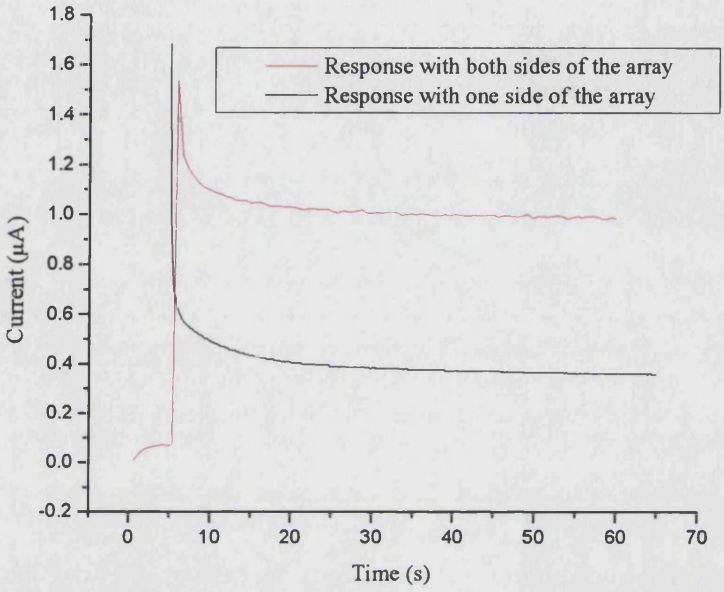

Fig. 5.24. Potential Step Voltammogram observed for microband electrode array with a 20μm separation. Both sets of data were recorded for a volume flow of $3.51 \times 10^{-3} cm^3 s^{-1}$.

A series of measurements was carried out to see how the response would vary as a function of volume flow rate and the change in amount of material being regenerated (i.e. collection efficiency). In Figure 5.25a the response is shown for a given volume flow rate. From the data it is apparent that an approximate collection efficiency of 60% can be achieved using this array. The change in the collection efficiency due to volume flow rate was analysed and Figure 5.25b shows the data recorded for the 20μm separated array.

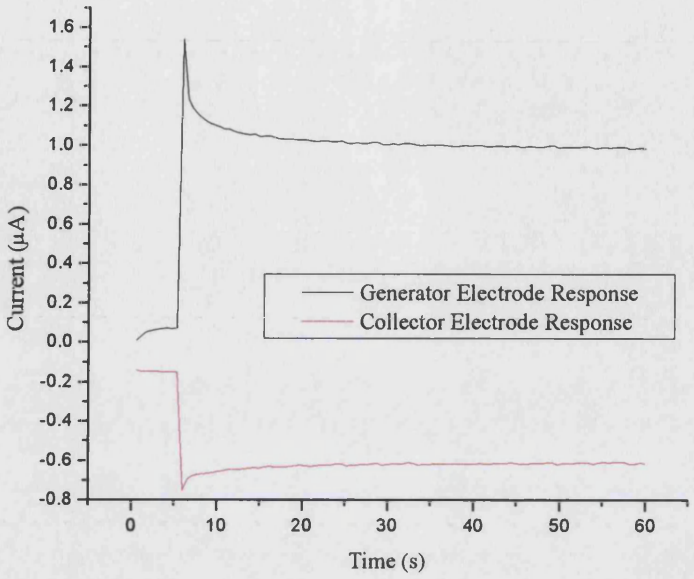

Fig. 5.25a. Potential Step Voltammogram observed for microband electrode array with a 20μm separation. Data was recorded for a volume flow of $3.51 \times 10^{-3} cm^3 s^{-1}$.

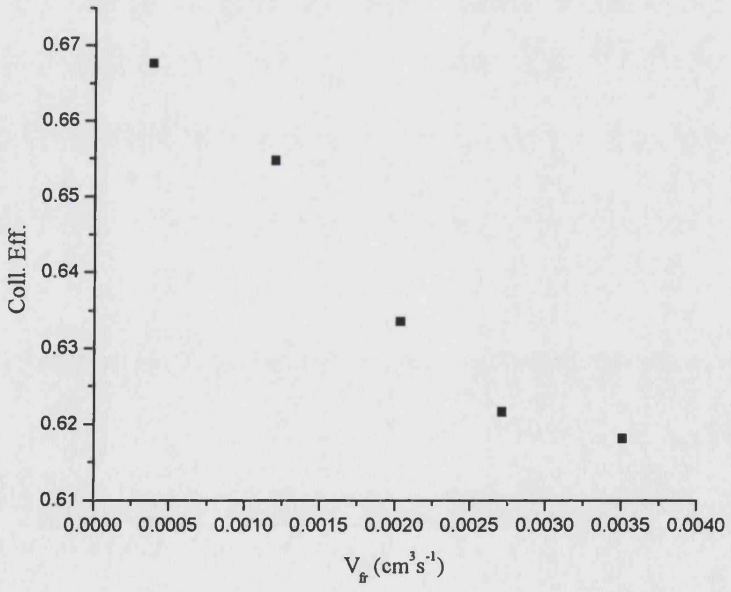

Fig. 5.25b. Change in collection efficiency due to volume flow rate observed for a microband electrode array with 20μm separations.

The above data shows that a series of microband electrodes behave in a manner which allows the voltammetric measurement to integrate the signal relative to the material being regenerated along the channel. This in turn causes an amplification of the signal within the MECR. To illustrate the ability to continue patterning microband electrodes and in order to rationalise the change in response with increasing numbers of microband electrodes, measurements were conducted using the following array design.

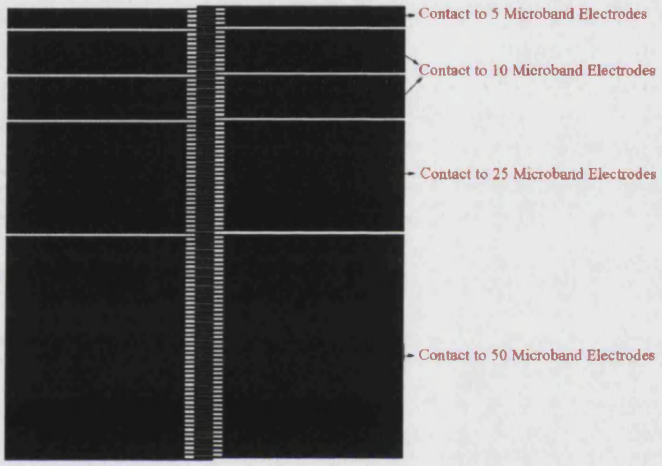

Fig. 5.26a. Schematic of Microband Electrode Array.

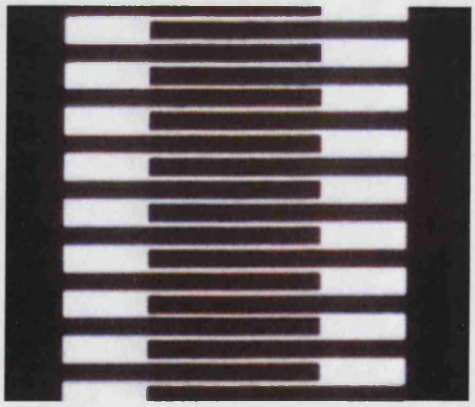

Fig. 5.26b. Image of Microband Electrode Array.

The illustration in Figure 5.26a shows how the microband electrode array design was optimised in order to interrogate a different number of microband electrodes. Individual

contacts were made to a series of the following microbands: 5, 10, 20, 25, 50 and 100. In all cases the microbands were separated by 20μm and had a length of 100 μm as shown in Figure 5.26b.

Measurements were carried out in a stagnant system, using a solution of 1mM ferrocene in acetonitrile with 0.1M TBAP as background electrolyte. Figure 5.27a details the response seen and shows that increasing the number of microband electrodes has a substantial influence on the transport limited current. The increase in response should be linear and Figure 5.27b details a plot of the transport limited current against the number of arrays.

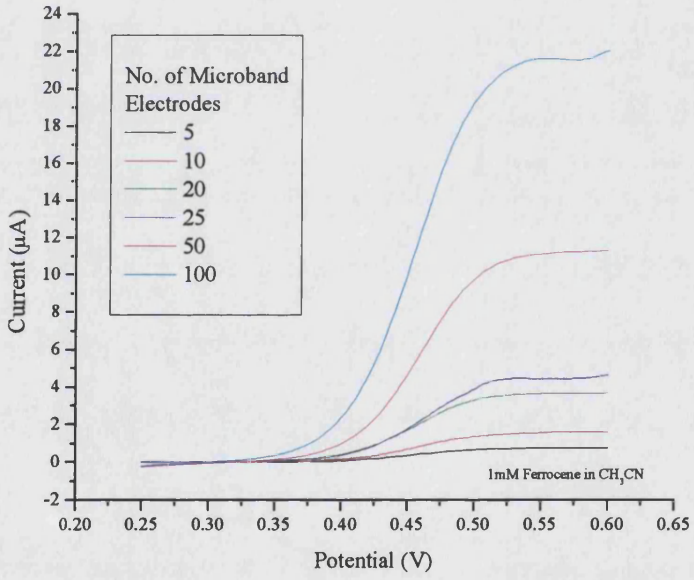

Fig. 5.27a. Linear sweep voltammograms recorded using 1mM ferrocene in acetonitrile.

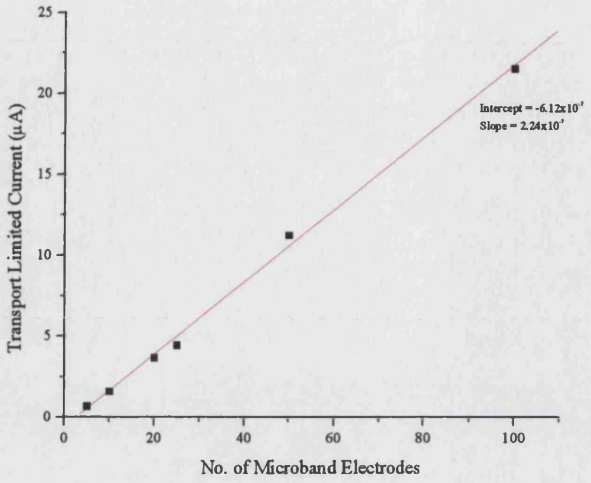

Fig. 5.27b. Plot to illustrate linear relationship of the transport limited current relative to the number of microband electrodes.

From Figure 5.27 it can be seen that a current of the magnitude of 25 μA can be observed using this system, and that the current measured scales respectively with the change in concentration. Preliminary measurements were carried out using a 100 set of arrays with a solution 1μM ferrocene in acetonitrile with no background electrolyte, and a typical current-voltage curve is detailed in Figure 5.28.

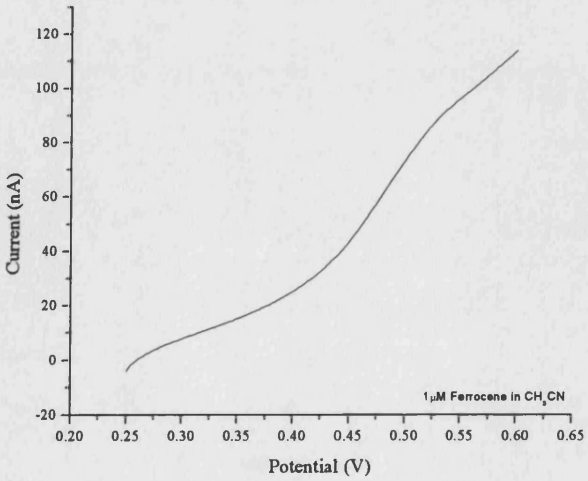

Fig. 5.28. Linear sweep voltammogram recorded using 1μM ferrocene in acetonitrile.

Chapter 6

Immiscible Liquid-Liquid Interfaces

6.0. Introduction

The study of interfacial processes is an important aspect of many chemical reactions. In previous chapters, studies into understanding the electrified interface on metal surfaces have been discussed for hydrodynamic systems and a demonstration of how these processes can be governed and examined have also been presented. In this chapter, the study of interfacial properties between two immiscible electrolyte solutions (ITIES) is presented and investigations into how electrochemical techniques combined with MECRs can be used are discussed.

The first direct electrochemical study of ITIES was reported by Nernst and Riesenfeld in 1902. Using coloured inorganic electrolytes as partition equilibrium between water and phenol, they observed the transfer of ions during the passage of current through the system water/phenol/water. Since then, much work has been developed in determining many processes occurring at the ITIES. In this chapter, a short review of the more recent studies reported will be presented, along with the development of a novel range of hydrodynamic devices that present an elegant solution to many studies of liquid-liquid systems.

A quantitative description of the processes occurring at liquid-liquid interfaces is vital for the development of a diverse range of industrial technologies, including colloid science, metal extraction, two-phase synthesis and phase transfer catalysis[202-205]. Electrochemical methods have been used with significant success in stagnant solution to study these interfacial processes and have provided a range of thermodynamic and

kinetic data for a variety of interfacial charge transfer reactions. In one popular approach, external polarisation of the liquid-liquid interface induces the transfer of ions and electrons across the interface, with the resultant current detected in an external circuit[206-211]. A more recent alternative, which does not rely on a polarised interface, exploits scanning electrochemical microscopy to establish kinetic information for a variety of systems[212-217]. Other recent developments include micropipette[218] and microdroplet approaches[219].

All of the above studies have been performed within stagnant solution. However, it has been demonstrated that within single solvent phases introduction of an element of forced convection can offer potential advantages[28,41,46,219-221]. In particular, the ability to vary the transport rate over three or four orders of magnitude can provide significant benefits in mechanistic analysis[28]. Despite the potential advantages, the application of hydrodynamic electrochemical strategies to investigate processes at immiscible liquid-liquid interfaces remains poorly exploited. In early measurements[222], two phases were stirred using a paddle arrangement, with the progress of the reaction monitored *ex-situ* and a modified rotating disc with impaired hydrodynamics reported[223]. However, the device has not been widely adopted due to the build up of reaction products in the cell and difficulties in modelling the processes occurring. A methodology based on the wall-jet configuration has been applied to a membrane supported liquid-liquid interface by Hundhammer and co-workers[224,225]. This approach led to the development of liquid-liquid flow injection systems for analytical determinations of ionic concentrations[225,226]. An expanding droplet approach has also been applied to the analysis microelectrochemical measurements of electron transfer reactions at the interface between two immiscible electrolyte solutions (ITIES).

In related non-electrochemical studies, it has been demonstrated that microchannel arrangements can provide a stable environment in which multiphase flow can be established[227,228]. This approach has permitted the spectroscopic monitoring of chemical transfer processes[77,229].

Recently, an outline of the application of thin layer flow cell arrangements[230,231] using a membrane separator has been reported with the aim of extracting kinetic and mechanistic details of ion transfer reactions. In this chapter, the potential benefits of flow cells will be exploited and, using the concept of MECRs, a novel hydrodynamic device that allows immiscible liquid streams to flow in direct contact to one another will be presented. The development of a microeletrochemical liquid-liquid technique (MELL) will be discussed, where the approach utilises a confluence reactor design. The design, fabrication and experimental characterisation of this range of analytical devices using an electrochemical approach will also be presented.

6.1. Development of Microelectrochemical Liquid-Liquid Techniques (MELL)

The concept detailed in Chapter 5 describes the characteristics of hydrodynamic systems and how the process of well-defined mass transport plays a critical role in determining their quantitative description. In this section, an approach to adopt these unique properties to interrogate liquid-liquid interfacial systems within a flow through arrangement will be given.

A micro reactor design which incorporates a channel with two inlet and outlet openings was developed and a schematic of the flow cell design can be found in Figure 6.1. The concept of the design was to achieve a parallel flow regime of the two immiscible liquids that retained stable and laminar flow, in order to characterise a quantitative analysis of the processes occurring at an ITIES. Microelectrodes were sited and aligned on one wall of the channel, and electrochemical measurements were carried out to interrogate transport of material within each of the two flowing phases.

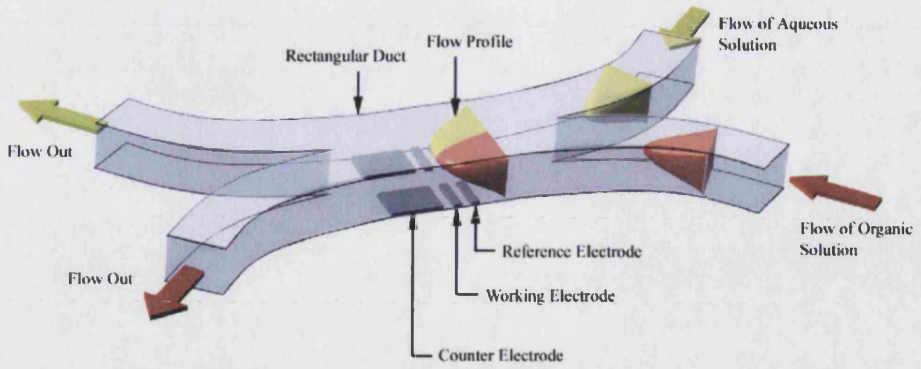

Fig. 6.1. Schematic of a Liquid-Liquid Microelectrochemical Reactor.

In the following sections, a description of the work carried out in developing the design of the micro reactors to achieve stable flow will be presented, as well as an electrochemical approach illustrating the mass transport properties within the individual liquid phases.

6.1.1 Study of the Liquid-Liquid Interface Stability within Flowing Regimes

In order to achieve a stable flow environment where the two immiscible liquids could flow in parallel, critical aspects of the cell design needed to be considered, such as the manner in which the two liquids were to be introduced into a single channel and the placement of microelectrodes. An approach where the two liquid streams were introduced after a lead in length was used, so that once they were in contact with one another they were already flowing under laminar conditions. Figure 6.1 illustrates the two individual channels meeting at a junction after which the single channel continues downstream to another junction point where the channel splits into two again. It was found that a 'Y' junction at the point where the two liquids met and a 'T' junction where the two liquids separated and flowed out proved to be a good geometry to work in.

The viscosities of the individual liquids also needed to be considered, and fluid mechanical studies have shown that the viscosities of the two liquids play an important role. Figure 6.2 reveals a finite element simulation of two immiscible liquids flowing parallel in contact and the effect of various viscosity ratios of the liquids on the flow profile. As illustrated, varying the viscosity had a profound effect over the flow profile and it is apparent that the transport properties in the two liquid regimes with different viscosities can prove to be very different. In order to do comparative studies, the two liquids needed to have similar viscosities and for these reasons the studies presented in this chapter were mostly carried out using 1,2-dicholorethane (DCE) and water as a model liquid-liquid system, due to the viscosity ratio of the two liquids being similar.

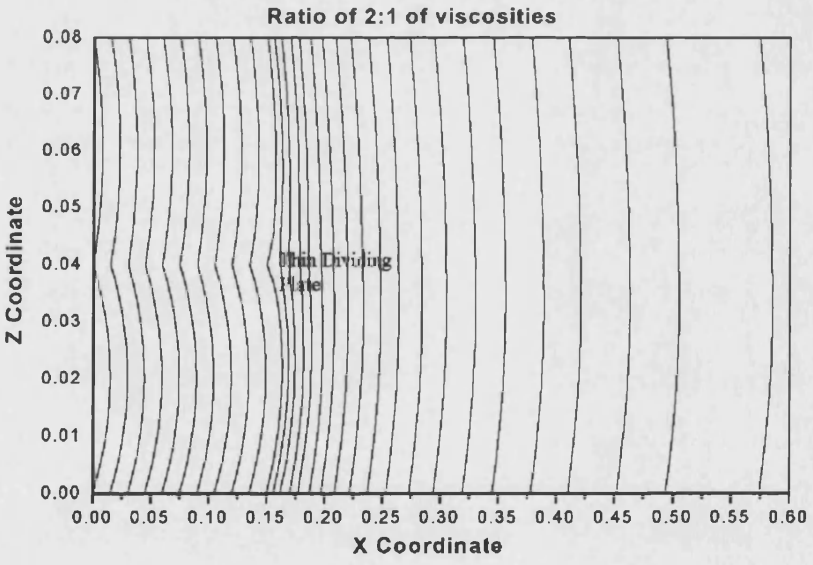

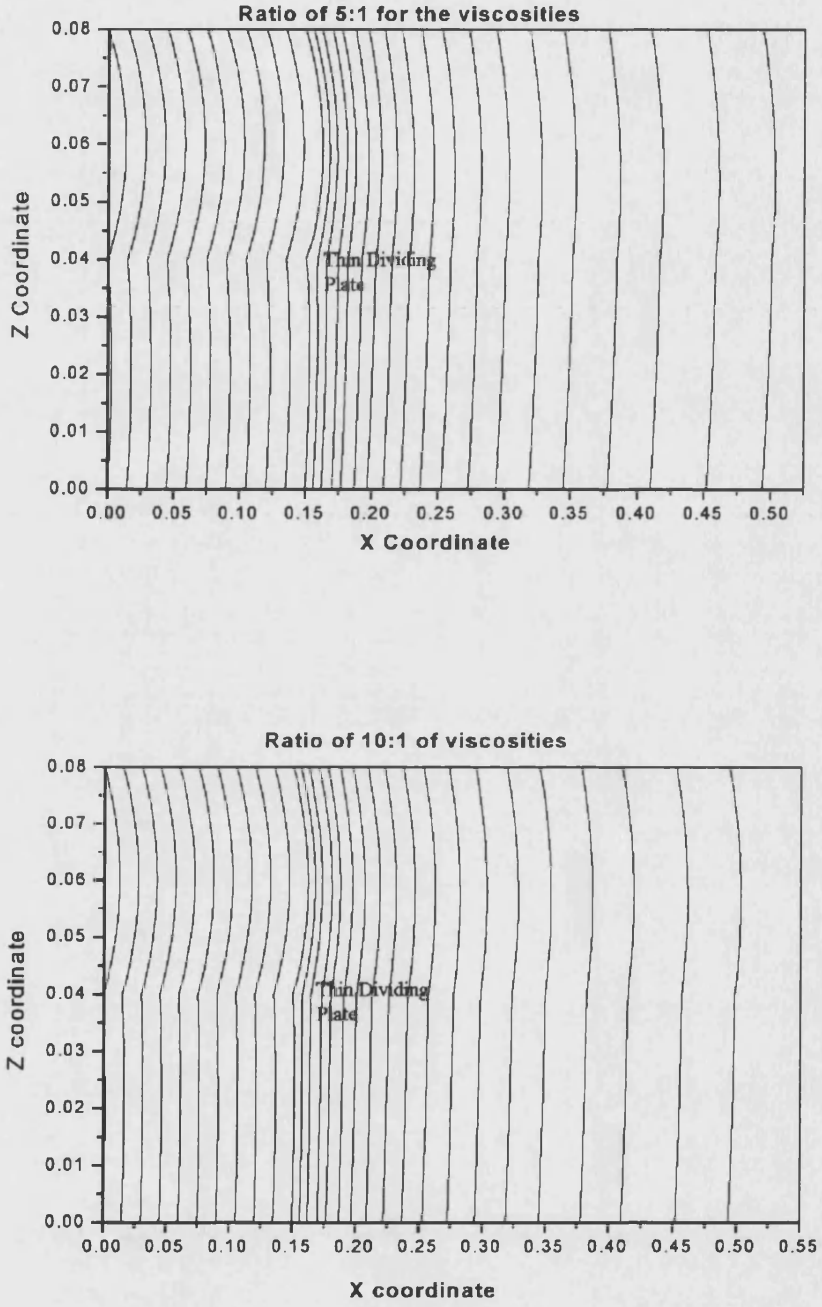

Fig. 6.2. Flow profiles predicted using finite element modelling for varying fluid viscosities.[6]

Using flow cell construction procedures outlined in Section 3.1.1.1, a range of micro flow cells of dimensions: width 5-1 mm, height 300 – 100 μm and length 10 – 1 cm, was constructed for preliminary studies on the stability of an ITIES in a flow

[6] Simulated results achieved from calculations by K. A. Gooch.

environment. It was found that the channel dimensions were a key feature of the cell designs, where the height to width of the channel had to be within the proximity of a ratio of 1:5. Figure 6.3 details a cell design used to investigate the channel's height to width ratio effect on the ITIES stability. The flow cell was constructed to have a height of 200 μm and width which started at 1 mm and opened up to 5 mm.

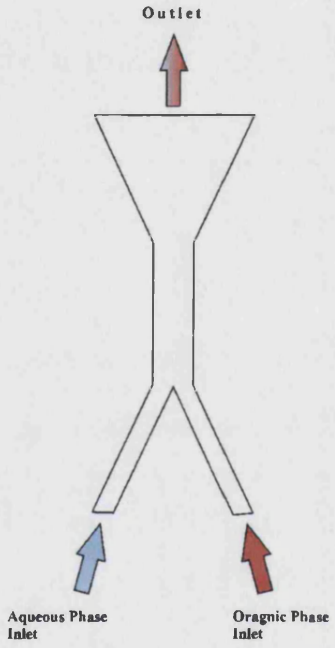

Fig. 6.3. Schematic of flow cell design used to interrogate the effect of channel dimensions on ITIES stability.

A solution of water containing a concentrate of potassium ferricyanide and DCE containing a concentration of TMPD was used. The individual liquids were introduced via their respective inlets under the influence of gravity as detailed in Section 2.4.1. An interfacial electron transfer reaction was found to occur at the point where the two liquid streams came into contact and the formed product had a distinctive blue colour, which was believed to be the TMPD cation. The pathway of the interface flowing along the length of the channel could be imaged by tracing the blue cation and Figure 6.4 shows an image recorded for the stability analysis using the cell design in Figure 6.3.

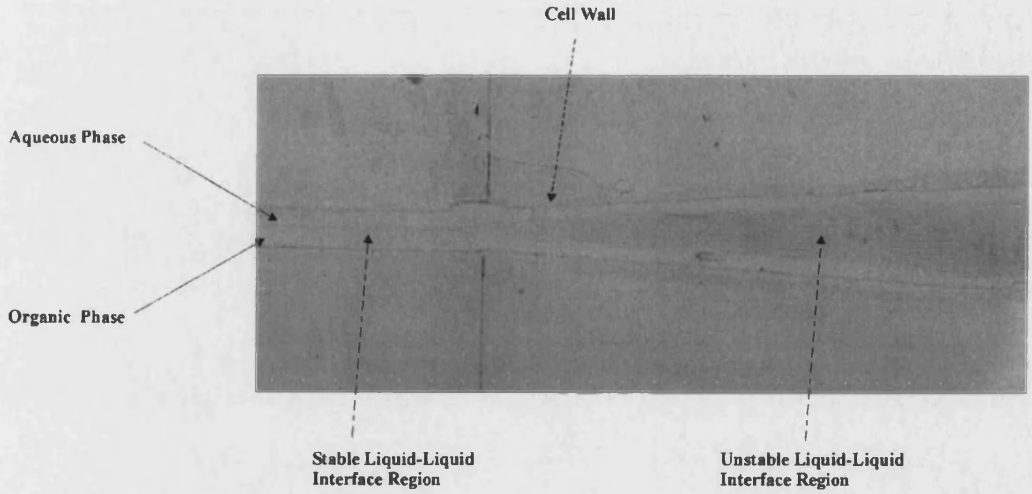

Fig. 6.4. An image of the effect of channel dimensions on DCE/Water interface stability.

From the above image it can be seen that the interface is most stable within the channel region where the height 200 μm and width is 1 mm (i.e. 1:5). Another flow stability analysis revealed that when the two liquids were introduced from the opposite end of the cell, i.e. flowed in from the wider end and out of the narrow end, a similar behaviour of the flow was observed where a stable ITIES was created once the liquids entered into the region where the channel height and width ratio was 1:5.

It became apparent from the studies that the central velocities of the liquids had an influence over the stability of interface formed. Further analysis of a flow cell which had the dimensions: height 1 mm and width 5 mm showed that a stable interface between DCE and water was not observed, even though the height and width obeyed the 1:5 ratio rule. This was because the gravity fed flow setup used was not able to apply a pressure high enough to increase the central velocities of the fluid within the channel to a point at which parallel laminar flow of the two liquids would occur.

It was concluded that a combination of the force being applied to the liquid when flowing through a channel, and the path of least resistance it took, governed the behaviour and stability of the formed interface. Two immiscible liquids flowing through a channel required a central velocity to be high enough to create an environment where

parallel and laminar flow would be the more dominating process. The use of micro channels proved useful, as it allowed the ability to achieve high transport rates with relatively low pressures that could be applied by a gravity fed flow system. As well as having all the potential benefits that were outlined in earlier chapters incorporated the motivations of micro devices, the micro flow cells had a diffusion path length where the interfacial region and the individual two phases were in the order of microns apart, offering efficient means of studying diffusion related processes occurring at an ITIES.

Figure 6.5 shows an image of a channel of dimensions: width 1 mm, height 200 μm and length 3cm, based on the design described in Figure 6.1 using thin glass slides. A similar approach using a gravity flow system with potassium ferricyanide and TMPD to image the stability of the formed interface was carried out and is detailed in Figure 6.5. An analysis of the interface at a range of volume flow rates revealed that a stable interface was apparent with a range of volume flow rates, due to the transport rates being high as explained earlier.

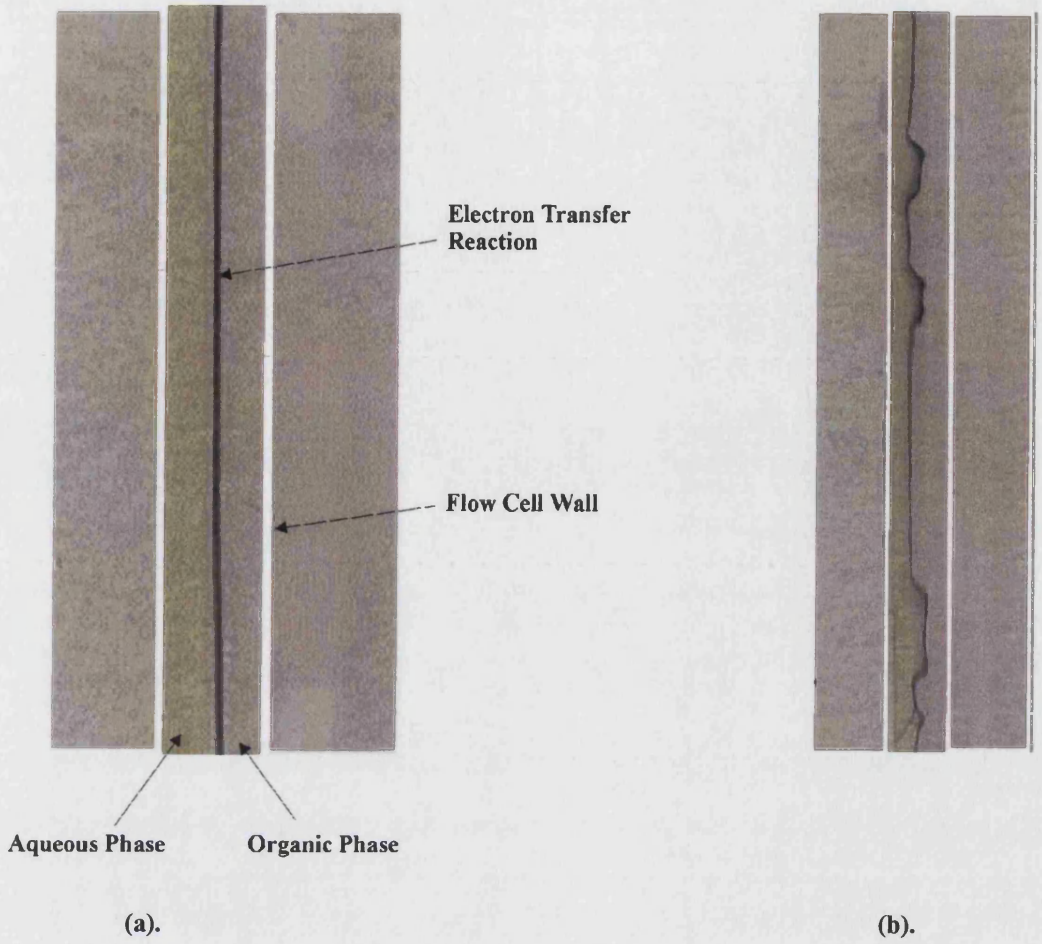

Fig. 6.5. Images of DCE-Water flow behaviour at different volume flow rates. **(a).** image recorded at a high volume flow rate, **(b).** image recorded at a low volume flow rate.

An effort to broaden the range of applicable volume flow rates required further miniaturisation of the channel dimensions, and the use of Foturan Glass was exploited to develop a range of channel designs and dimensions. Testing of flow cell designs and fabricated channel dimensions, revealed that a channel with dimensions: width 500 μm and height 100 μm, produced a stable ITIES for a range of volume flow rates. Figure 6.6 shows an image of a micro flow cell fabricated with Foturan Glass, were the channel dimensions were: 500 μm wide, 100 μm high and 2 cm long. In the analysis a blue dye (tris(4-bromophenyl)aminium hexachloroantimonate) which did not partition into the

aqueous phase was dissolved in DCE and was used to trace the stability of the liquid-liquid interface.

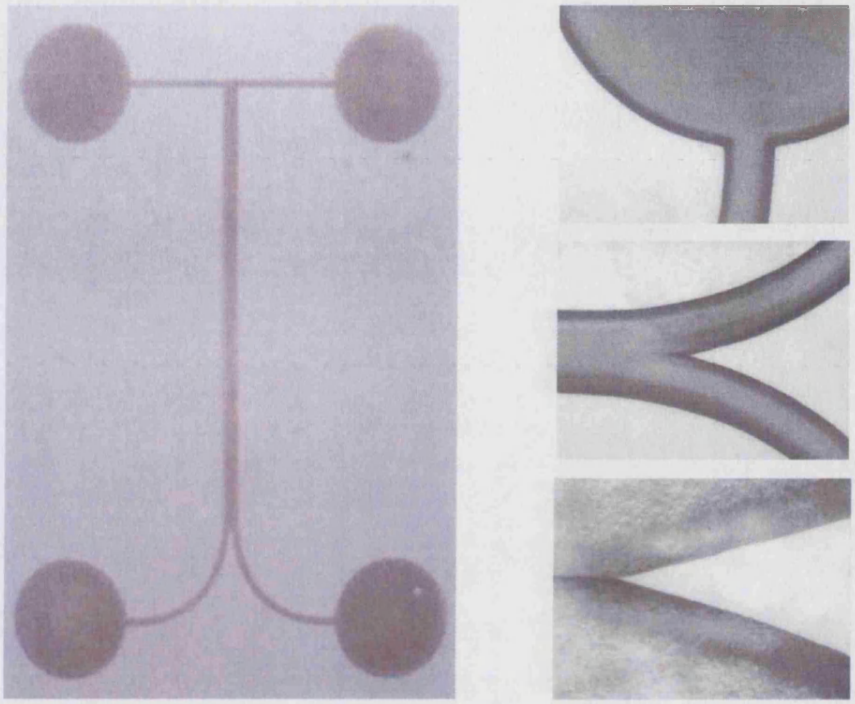

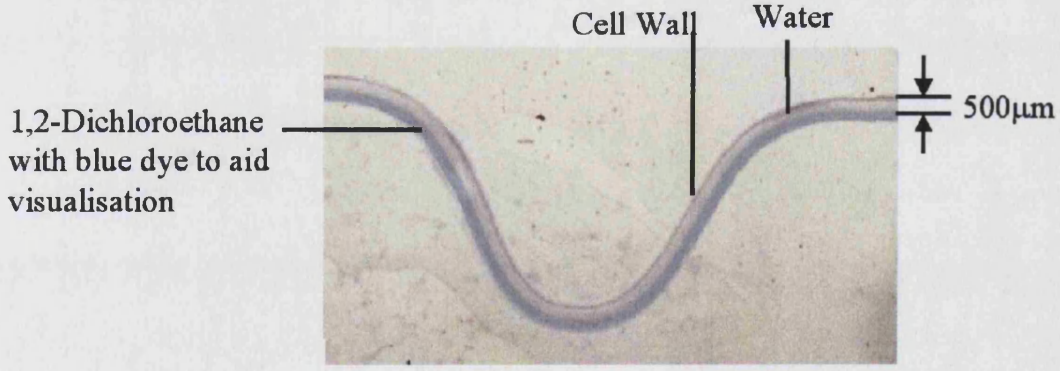

(b).

Fig. 6.6. (a). Image of channel profiles fabricated with Foturan Glass. **(b).** Image of flow behaviour of DCE-Water within a 'U' shaped microchannel.

The studies revealed that stable parallel laminar flow between two immiscible liquids could be achieved, provided that the cell dimensions obeyed a logical rule of height and width ratio depending on the viscosities of the liquids. It was also found that the central velocities of the two liquids needed to be high enough to create a scenario where the laminar parallel flow would be the path of least resistance for the two liquids to follow. Overall, the use of micro reactor devices was found to play a key role, as the inherent properties of these devices provided high transport rates with relatively low pressures, as well as short diffusion path lengths of the two individual liquid phases to the interfacial region. Another potential benefit of increased surface area of the interface to volume ratio was also apparent when using micro reactor devices.

In the next section, a similar approach adopted for studying flow in a single phase as detailed in Chapter 5, is illustrated. This shows how electrochemical techniques can be used to quantify the mass transport behaviour which occurs within the two individual phases of a liquid-liquid flow regime.

6.1.2. An Electrochemical Quantification of Liquid-Liquid Flow Systems

In the above section, the results illustrate that well-defined and parallel flow can be achieved in liquid-liquid flowing regimes in direct contact. In this section an attempt into defining the fluid dynamics and mass transport that is occurring within each of the two liquid phases is detailed. An electrochemical approach similar to that described for MECRs in Chapter 5 is detailed.

A microchannel as detailed in Figure 6.7 was fabricated using Foturan glass with the techniques described earlier in Section 3.1.1.3. The channel had the dimensions: width 500 μm and height 100 μm and length 2 cm. Gold microelectrodes were fabricated on the cover plate to yield the electrode design as shown in Figure 6.8, where two electrodes of dimensions 60 and 20 μm in length and 100 μm in width acted

as a pseudo-reference and working electrode (see Section 2.2 for details on the fabrication procedure). A counter electrode was placed further downstream from the working electrodes and all electrodes had a separation of approximately 50 μm. The electrodes were placed either side of the channel walls and had a space of 200 μm where the liquid-liquid interface was established while flowing.

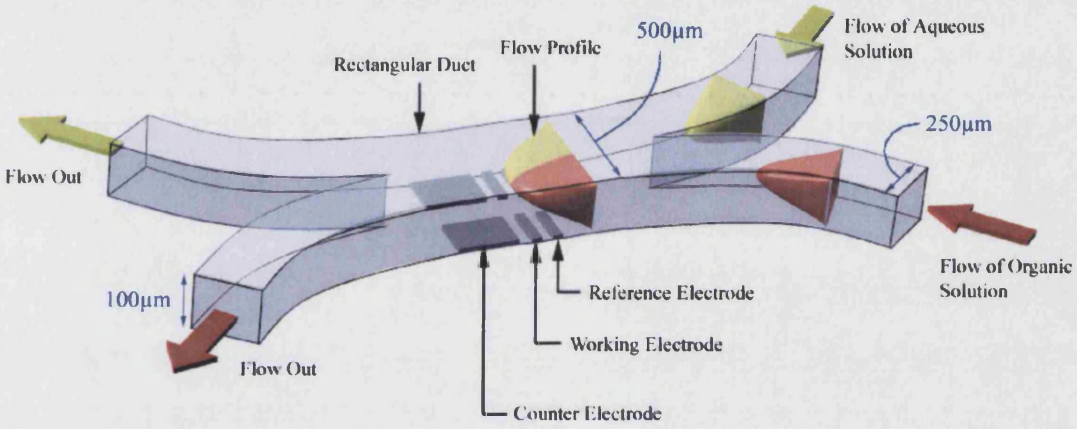

Fig. 6.7. Schematic of Microelectrochemical Liquid-Liquid Reactor.

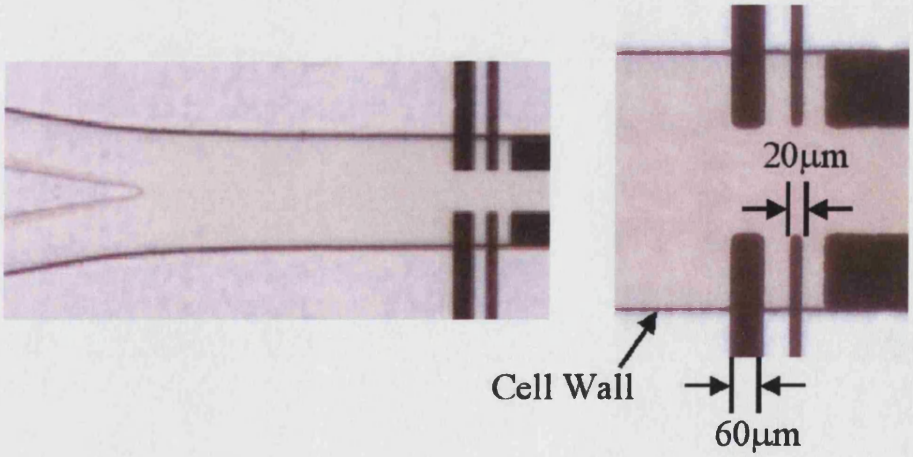

Fig. 6.8. Image of Gold Microelectrode sited with the Microreactor.

The concept of this micro flow cell was to determine the mass transport and fluid dynamic properties that would occur with the two liquid phases flowing using

voltammetric techniques. A solution of DCE containing 0.1 mol dm^{-3} TBAP and TMPD, and an aqueous solution using Millipore Water (18.2 M Ω cm) containing 1 mol dm^{-3} KCl with Hexaaminеruthenium(III)chloride were prepared. Both solutions were fed through the cell under gravity with balanced volume flow rates (within 1% of one another) and were purged with predried nitrogen for 15 minutes prior to measurements. A set of linear sweep voltammograms was recorded in turn for each phase, for the electrolysis occurring in that phase at various volume flow rates. Figure 6.9 shows the current voltage curves observed for a solution of $1x10^{-3}$ mol dm^{-3} TMPD in DCE and $1x10^{-3}$ mol dm^{-3} Hexaaminеruthenium(III)chloride in water using a working electrode with the dimensions: length 20 μm and width 100 μm.

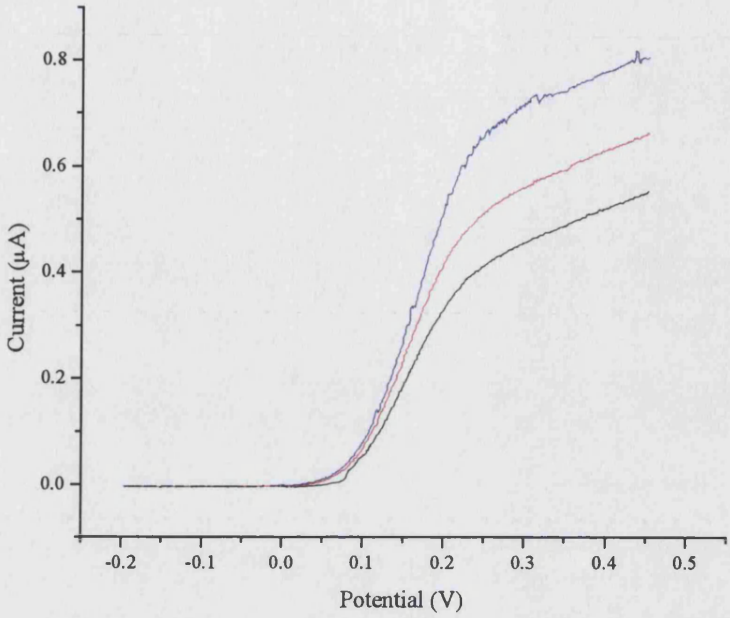

(a).

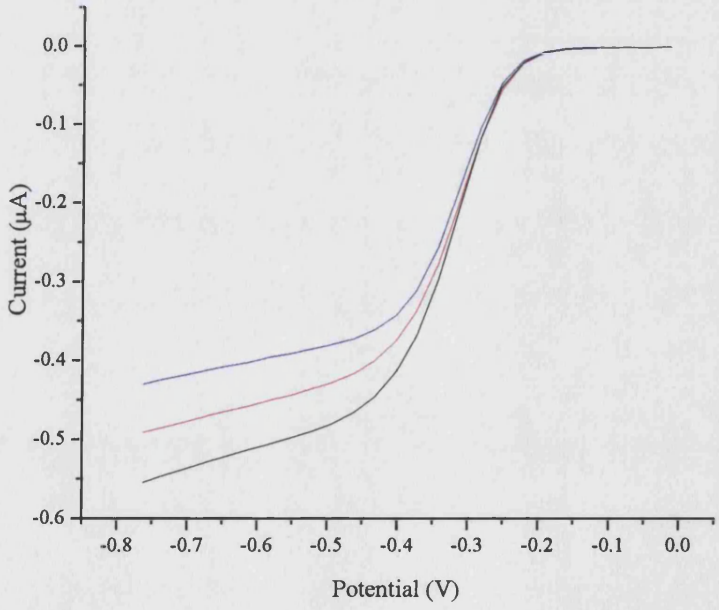

(b).

Fig. 6.9. Linear sweep voltammograms recorded at a 20 μm long working electrode. **(a).** current-voltage curves recorded in DCE with 1mM TMPD, **(b).** current-voltage curves recorded in water with 1mM Hexaaminеruthenium(III)chloride.

It is apparent that a change in the transport limited current increases with increasing volume flow rate in both liquid phases. This behaviour is analogous to hydrodynamic voltammetric measurements reported in single phase solvents using macro- and micro-channel electrode configurations and consistent with the studies detailed in Chapter 5. Figure 6.10 shows the variation of the transport limited current as a function of volume flow rate for the data collected using the $1x10^{-3}$ mol dm^{-3} solutions of TMPD in DCE and Hexaaminеruthenium(III)chloride in the aqueous phase. It is interesting to note that the absolute magnitude of the currents varies within each phase due to the different diffusive properties of the reagents.

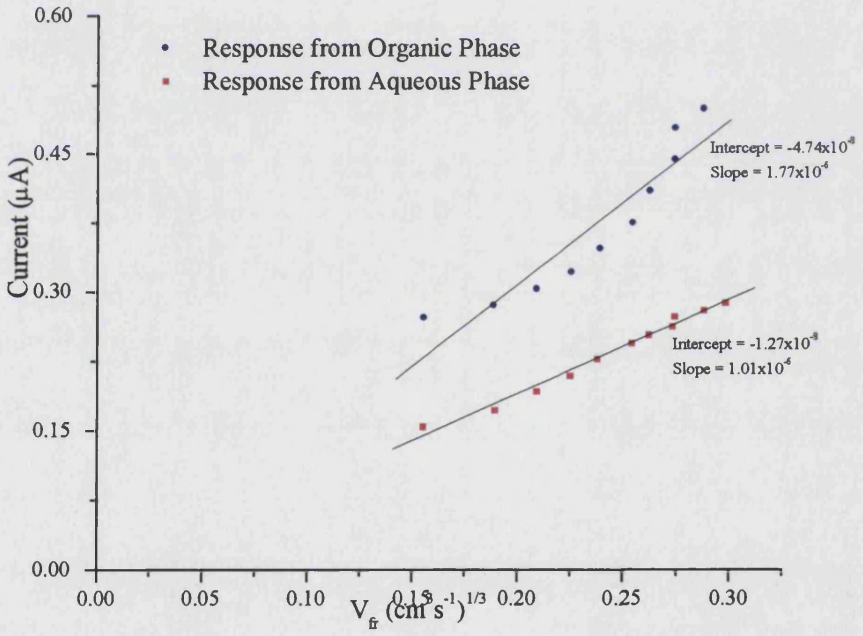

Fig. 6.10. Comparison of the transport limited current observed in the DCE and Water, for 1mM TMPD in DCE and 1mM Hexaaminеruthenuim(III)chloride in water.

In addition, further measurements were carried out with a range of different concentrations of TMPD and Hexaaminеruthenium(III)chloride in their respective liquid media. Figure 6.11 details the comparative analysis of the transport-limited current for

$1x10^{-3}$ mol dm^{-3} and $2x10^{-3}$ mol dm^{-3} concentrated reagents in the two individual liquid phases. The data show that the magnitude of current scales proportionally to the change in concentration as would be expected. This is a response that is analogous to that reported in previous macro and micro channel electrodes and to that reported for the MECRs in Chapter 5.

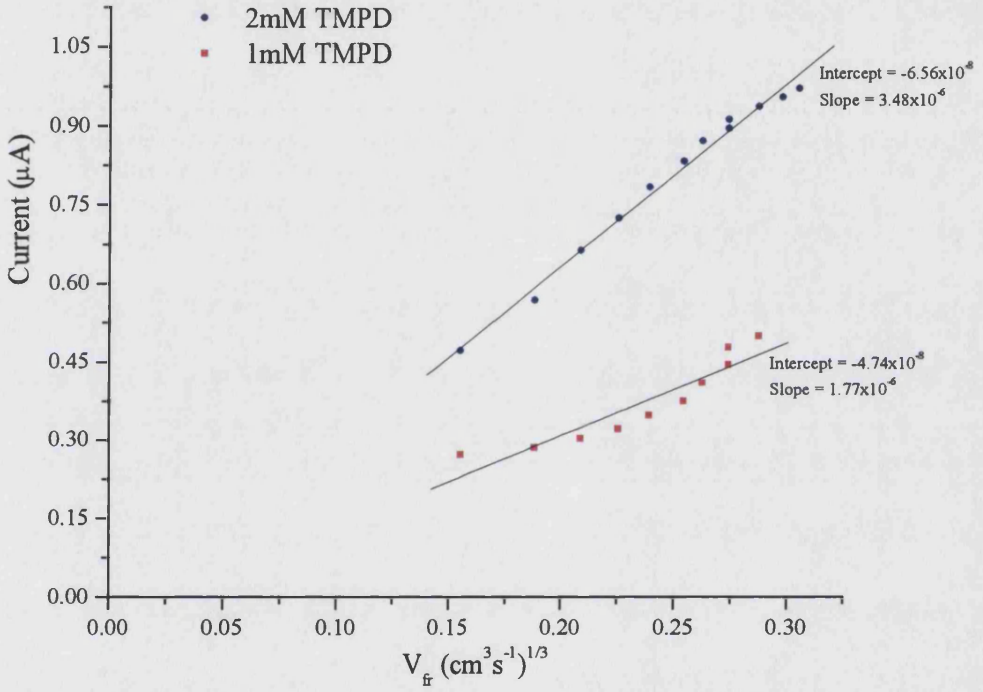

(a).

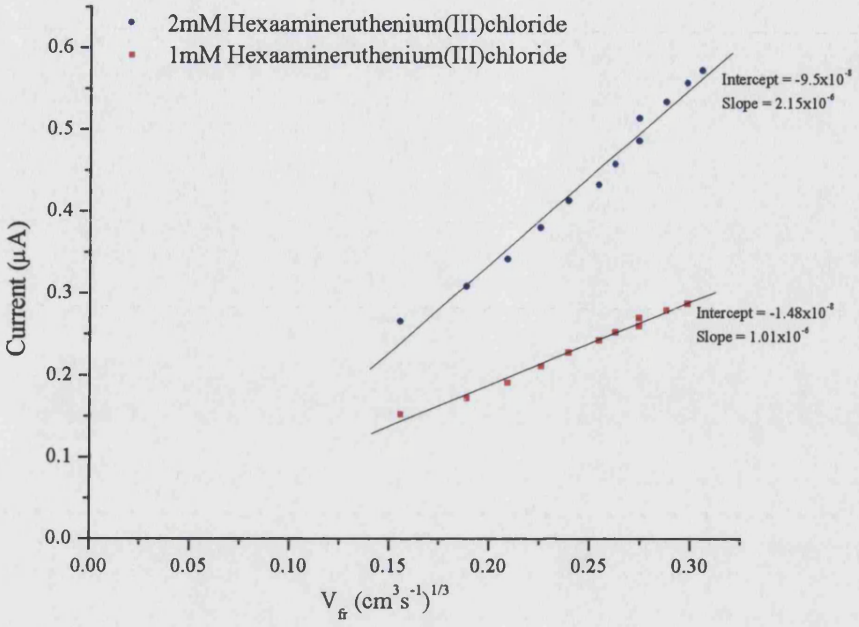

(b).

Fig. 6.11. Change in transport limited current due to change in electroactive reagent and volume flow rate. **(a).** response observed in the DCE phase, **(b).** response observed in aqueous phase.

Due to the dimensions of the channels used in the study of liquid-liquid flow systems, the central velocities of the two liquids were in the order of 1-2m/s. Although this property of microchannels can prove to be a useful tool to resolve chemical processes that occur at high reaction rates, it would be difficult to yield useful kinetic and mechanistic information for slower chemical processes. Many processes occurring at a liquid-liquid interface such as ion transfer can be dependent on the chemical system under analysis. Hence, in order to accommodate slower chemical processes at a liquid-liquid interface a microreactor design was employed which incorporated large reaction vessels that would slow the transport rate of material within these larger volume regions of the reactor.

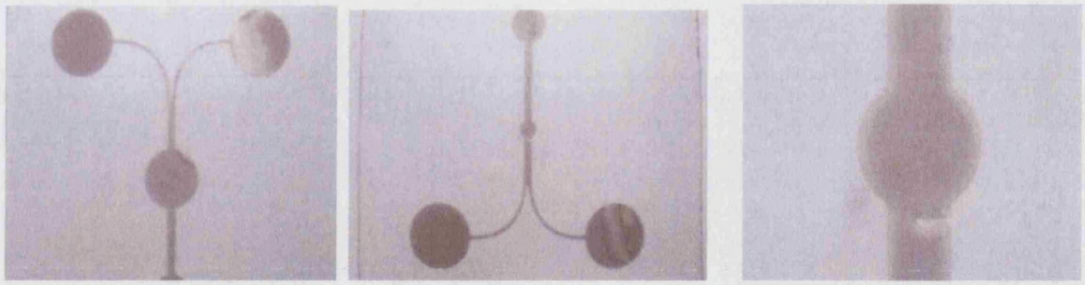

Fig. 6.12. Images of Liquid-Liquid Microreactor with circular vessels.

Figure 6.12 shows images of a reactor design fabricated using Foturan glass. The design was based on the schematic detailed earlier in Figure 6.7, but with the addition of three reaction vessels with increasing widths. The channels had the dimensions: width 500 μm, height 100 μm and length 2cm and the three reaction vessels had a diameter of 1, 2 and 5 mm. Preliminary studies were carried out by dyeing the DCE phase with tris(4-bromophenyl)aminium hexachloroantimonate (0.5 mol dm^{-3}) to determine the stability of the liquid-liquid interface when flowing solution through these reaction vessels. The analysis showed that even though the aspect ratios of the channel dimensions were being changed the interface created remained stable throughout the length of the channel. Measurements were carried out to characterise the voltammetric response for a non reacting/mixing flow system as a means of quantifying the mass transports after the liquids had flowed through each reaction vessel. Electrode sensors (of approximate dimension 60 and 20 μm in length) were placed 1 mm, downstream of each circular vessel (Figure 6.13) and were used in voltammetric measurements.

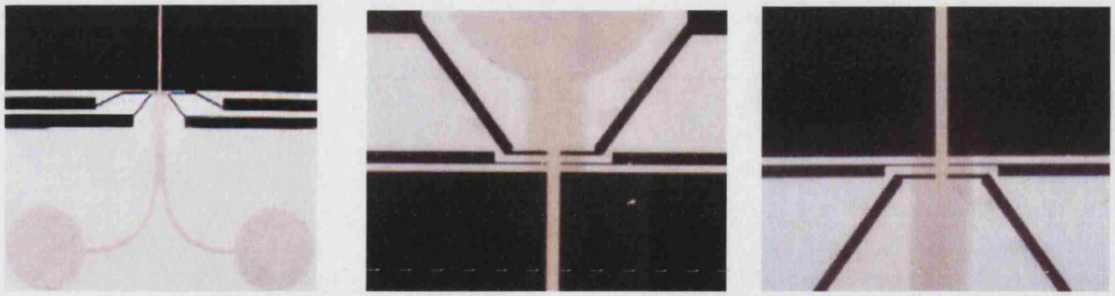

Fig. 6.13. Images of microelectrodes sited within a liquid-liquid microreactor.

DCE solutions containing $1x10^{-3}$ mol dm^{-3} TMPD and 0.1 mol dm^{-3} TBAP, and aqueous solutions containing $1x10^{-3}$ mol dm^{-3} Hexaammineruthenium(III)chloride and 1 mol dm^{-3} KCl, were flowed through the reactor with voltammetric sensing performed, as above. An identical response was obtained for each set of electrodes sited after the three circular reactors (no reagent transfer occurs between the two phases) and analogous behaviour to that observed for the flow cell discussed earlier (Figure 6.11). These observations confirm the retained stability of the flow and transport characteristics within the cells and highlight the potential of these larger reactor regions. Figure 6.14 illustrates the measurements recorded using microelectrodes located after the 5mm diameter vessel.

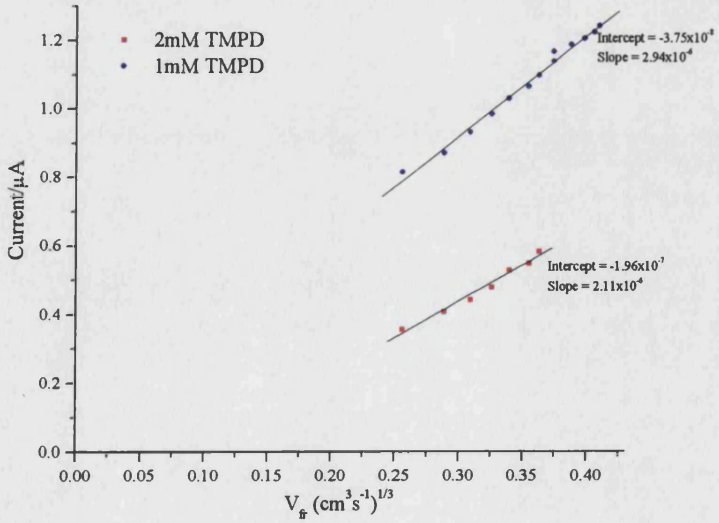

(a).

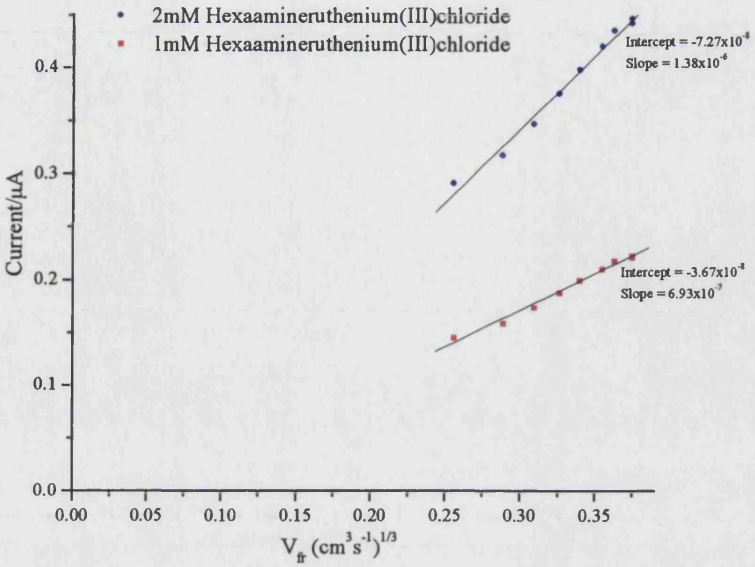

(b).

Fig. 6.14. Change in transport limited current due to change in electroactive reagent concentration and volume flow rate. Measurements carried out 1 mm downstream of 5 mm reactor vessel. **(a).** response observed in the DCE phase, **(b).** response observed in aqueous phase.

6.1.3. Integrated Multilayer Flow Systems in Microreactors

The study of susceptibility of drugs by the human body has always been an area of science that has been studied for decades. Pharmaceutical industries have an invested interest in classifying and screening vast quantities of drugs efficiently. The methodology of micro reactors holds a potential role in resolving many concepts for analysing drugs due to their ability of high through put screening. A critical area of drug development is to study their ability to penetrate and transverse through many cells to reach their site of action within the human body. The membrane permeability of drugs is an important biopharmaceutical parameter that governs the absorption, distribution, metabolism and excretion of drugs and holds a key role in new pharmaceutical formulations. Simple organic solvents such as Octanol have been studied to mimic biological membranes, and systems have been designed to monitor the partition between

biomass and water to describe the lipophilic or hydrophilic properties of chemical compounds. More recently three phase flow system of water-organic-water has been reported, where the central organic phase has been designed to act as a biological membrane between the two aqueous streams which act as donors or receptors. Other commercial areas where multilayer liquid systems have potential benefits include processes such as solvent extraction procedures or organic synthesis.

In this section, the concepts of microreactors are taken further to develop a range of fluidic devices that allow multilayer liquid regimes to flow in direct contact. A similar electrochemical approach detailed earlier for two phase systems is taken to quantify the mass transport and fluid dynamic properties of these reactors.

6.1.3.1. Development of Three Phase Micro Flow Cells

Similar fabrication techniques using Foturan glass and cell designs as outlined in Section 3.1.1.3 have been used to develop a three phase micro flow cell. The cell consisted of three channels which merged into a single channel before separating out into three channels once again. Figure 6.15 shows a schematic of the cell design, where the height of the channels were 100 μm and widths of the individual channels were 300 μm and combined to make a single central channel of 600 μm.

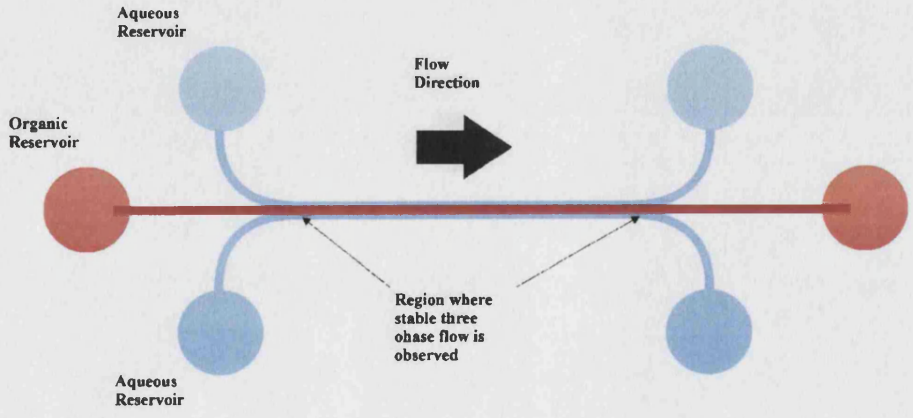

Fig. 6.15. Schematic of Three Phase Micro Flow Cell.

An arrangement where the central channel was flowing DCE dyed blue with tris(4-bromophenyl)aminium hexachloroantimonate (0.5 mol dm^{-3}), and the channels either side were flowing water, was setup so that a three phase flow of water-DCE-water could be assembled. Figure 6.16 shows the flow images recorded, and it is apparent that a stable and well-defined three layer flow regime can be achieved. Measurements revealed that the volume flow rates of either the organic or the two aqueous phases had a profound effect over the three phase flow profile.

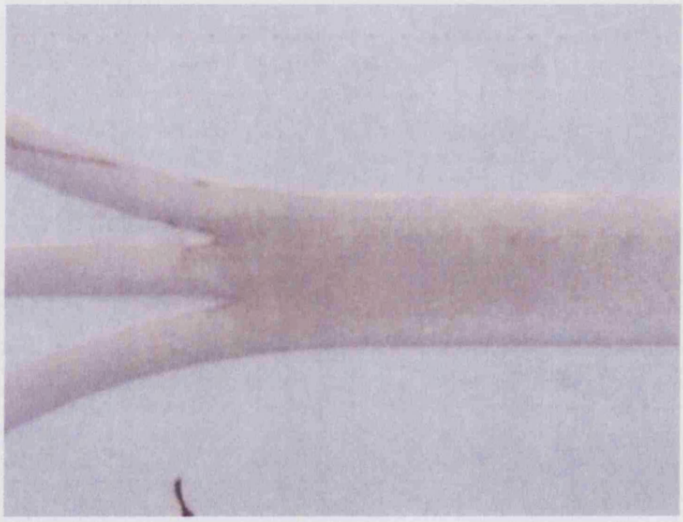

(a).

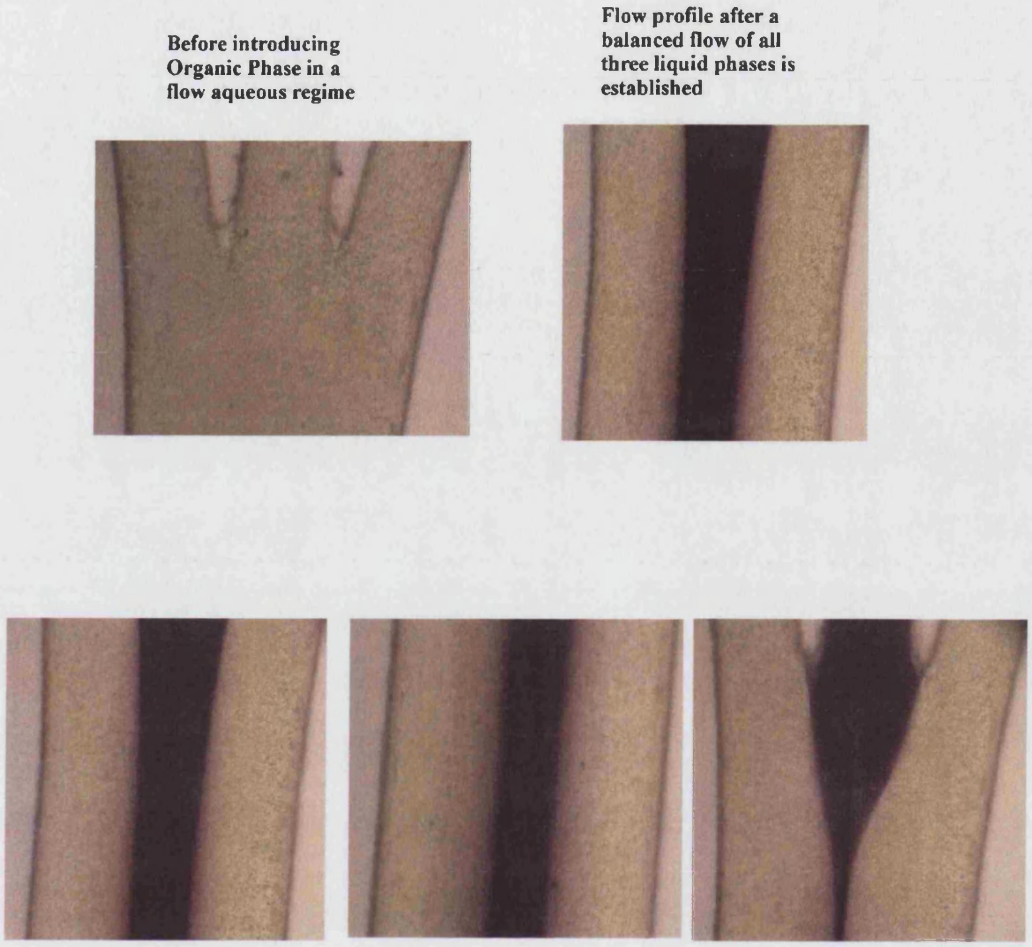

Fig. 6.16. (a). Images of three phase reactor. **(b).** Images of Three Phase Flow.

Microelectrodes were fabricated as detailed in Section 2.2, and were sited along the width of the central channel. The dimensions of the electrodes were as follows: reference electrode length 90 μm, width 600 μm; working electrode length 90 μm, width 600 μm; and counter electrode length 5 mm width 600 mm. Voltammetric measurements similar to those reported above for two phase flow systems were carried out using the microelectrodes. Solutions of DCE containing TBAP and TMPD were flowed through the cell with two aqueous streams either side under the influence of gravity. A series of linear sweep voltammograms revealed a change in the transport limited current relative to the volume flow rate. Figure 6.17 illustrates the linear sweep

voltammograms recorded at various volume flow rates for $1x10^{-3}$ mol dm^{-3} TMPD with 0.1 mol dm^{-3} TBAP in DCE. Further analysis of the transport limited current against the volume flow rate showed analogous behaviour as reported earlier and is illustrated in Figure 6.18.

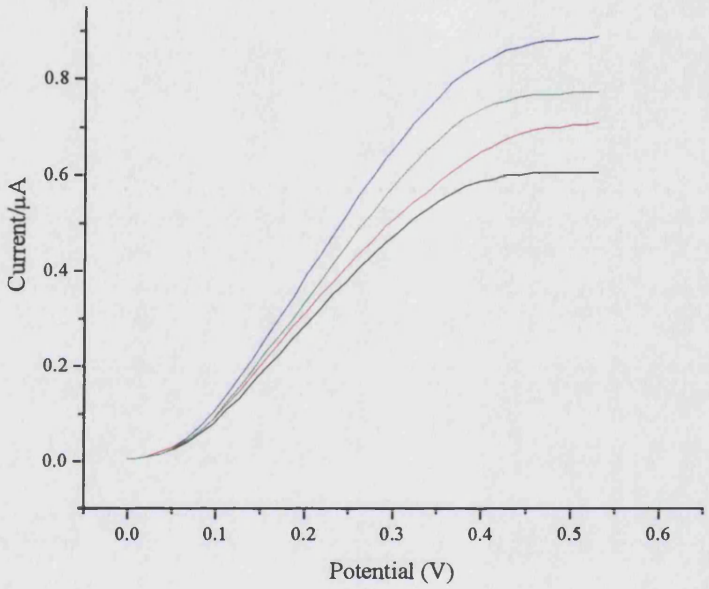

Fig. 6.17. Series of linear sweep voltammograms recorded at various volume flow rates using 1mM TMPD in DCE.

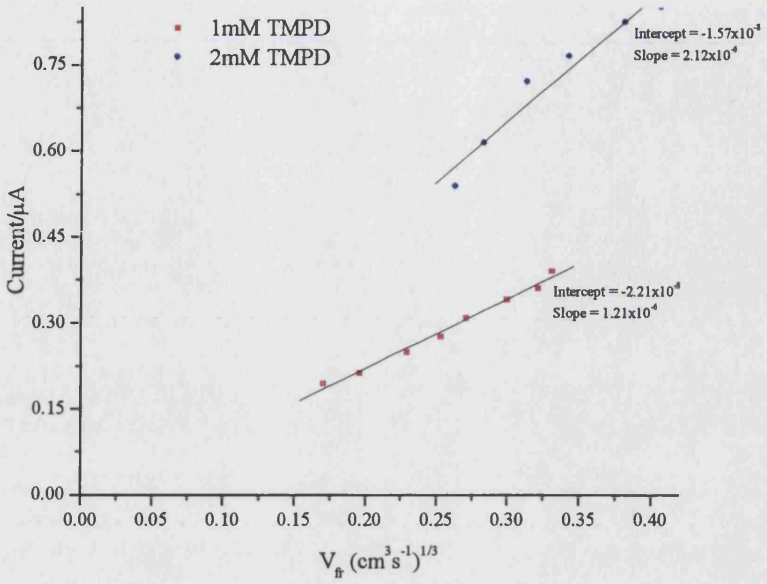

Fig. 6.18. Change in transport limited current due to change in volume flow rate with 1mM and 2mM TMPD in DCE.

From the above studies it can be concluded that the use of microreactor devices can be extended to studies of multilayer liquid-liquid flowing regimes to produce well-defined and reproducible electrochemical measurements. The technique has the potential of being applied in commercial and industrial applications. Experimental investigations into studying organic synthesis, phase transfer catalysis, solvent extraction and flow injection analysis have been demonstrated with liquid-liquid flow systems. The development of this novel range of devices now allows potential benefits of probing the analysis using an integrated system that contains all the components required for interpreting processes occurring at the liquid-liquid interface.

Conclusions

A range of microfabrication techniques have been demonstrated in developing a novel range of microelectrochemical reactor devices. The use of various substrates have been explored and and shown to construct structurally well-defined microchannels. In particular photolithographic techniques have been presented and used to fabricate a range of microelectrodes.

A new flow visualisation technique using an electrochemical approach has been illustrated and a qualitative analysis has shown potential applications in studying fluid dynamic properties in macro and micro scaled flow through devices.

A qualitative and quantitative analysis of the voltammetric response observed on MECR devices has been presented. Experimental measurements revealed quantitative trends identical to those predicted numerically for the transport limited current seen for a microband electrode within a microchannel. Further investigations show that good agreement with the analytical expression reported by Levich is also seen. Preliminary studies have shown the potential applications of MECR devices aswell and the use of dual working electrode flow through devices have been detailed.

A demonstration of MECR techniques to develop a range of microreactor devices with an environment of parallel immiscible flow regime has also been demonstrated. Results have been presented on the use of microchannels to interrogate the liquid-liquid interface between two and three immiscible liquids. Qualitative studies of the mass transport and fluid dynamic properties using voltammetric techniques have been shown, and a linear relationship between the transport limited current and volume flow rate have been shown.

In summary, the work detailed in this Thesis, has outlined the fundamentals of electrochemical techniques for exploring the application of microreactor devices in the field of chemical sensors. The concepts covered in this research characterise the

electrochemical behaviour seen in microelectrochemical reactors devices, and provide a foundation for technological advances in developing novel and more sophisticated microchemical sensors.

Appendix 1

Appendix 1

The Finite Element Method

Introduction

The simulation results presented within this Thesis have been performed using the finite element method.

The FEM is part of group of numerical strategies that exploits the use of weighted residuals (MWR). In this approach a set of weighting functions is employed to allow approximation of a variable over a region of interest. The selection of an appropriate weighting function gives rise to a number of different formulations strategies, including the collocation method, sub domain method, method of moments and the Galerkin method.

The FEM can trace its history back to structural analysis, the phrase, finite element, however, was not widely adopted until Clough[232] used it for a title of a paper in 1960. The method has subsequently been applied to a vast range of problems, including, importantly in this Thesis for the application of electrochemical reactivity under diffusional and convective diffusional transport conditions. In the following sections the basic formulation and application of FEM analysis for one-dimensional diffusional transport is outlined. .

Mathematical Formulation

A one-dimensional diffusional problem, under steady-state conditions can be predicted using the following expression

$$D\frac{\partial^2 c}{\partial x^2} = 0$$

Equ. A1.1

The FEM uses a mesh of elements to cover the domain, as shown in figure A1 below

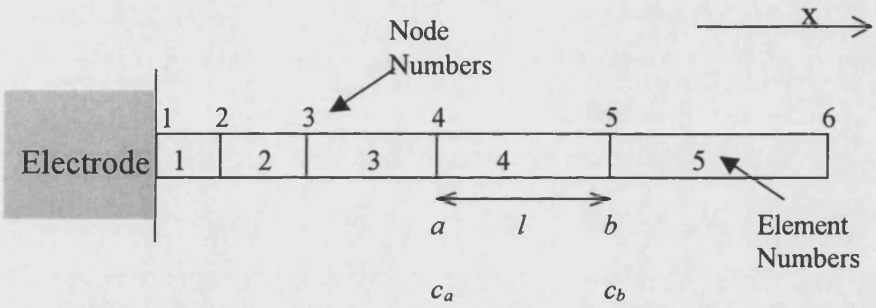

Figure A1: One-dimensional element mesh.

The concentration variation as a function of distance (x) $c(x)$ along the element can be defined by an interpolation function with the concentrations related to the values at the nodal points (figure A1) c_a and c_b:

$$c(x) = N_a c_a + N_b c_b$$

Equ. A1.2

here the interpolation functions employed are

$$N_a = \frac{1}{l}(x_b - x)$$

Equ. A1.3

$$N_b = \frac{1}{l}(x - x_a)$$

Equ. A1.4

where x_a and x_b are as noted above. For each individual element these relationships may be cast into a matrix form using

$$c = \vec{N}^e \vec{c}^e$$

Equ. A1.5

where

$$\vec{N}^e = [N_a \quad N_b]$$

Equ. A1.6

Assuming ne elements are employed to cover the domain of interest the total concentration may be predicted by a summation:

$$c = \sum_{e=1}^{ne} \vec{N}^e \vec{c}^e$$

Equ. A1.7

A weighted residual formulation is then used to solve Equation A1.7. Essentially this approach sets out to approximate the concentration variation over a specific region in space using a residual *R(x)* and this must obey:

$$R(x) - \frac{\partial^2 c}{\partial x^2} = 0$$

Equ. A1.8

Therefore the numerical procedure is implemented such that the residual is minimised within the domain. This can be achieved by numerically forcing *R(x)* to take an average value of zero over the finite region, defined by the element. Mathematically this is carried out by multiplying by a weighting function *w(x)*

$$\int_a^b w(x)R(x)\,dx = 0$$

Equ. A1.9

This weighting function distributes the residual error over the elemental interval (defined by the bounds *a* and *b*). A popular approach to achieve this is via the Galerkin method, which exploits weighting functions of the same form as the interpolation functions (Equations A1.3 and 1.4 above). The residual thus takes the same form as the original differential

$$R(x) - \frac{\partial^2 C}{\partial x^2} = 0$$

Equ. A1.10

where C now represents an approximate solution for the concentration (not the real solution denoted by c) . Recasting Equation A1.10 in residual form yields

$$D\int_a^b N^e \frac{\partial^2 C}{\partial x^2} dx = 0$$

Equ. A1.11

Equation A1.11 is then integrated (by parts) to yield

$$D\int_a^b \frac{\partial \vec{N}^e}{\partial x}\frac{\partial C}{\partial x} dx \; - \; D\left(\vec{N}^e \frac{\partial C}{\partial x}\right)\Big|_a^b \; = \; 0$$

Equ. A1.12

Therefore

$$\frac{\partial C}{\partial x} = \frac{\partial \vec{N}^e}{\partial x}\vec{C}$$

Equ. A1.13

and this yields the form of the equation, which can then be solved (subject to the application of appropriate boundary conditions).

$$D\int_a^b \frac{\partial \vec{N}^e}{\partial x}\frac{\partial \vec{N}^e}{\partial x} dx \vec{C} - D\frac{\partial c}{\partial x}\left(\vec{N}^e\right)\Big|_a^b \; = \; 0$$

Equ. A1.14

Noting the second term of Equation A1.14 actually corresponds to the boundary of the element and may be applied as a boundary condition solution of Equation A1.14 now

requires the remaining integral on the left hand side of A1.14 to be discretised and solved. We can show that

$$\frac{\partial \vec{N}}{\partial x} = \begin{bmatrix} -\frac{1}{l} & \frac{1}{l} \end{bmatrix}$$

Equ. A1.15

it also follows that

$$\frac{D}{l}\begin{bmatrix} 1 & -1 \\ -1 & 1 \end{bmatrix}\vec{C} = 0$$

Equ. A1.16

thus an individual element in matrix from may be represented by

$$[K]^e \vec{C} = \vec{P}$$

Equ. A1.17

where

$$[K]^e = \begin{bmatrix} 1 & -1 \\ -1 & 1 \end{bmatrix}$$

Equ. A1.18

($[K]^e$ is usually referred to as the characteristic matrix of the element).

For a mesh of *ne* elements (figure *.6) a global matrix is now constructed with contributions from each node summed into the relevant matrix position

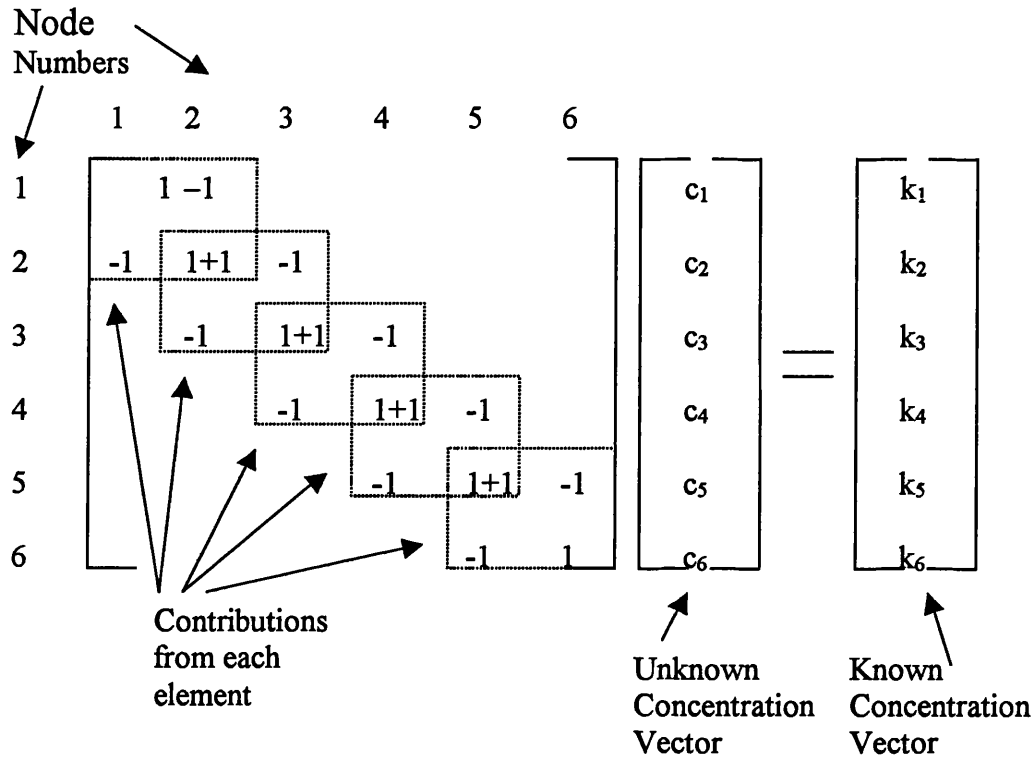

Figure A2: Global Matrix for a problem where *ne = 5*

Once the matrix has been constructed from the individual elemental matrices and the known interconnectivity of the grid, then any boundary conditions for the problem can be introduced (e.g. electron transfer rates at the electrode surface etc). The boundaries at the internal nodes are assumed to have a continuous flux between each element and are therefore balance, leaving only the two values of flux at the external points of the mesh to be defined (if required). Left undefined, the values correspond to the Neumann boundary condition of no flux. However, a fixed concentration, Dirichlet boundary condition, may be routinely introduced. It is apparent that the matrix formed is symmetric and banded around the centre diagonal and this permits standard Gaussian

elimination routines to be employed for solution of the matrices. Modification of the above formulation to permit the simulation of convective diffusional transport provides no significant conceptual difficulties and readers are referred to the article by Stevens[162,233] where a similar procedure has been adopted to formulate two-dimensional convective diffusion problems.

References

(1) Fisher, A. C. *Oxford Chemstry Primers* **1996**, 4.

(2) Butler, J. A. V. *Trans. Faraday Soc.* **1924**, *734*, 19.

(3) Bard, A. J.; Faulkner, L. R. **1980**.

(4) Cottrell, F. G. Z. *Physical Chemistry* **1903**, *42*, 385.

(5) Heinze, J. *Angewandte Chemie-International Edition* **1993**, *32*, 1268.

(6) Bond, A. M.; Eklund, J. C.; Tedesco, V.; Vu, T.; Wedd, A. G. *Inorganic Chemistry* **1998**, *37*, 2366.

(7) Sarfarazi, J. G. F.; Cassidy, T. D. J.; J-J., S.; Russel, A.; Dunmore, G.; Fleischmann, M.; Pons, S. *Analytical Chemistry* **1986**, *58*, 2278.

(8) Bond, A. M.; Man, T. F. *Electrochimica Acta* **1987**, *32*, 863.

(9) Vetter, K. J. **1961**.

(10) Delahay, P. **1954**.

(11) Bard, A. J. *Analytical Chemistry* **1962**, *33*, 11.

(12) Lingane, P. J. *Analytical Chemistry* **1964**, *36*, 1723.

(13) Soos, Z. G.; Lingane, P. J. *Journal of Physical Chemistry* **1964**, *68*, 3821.

(14) Pnchon, J.-L.; Cespuglio, R.; Gonon, F.; Jouvet, M.; Pujol, J.-F. *Analytical Chemistry* **1979**, *51*, 1483.

(15) Storzbach, M. **1991**.

(16) Fleischmann, M.; Lasserre, F.; Robinson, J.; Swan, D. *Journal of Electroanalytical Chemistry* **1984**, *177*, 97.

(17) Dayton, M. A.; Ewing, A. S.; Wightman, R. M. *Analytical Chemistry*, *52*, 2392.

(18) Marcoux, S.; Adams, R. N.; Feldberg, S. W. *Journal of Physical Chemistry* **1969**, *73*, 2611.

(19) Montengero, M. I.; Pletcher, D. *Journal of Electroanalytical Chemistry* **1990**, *290*, 155.

(20) Montengero, M. I.; Pletcher, D.; Mazur, L. D. J.; Zawodzinski, C. *Journal of Applied Electrochemistry* **1990**, *20*, 54.

(21) Howell, J. W.; Wightman, R. M. *Journal of Physical Chemistry* **1984**, *88*, 3915.

(22) Meerholz, K.; Tschuncky, P.; Heinze, J. *Journal of Electroanalytical Chemistry* **1993**, *347*, 425.

(23) Fitch, A.; Evans, D. H. *Journal of Electroanalytical Chemistry* **1986**, *202*, 83.

(24) Andrieux, C. P.; Saveant, P. H. J.-M. *Journal of Physical Chemistry* **1988**, *92*, 5987.

(25) Shoup, D.; Szabo. *Journal of Electroanalytical Chemistry* **1984**, *160*, 19.

(26) Nuzaki, K.; Oyama, M.; Hatano, H.; Ozakazi, S. *Journal of Electroanalytical Chemistry* **1989**, *270*, 191.

(27) Sleszyniski, N.; Carter, O. M. *Analytical Chemistry* **1984**, *56*, 130.

(28) Brett, C. M. A.; Brett, A. M. C. F. O. *Comprehensive Chemical Kinetics* **1986**, *26*, 355.

(29) Eklund, J. C.; Bond, A. M. *Advances in Physical Organic Chemistry* **1999**, *31*, 1.

(30) Howe, J. O.; Wightman, R. M. *Analytical Chemistry* **1985**, *56*, 524.

(31) Howell, J. O.; Kuhr, W. G.; Ensman, R. E.; Wightman, R. M. *Journal of Electroanalytical Chemistry* **1986**, *243*, 321.

(32) Saito, Y. *Rev. Polarogr.* **1968**, *15*, 177.

(33) Kwak, J.; Bard, A. J. *Analytical Chemistry* **1989**, *61*, 1221.

(34) Bard, A. J.; Fan, F. R. F.; Peierce, D. T.; Unwin, P. R.; Widpf, D. O.; Zhou, F. *Science* **1991**, *254*, 68.

(35) Bard, A. J.; Fan, F. R. F. **1993**, *18*, 243.

(36) Bard, A. J.; Mirkin, M. V.; Unwin, P. R.; Wipf, D. O. *Journal of Physical Chemistry* **1992**, *96*, 1861.

(37) Unwin, P. R.; Bard, A. J. *Journal of Physical Chemistry* **1991**, *96*, 4917.

(38) Zhou, F.; Unwin, P. R.; Bard, A. J. *Journal of Physical Chemistry* **1992**, *96*, 4917.

(39) Bernstein, C.; Heindrichs, A.; Vielstich, W. *Journal of Electroanalytical Chemistry* **1978**, *87*, 81.

(40) Herrman, J.; Schmidt, H.; Vielstich, W. *Journal of Physical Chemistry* **1984**, *139*, 83.

(41) Unwin, P. R.; Compton, R. G. *Comprehensive Chemical Kinetics* **1989**, *29*, 173.

(42) Rees, N. V.; Dryfe, R. A. W.; Cooper, J. A.; Coles, B. A.; Compton, R. G.; Davies, S. G.; McCarthy, T. D. *Journal of Physical Chemistry* **1995**, *99*, 7096.

(43) Qiu, F. L.; Gooch, K. A.; Fisher, A. C.; Stevens, N. P. C.; Compton, R. G. *Analytical Chemistry* **2000**, *72*, 3480.

(44) Baars, A.; Sluyters-Rehbach, M.; Sluyters, J. H. *Journal of Electroanalytical Chemistry* **1990**, *283*, 99.

(45) Macpherson, J. V.; Simjee, N.; Unwin, P. R. *Electrochimica Acta* **2001**, *47*, 29.

(46) Levich, V. G. **1962**.

(47) Terry, S. C.; Jerman, J. H.; Angell, J. B. *Ieee Transactions on Electron Devices* **1979**, *26*, 1880.

(48) van Lintel, H. T. G.; M., v. d. P. F. C.; Bouwstra, S. *Sensors and Actuators* **1988**, *15*, 153.

(49) Shoji, S.; Esashi, M.; Matsuo, T. *Sensors and Actuators* **1988**, *14*, 101.

(50) Esashi, M. *Sensors and Actuators* **1990**, *21*, 161.

(51) Manz, A.; Graber, N.; Widmer, H. M. *Sensors and Actuators* **1990**, *B1*, 244.

(52) Widmer, H. M. *Trends in Analytical Chemsitry* **1983**, *2*, viii.

(53) Kovacs, G. T. A. **1998**.

(54) Madou, M. J. **1997**.

(55) Raymond, D. E.; Manz, A.; Widmer, H. M. *Analytical Chemistry* **1994**, *66*, 2858.

(56) Jeong, Y.; Kim, S.; Chun, K.; Chang, J.; Chung, D. S. *Lab on a Chip* **2001**, *1*, 143.

(57) Burns, M. A.; Mastrangelo, C. H.; Sammasrco, T. S.; Man, F. P.; Webster, B. N.; Johnson, B. N.; Forester, B.; Jones, D.; Fields, Y.; Kaiser, A. R.; Burke, D. T. *Proc. Nat. Acad. Sci.* **1996**, *93*, 5556.

(58) Manz, A.; Miyahara, Y.; Miura, J.; Watanabe, Y.; Miyagi, H.; Sato, K. *Sensors and Actuators B-Chemical* **1990**, *1*, 249.

(59) Verpoorte, E.; Manz, A.; Ludi, H.; Bruno, A. E.; Maystre, F.; Krattiger, B.; Widmer, H. M.; van der Schoot, B. H.; de Rooij, N. F. *Sensors and Actuators B-Chemical* **1992**, *6*, 66.

(60) Losey, M. W.; Jackman, R. J.; Firebaugh, S. L.; Schmidt, M. A.; Jensen, K. F. *Journal of Microelectromechanical Systems* **2002**, *11*, 709.

(61) Verpoorte, E. M. J.; Vanderschoot, B. H.; Jeanneret, S.; Manz, A.; Widmer, H. M.; Derooij, N. F. *Journal of Micromechanics and Microengineering* **1994**, *4*, 246.

(62) Kikutani, Y.; Horiuchi, T.; Uchiyama, K.; Hisamoto, H.; Tokeshi, M.; Kitamori, T. *Lab on a Chip* **2002**, *2*, 188.

(63) Abe, T.; Esashi, M. *Sensors and Actuators a-Physical* **2001**, *87*, 139.

(64) Dietrich, T. R.; Ehrfeld, W.; Lacher, M.; Krämer, M.; Speit, B. *Microelectronic Engineering* **1996**, *30*, 497.

(65) Becker, H.; Arundell, M.; Harnish, A.; Hulsenberg, D. *Sensors and Actuators B-Chemical* **2002**, *86*, 271.

(66) Xia, Y. N.; Whitesides, G. M. *Annual Review of Materials Science* **1998**, *28*, 153.

(67) Michel, B.; Bernard, A.; Bietsch, A.; Delamarche, E.; Geissler, M.; Juncker, D.; Kind, H.; Renault, J. P.; Rothuizen, H.; Schmid, H.; Schmidt-Winkel, P.; Stutz, R.; Wolf, H. *IBM J. Res. Dev.* **2001**, *45*, 697.

(68) Duffy, D. C.; McDonald, J. C.; Schueller, O. J. A.; Whitesides, G. M. *Analytical Chemistry* **1998**, *70*, 4974.

(69) Ceriotti, L.; De Rooij, N. F.; Verpoorte, E. *Analytical Chemistry* **2002**, *74*, 639.

(70) Jo, B. H.; Van Lerberghe, L. M.; Motsegood, K. M.; Beebe, D. J. *Journal of Microelectromechanical Systems* **2000**, *9*, 76.

(71) Anderson, J. R.; Chiu, D. T.; Jackman, R. J.; Cherniavskaya, O.; McDonald, J. C.; Wu, H. K.; Whitesides, S. H.; Whitesides, G. M. *Analytical Chemistry* **2000**, *72*, 3158.

(72) Becker, H.; Gartner, C. *Electrophoresis* **2000**, *21*, 12.

(73) McCormick, R. M.; Nelson, R. J.; Alonso-Amigo, M. G.; Benvegnu, D. J.; Hooper, H. H. *Analytical Chemistry* **1997**, *69*, 2626.

(74) Belgrader, P.; Hansford, D.; Kovacs, G. T. A.; Venkateswaran, K.; Mariella, R.; Milanovich, F.; Nasarabadi, F.; Okuzumi, S.; Pourahmadi, F.; Northrup, M. A. *Analytical Chemistry* **1999**, *71*, 4232.

(75) Shaw, J.; Nudd, R.; Naik, B.; Turner, C.; Rudge, D.; Benson, M.; Garman, A. *Proceedings of Micro Total Analysis Systems* **2000**.

(76) Hisamoto, H.; Horiuchi, T.; Uchiyama, K.; Tokeshi, M.; Hibara, A.; Kitamori, T. *Analytical Chemistry* **2001**, *73*, 5551.

(77) Tokeshi, M.; Minagawa, T.; Kitamori, T. *Journal of Chromatography A* **2000**, *894*, 19.

(78) Tokeshi, M.; Minagawa, T.; Kitamori, T. *Analytical Chemistry* **2000**, *72*, 1711.

(79) Yu, C.; Davey, M. H.; Svec, F.; Frechet, J. M. J. *Analytical Chemistry* **2001**, *73*, 5088.

(80) Floyd, T. M.; Schmidt, M. A.; Jensen, K. F. *Proceedings of Micro Total Analysis Systems* **2001**, 277.

(81) Yasuda, K.; Ichiki, M. *Transducers 99* **1999**, 128.

(82) Eijkel, J. C. T.; Prak, A.; Cowen, S.; Craston, D. H.; Manz, A. *Journal of Chromatography A* **1998**, *815*, 265.

(83) Yamamoto, T.; Nojima, T.; Fujii, T. *Lab on a Chip* **2002**, *2*, 197.

(84) Hostis, L.; Michel, E.; Fiaccabrino, P. E.; Strike, G. C.; De Rooij, N. F.; Koudelka-Hep, M. *Sensors and Actuators* **2000**, *64*, 156.

(85) Hatch, A.; Kamholz, A. E.; Hawkins, K. R.; Munson, M. S.; Schilling, E. A.; Weigl, B. H.; Yager, P. *Nat. Biotechnol.* **2001**, *19*, 461.

(86) Auroux, P. A.; Iossifidis, D.; Reyes, D. R.; Manz, A. *Analytical Chemistry* **2002**, *74*, 2637.

(87) Roulet, J. C.; Fluri, K.; Verpoorte, E.; Wolkel, R.; Herzig, H. P.; De Rooij, N. F.; Dandliker, R. *Proceedings of Micro Total Analysis Systems* **1998**, 287.

(88) Burggraf, N.; Krattiger, B.; de Mello, A. J.; De Rooij, N. F.; Manz, A. *Analyst* **1998**, *123*, 1443.

(89) Pan, D. H.; Mathies, R. A. *Biochemistry* **2001**, *40*, 7929.

(90) Li, J.; Thibault, P.; Bings, N. H.; Skinner, C. D.; Wang, C.; Coyler, C. L.; Harrison, D. J. *Journal of Analytical Chemistry* **1999**, *71*, 3036.

(91) Deng, Y. Z.; Henion, J.; Li, J. J.; Thibault, P.; Wang, C.; Harrison, D. J. *Proteomics* **2001**, *1*, 975.

(92) Fister, J. C.; Jacobson, S. C.; Davis, L. M.; Ramsey, J. M. *Analytical Chemistry* **1998**, *70*, 431.

(93) Sato, K.; Kawanishi, H.; Tokeshi, M.; Kitamori, T.; Sawada, T. *Analytical Sciences* **1999**, *15*, 525.

(94) Schawrz, M. A.; Hauser, P. C. *Lab on a Chip* **2001**, *1*, 1.

(95) Lacher, N. A.; Garrison, K. E.; Martin, R. S.; Lunte, S. M. *Electrophoresis* **2001**, *22*, 2526.

(96) Haber, C. *Handbook of Capillary Electrophoresis* **1997**, 425.

(97) Manz, A.; Harrison, D. J.; Verpoorte, E.; Widmer, H. M. *Advances in Chromatography* **1993**, *33*, 1.

(98) Gawron, A. J.; Martin, R. S.; Lunte, S. M. *Electrophoresis* **2001**, *22*, 242.

(99) Galloway, M.; Stryjewski, W.; Henry, A.; Ford, S. M.; Llopis, S.; McCarley, R. L.; Soper, S. A. *Analytical Chemistry* **2002**, *74*, 2407.

(100) Wang, J.; Tian, B. M.; Sahlin, E. *Analytical Chemistry* **1999**, *71*, 5436.

(101) Hilmi, A.; Luong, J. H. T. *Analytical Chemistry* **2000**, *72*, 4677.

(102) Brookes, B. A.; Davies, T. J.; Fisher, A. C.; Evans, R. G.; Wilkins, S. J.; Yunus, K.; Wadhawan, J. D.; Compton, R. G. *Journal of Physical Chemistry B* **2003**, *107*, 1616.

(103) Davies, T. J.; Brookes, B. A.; Fisher, A. C.; Yunus, K.; Wilkins, S. J.; Greene, P. R.; Wadhawan, J. D.; Compton, R. G. *Journal of Physical Chemistry B* **2003**, *107*, 6431.

(104) Wadhawan, J. D.; Welford, P. J.; Yunus, K.; Fisher, A. C.; Compton, R. G. *Journal of Brazilian Chemical Society* **2003**, *14*, 1.

(105) Yunus, K.; Marks, C. B.; Fisher, A. C.; Allsopp, D. W. E.; Ryan, T. J.; Dryfe, R. A. W.; Hill, S. S.; Roberts, E. P. L.; Brennan, C. M. *Electrochemistry Communications* **2002**, *4*, 579.

(106) Fisher, A. C.; A., G. K.; Henley, I. E.; Yunus, K. *Analytical Sciences* **2001**, *17*, i371.

(107) Henley, I. E.; Yunus, K.; Fisher, A. C. *Journal of Physical Chemistry B* **2003**, *107*, 3878.

(108) Okazaki, J. *Journal of Vacuum Science & Technology B* **1991**, *9*, 2829.

(109) Jeong, H. J.; Markle, D. A.; Owen, G.; Pease, F.; Grenville, A.; von Bünau, R. *Solid State Technology* **1994**, *37*, 39.

(110) Levenson, M. D. *ibid.* **1995**, *38*, 57.

(111) Geppert, L. *IEEE Spectrum* **1996**, *33*, 33.

(112) O'Brien, C. S. *Chemistry Society Review* **1996**, 393.

(113) Bowden, N.; Arias, F.; Deng, T.; Whitesides, G. M. *Langmuir* **2001**, *17*, 1757.

(114) Madou, M. J. *Fundamentals of Microfabrication: The Science of Miniaturisation*, 2nd ed.; CRC Press: Boca Raton, 2002.

(115) Rai-choudhury, P. *Handbook of Microlithography, Micromachining, and Microfabrication*, 1st ed.; SPIE Press, Bellingham, WA, 1997; Vol. 2.

(116) Qin, D.; Xia, Y. N.; Black, A. J.; Whitesides, G. M. *Journal of Vacuum Science & Technology B* **1998**, *16*, 98.

(117) Kyung, J. H.; Lawandy, N. M. *Optics Letters* **1996**, *21*, 174.

(118) Daykin, R. N. C.; Haswell, S. J. *Analytica Chimica Acta* **1995**, *313*, 155.

(119) Tantra, R.; Manz, A. *Analytical Chemistry* **2000**, *72*, 2875.

(120) Cooper, J. A.; Compton, R. G. *Electroanalysis* **1998**, *10*, 141.

(121) Compton, R. G.; Coles, B. A. *Journal of Electroanalytical Chemistry* **1983**, *144*, 87.

(122) Schlichting, H. *Boundary Layer Theory*; Pergamon Press, London, 1995.

(123) Abe, T.; Esashi, M. *Sensors and Actuators a-Physical* **2000**, *82*, 139.

(124) *http://www.mikroglas.com/index_e.html*.

(125) *http://www.el.utwente.nl/tt/projects/wetchem/*.

(126) Kumar, A.; Whitesides, G. M. *Applied Physics Letters* **1993**, *63*, 2002.

(127) Kim, E.; Xia, Y. N.; Whitesides, G. M. *Journal of the American Chemical Society* **1996**, *118*, 5722.

(128) Xia, Y.; Kim, E.; Zhao, X. M.; Rogers, J. A.; Prentiss, G. M.; Whitesides, G. M. *Science* **1996**, *273*, 347.

(129) Kim, E.; Xia, Y.; Whitesides, G. M. *Nature* **1995**, *376*, 587.

(130) Kim, E.; Xia, Y.; Zhao, X. M.; Whitesides, G. M. *Advanced Materials* **1997**, *9*, 651.

(131) Hutley, M. C. *Diffraction Gratings*; Academic Press, New York, 1982.

(132) Terris, B. D.; Mamin, H. J.; Best, M. E.; Logan, J. A.; Rugar, D. *Applied Physics Letters* **1996**, *69*, 4262.

(133) Kiewit, D. A. *Rev. Sci. Instrum.* **1973**, *44*, 1741.

(134) Wang, H. Y.; Foote, R. S.; Jacobson, S. C.; Chneibel, J. H.; Ramsey, J. M. *Sensors and Actuators B-Chemical* **1997**, *45*, 199.

(135) Roggendorf, H.; Boschel, D.; Trempler, J. *Journal of Non-Crystalline Solids* **2001**, *293*, 6.

(136) Adrian, R. J. *Int. J. Heat Fluid Flow* **1986**, *7*, 127.

(137) Adrian, R. J. *Annual Review of Fluid Mechanics* **1991**, *23*, 261.

(138) Hesselink, L. *Annual Review of Fluid Mechanics* **1988**, *20*, 421.

(139) Ohba, K. *J. Flow Visualisation* **1987**, *7*, 77.

(140) Fujimoto, T.; T., N.-i. *J. Flow Visualisation* **1980**, *5*, 203.

(141) Kawahashi, M. *J. Flow Visualisation* **1987**, *7*, 84.

(142) Hosoi, K. *J. Flow Visualisation* **1980**, *3*, 247.

(143) Kobayashi, T.; Saga, T.; Segawa, S. *Flow Visualisation* **1990**.

(144) Kanamori, H.; Lee, Y. H.; Kobayashi, T.; Saga, T. *The 3rd Trennial International Symposium on Fldui Control, Measurement and Visualisation* **1991**, 401.

(145) Chen, L. J.; Chen, C. J. *The 3rd Trennial International Symposium on Fldui Control, Measurement and Visualisation* **1991**, 407.

(146) David, L.; A., T. *The 4th Triennial Symposium on Fluid Control, Fluid Measurement and Visualisation* **1994**, 515.

(147) Dimotakis, P. E.; Debussy, F. D.; Koochesfahani, M. M. *Phys. Fluids* **1981**, *24*, 995.

(148) Kobayashi, T.; Ishihara, T.; Saski, N. *Flow Visualisation III* **1985**.

(149) Khalighi, B. *Flow Visualisation Conference* **1989**.

(150) Walter, J. A.; Chen, C. J. *Flow Visualisation Conference* **1989**, *85*.

(151) Lourenco, L.; Kirothapali. *Exp. Fluids* **1987**, *5*, 29.

(152) Erbeck, R.; Merzkirch, W. *Exp. Fluids* **1988**, *6*, 89.

(153) Kuhnel, W.; Kottke, V. *The 4th Triennial Symposium on Fluid Control, Fluid Measurement and Visualisation* **1994**, 989.

(154) Nakayama, Y. *The 3rd Trennial International Symposium on Fldui Control, Measurement and Visualisation* **1991**, 355.

(155) JSME. *Flow Visualisation Hanbook* **1986**.

(156) Hori, K.; Sugiyama, S.; Akai, A. *The 4th Triennial Symposium on Fluid Control, Fluid Measurement and Visualisation* **1994**, 289.

(157) Kawamura, K.; Siaito, A.; Tanasawa, Y. *Trans. JSAE, 36*, 33.

(158) Woods, W. A.; Clark, D. G. *Visualised Flow, Fluid Motion in Basic and Engineering Situations Revealed by Flow Visualisation* **1991**, 231.

(159) Tskuiji, T. *The 3rd Trennial International Symposium on Fldui Control, Measurement and Visualisation* **1991**, 231.

(160) Compton, R. G.; Pilkington, M. B. G.; Stearn, G. M. *J. Chem. Soc.* **1988**, *84*, 2155.

(161) Coles, B. A.; Dryfe, R. A. W.; Rees, N. V.; Compton, R. G.; Davies, S. G.; McCarthy, T. D. *Journal of Electroanalytical Chemistry* **1996**, *411*, 121.

(162) Stevens, N. P. C.; Fisher, A. C. *Journal of Physical Chemistry B* **1997**, *101*, 8259.

(163) Jeong, D. A.; Markel, F.; Pease, A.; CVonBunau. *Solid State Technology* **1994**, *37*, 39.

(164) Levenson, M. D. *Solid State Technology* **1995**, *38*, 57.

(165) Compton, R. G.; Fisher, A. C.; Wellington, R. G.; Winkler, J. *Journal of Physical Chemistry* **1992**, *96*, 8153.

(166) Compton, R. G.; Fisher, A. C.; Spackman, R. A. *Electroanalysis* **1992**, *22*, 38.

(167) Fisher, A. C.; Compton, R. G. *Electroanalysis* **1992**, *4*, 311.

(168) Alden, J. A.; Compton, R. G.; Leslie, W. M.; Silk, T. *Journal of Physical Chemistry* **1996**, *100*, 14130.

(169) Ranger, C. B. *Analytical Chemistry* **1981**, *20A*, 53.

(170) Stewart, K. K. *Analytical Chemistry* **1983**, *931A*, 55.

(171) Ruzicka, J. *Analytical Chemistry* **1983**, *1040A*, 55.

(172) Albery, W. J.; Jones, C. C.; Mount, A. R. *Comprehensive Chemical Kinetics* **1989**, *29*, 129.

(173) Waller, A. M.; Compton, R. G. *Comprehensive Chemical Kinetics* **1989**, *29*, 297.

(174) Dryfe, R. A. W.; Compton, R. G. *Prog. Reaction Kinetics* **1995**, *20*, 245.

(175) Kissinger, P. T. *Analytical Chemistry* **1977**, *447A*, 49.

(176) Wightman, R. M.; Paik, E. C.; Borman, S.; Dayton, M. A. *Analytical Chemistry* **1978**, *1410*, 50.

(177) Kastening, B. *Z. Anal. Chem.* **1967**, *224*, 196.

(178) Dohrmann, J. K.; Galluser, F.; Wittchen, H. *Faraday Discussions Chem. Soc.* **1973**, *56*, 350.

(179) Webster, B. N.; Dryfe, R. A. W.; Eklund, J. C.; Lee, C. W.; Compton, R. G. *Journal of Electroanalytical Chemistry* **1996**, *402*, 167.

(180) Compton, R. G.; Coles, B. A.; Pilkington, M. B. G.; Bethell, D. *J. Chem Soc. Faraday Trans.* **1990**, *86*, 663.

(181) Fisher, A. C.; Coles, B. A.; Compton, R. G.; Bethell, D.; Tripathi, S. *Journal of the Chemical Society-Faraday Transactions* **1990**, *86*, 3603.

(182) Compton, R. G.; Eklund, J. C.; Fisher, A. C.; Waller, A. M. *Journal of the Chemical Society-Faraday Transactions* **1990**, *86*, 2951.

(183) Compton, R. G.; Fisher, A. C.; Wellington, R. G.; Bethell, D.; Lederer, P. *Journal of Physical Chemistry* **1991**, *95*, 4749.

(184) Compton, R. G.; Fisher, A. C.; Wellington, R. G.; Bethell, D. *Portug. Electrochim. Acta* **1991**, *9*, 271.

(185) Compton, R. G.; Dryfe, R. A. W.; Fisher, A. C. *Journal of Electroanalytical Chemistry* **1993**, *361*, 275.

(186) Compton, R. G.; Dryfe, R. A. W.; Eklund, J. C.; Page, S. D.; Hirst, J.; Nei, L.; Fleet, G. W. J.; Hsua, K. Y.; Bethell, D.; Martingale, L. J. *J. Chem. Soc. Perkin II* **1995**, *8*, 1673.

(187) Gerischer, H.; Mattes, I.; Braun, R. *Journal of Electroanalytical Chemistry* **1963**, *10*, 553.

(188) Ysuru, T.; Nishimura, T.; Haryuma, S. *Denki Kagaku* **1984**, *52*, 532.

(189) Aoki, K.; Tokuda, K.; Matsuda, H. *Journal of Electroanalytical Chemistry* **1986**, *209*, 247.

(190) Compton, R. G.; Coles, B. A.; Fisher, A. C. *Journal of Physical Chemistry* **1994**, *98*, 2441.

(191) Compton, R. G.; Coles, B. A.; Gooding, J. J.; Fisher, A. C.; Cox, T. I. *Journal of Physical Chemistry* **1994**, *98*, 2446.

(192) Fisher, A. C.; Compton, R. G. *Journal of Physical Chemistry* **1991**, *95*, 7538.

(193) Naz, A.; Effenhauser, C. S.; Barggraf, N.; Verpoorte, E.; Raymond, D. E.; Widmer, H. M. *Analusis Mag.* **1994**, *M25*, 22.

(194) Ehrfeld, W.; Gratner, C.; Hessel, V.; Konard, R.; Lowe, H.; Richter, T.; Schulz, C. *Fabrication of Components and systems for Chemical Biochemical Microreactors* **1998**.

(195) Jackel, K. P. *Microtechnology* **1996**, *132*, 29.

(196) Aoki, K. *Electroanalysis* **1993**, *5*, 627.

(197) Qiu, F.; Stevens, N. P. C.; Fisher, A. C. *Journal Physical Chemistry B* **1998**, *102*, 3779.

(198) Coles, B. A.; Compton, R. G.; Spackman, R. A. *Electroanalysis* **1993**, *5*, 41.

(199) Sawyer, D. T.; Johnson, D. C. *Analytical Chemistry* **1980**, *52*, 1304.

(200) Compton, R. G.; Fisher, A. C.; Wellington, R. G.; Dobson, P. A.; Leigh, P. A. *Journal of Physical Chemistry* **1993**, *97*, 10410.

(201) Fulian, Q.; Stevens, N. P. C.; Fisher, A. C. *Journal of Physical Chemistry* **1998**, *102*, 3779.

(202) Aveyard, R.; Blankscheitn, D. *Cuur. Opinion Colloid Interface Sci.* **2001**, *4*, 338.

(203) Hardcastle, J. L.; Compton, R. G. *Analyst* **2001**, *126*, 2025.

(204) Atherton, J. H. *Res. Chem. Kinet.* **1993**, *2*.

(205) Uchiyama, Y.; Kitamori, T.; Sawada, T.; Tsuyumoto, I. *Langmuir* **2000**, *16*, 6597.

(206) Girault, H. H.; Schiffrin, D. J. *Electroanalytical Chemistry* **1989**, *15*, 1.

(207) Tan, S. N.; Dryfe, R. A. W.; Girault, H. H. *Helv. Chim. Acta.* **1994**, *77*, 231.

(208) Maracek, V.; Samec, Z.; Koryta, J. *Adv. Colloid Int. Sci.* **1988**, *29*, 1.

(209) Wilke, S.; Osbourne, M. D.; Girault, H. H. *Journal of Electroanalytical Chemistry* **1997**, *436*, 53.

(210) Osakai, T.; Jensen, H.; Nagatani, H.; Fermin, D. J.; Girault, H. H. *Journal of Electroanalytical Chemistry* **2001**, *510*, 43.

(211) Kong, Y.-T.; Kakiuchi, T. *Journal of Electroanalytical Chemistry* **1998**, *446*, 19.

(212) Wei, C.; Bard, A. J.; Mirkin, M. V. *Journal of Physical Chemistry* **1995**, *99*, 16033.

(213) Shao, Y.; Mirkin, M. V.; Rusling, J. F. *Journal Physical Chemistry B* **1997**, *101*, 3202.

(214) Shao, Y.; Mirkin, M. V. *Journal Physical Chemistry B* **1998**, *102*, 9915.

(215) Zang, J.; Unwin, P. R. *J. Chem. Soc. Perkin Trans.* **2001**, *9*, 1608.

(216) Ding, Z. F.; Quinn, B. M.; Bard, A. J. *Journal of Physical Chemistry* **2001**, *105*, 6367.

(217) Barker, A. L.; Unwin, P. R.; Zang, J. *Electrochem. Commun.* **2001**, *3*, 372.

(218) Liu, B.; Mirkin, M. V. *Electroanal. Chem.* **2000**, *12*, 1433.

(219) ulmeanu, S.; Lee, H. J.; Fermin, D. J.; Girault, H. H.; Shao, Y. H. *Electrochem. Commun.* **2001**, *3*, 219.

(220) Brett, C. M. A.; Brett, A.; Compton, R. G.; Fisher, A. C.; Tyley, G. P. *Electroanalysis* **1991**, *3*, 631.

(221) Fulian, Q.; Stevens, N. P. C.; Fisher, A. C. *Journal of Physical Chemistry B* **1998**, *102*, 3779.

(222) Lewis, J. B. *Chem. Eng. Sci.* **1954**, *3*, 248.

(223) Albery, W. J.; Couper, A. M.; Hadgraft, J.; Ryan, C. *J. Chem. Soc. Faraday Trans. I* **1974**, *70*, 1124.

(224) Hundhammer, B.; SDhawan, S. K.; Bekele, A.; Seidlitz, H. J. *Journal of Electroanalytical Chemistry* **1987**, *217*, 253.

(225) Hundhammer, B.; Wilke, S. *Journal of Electroanalytical Chemistry* **1989**, *266*, 133.

(226) Hundhammer, B.; Solomon, T.; Zerihun, T.; Abegaz, M.; Bekele, A.; Graichen, K. *Journal of Electroanalytical Chemistry* **1994**, *371*, 1.

(227) Surmeian, M.; Hibara, A.; Slyadnev, M.; Uchiyama, K.; Hisamoto, H.; Kitamori, T. *Analytical Letters* **2001**, *34*, 1421.

(228) Sato, K.; Tokeshi, M.; Sawada, T.; Kitamori, T. *Analytical Sciences* **2000**, *16*, 455.

(229) Hibara, A.; Tokeshi, M.; Uchiyama, K.; Hisamoto, H.; Kitamori, T. *Analytical Sciences* **2001**, *17*, 89.

(230) Stevens, N. P. C.; Qiu, F. L.; Gooch, K. A.; Fisher, A. C. *Journal of Physical Chemistry B* **2000**, *104*, 7110.

(231) Gooch, K. A.; Williams, N. A.; Fisher, A. C. *Electrochemistry Communications* **2000**, 51.

(232) Girijavallabhan, C. V.; Reese, L. C. *J. Soil Mech. Proc.* **1968**, *94*, 473.

(233) Stevens, N. P. C.; Hickey, S. J.; Fisher, A. C. *Anales De Quimica* **1997**, *93*, 225.